External Cavity Quantum Cascade Lasers

Sheffield University

Michael Hemingway

Tuesday 18th September, 2018

Abstract

In this thesis we deploy mid-infrared quantum cascade lasers (QCLs) in external linear cavity (EC) and external ring cavity (ERC) configurations, with the aim to develop the platform as a source for high resolution gas spectroscopy.

Initially, the temporal evolution of pulsed ERC-QCL system is compared to that of standard Fabry Perot (FP) QCLs to provide insight into the role played by the additional external feedback provided by ECs and ERCs. Time-resolved spectral measurements show that external feedback promotes single longitudinal mode operation on a shorter timescale than is the case for FP-QCLs. A room temperature wavelength tunable external ring cavity QCL is presented which shows improved performance over its linear counterpart due to its ability to support unidirectional emission regimes. Spectral comparisons between linear and ring cavities show that these regimes lead to improved performance due to the suppression of spatial hole burning (SHB), an instability common to linear laser resonators.

An active modulation scheme based on a number of bespoke power amplifiers and bias-tees is developed. These systems are used to produce mode-locked pulse trains in external cavity and external ring cavity QCLs by modulating the QCL gain medium's drive current at frequencies matching the cavity's round trip frequency. Spectral and temporal comparisons are made between these two cases. Asymmetric pulse propagation is observed in the case of the ERC-QCL which has been suggested as promising platform for ultrashort mode-locked mid-infrared pulses.

Publications

[1] DG Revin, M Hemingway, D Vaitiekus, JW Cockburn, N Hempler, GT Maker, and GPA Malcolm. Continuous wave room temperature external ring cavity quantum cascade laser. *Applied Physics Letters*, 106(26):261102, 2015.

[2] DG Revin, M Hemingway, Y Wang, JW Cockburn, and A Belyanin. Active mode locking of quantum cascade lasers in an external ring cavity. *Nature communications*, 7, 2016.

[3] Michael Hemingway, Deivis Vaitiekus, John Cockburn, Nils Hempler, Gareth Maker, Graeme Malcolm, and Dmitry G Revin. Continuous wave room temperature external ring cavity quantum cascade laser. In *CLEO: Science and Innovations*, pages STu4G–6. Optical Society of America, 2015.

Contents

Chapter 1

Introduction

1.1 Introduction

Quantum Cascade Lasers (QCLs) have already been established as a prominent source of coherent mid-infrared light for use in spectroscopic applications. They are high powered, operate at room temperature and can be engineered to cover a broad wavelength range spanning from 2.63[1] to 440 μm[2]. Since their first demonstration in 1994[3] these devices have undergone a great deal of technical revision and are now beginning to enjoying some commercial success where they are employed in a number of diverse applications that require coherent mid-infrared radiation. QCLs can be engineered to cover the technologically important region of the electromagnetic spectrum, between 3 and 8 μm, where the ro-vibrational resonances of organic compounds are found, often called the *molecular fingerprint* region. These resonances are many times stronger than at other frequencies and are the most promising target for future sensing applications.

These credentials have set the QCL in a dominant position for not only spectroscopy tasks such as medical diagnostics, environmental sensing, standoff detection, etc, but also, owing to their power and the natural characteristics of infrared radiation, in a diverse set of non-spectroscopic tasks such as military countermeasures and free-space communication.

In this thesis we deploy the QCL as a gain medium into external cavity (EC) and external ring cavity (ERC) systems to further develop their role as a tunable source. The increased photon lifetimes achieved in external cavities leads to a reduction in emission linewidths which is beneficial to high resolution spectroscopic applications which require increasing selectivity. Furthermore, the free air coupling of external cavities allows dispersive feedback elements to be used to tune the emission over the QCLs naturally broad gain bandwidth.

ERCs allow for the decoupling of the propagation directions which can lead to unidirectional emission and subsequently the suppression of spatial hole burning (SHB), an instability common to linear laser resonators. Developing tuning schemes for these systems could lead to a tunable mid-infrared source of greater stability than Littrow/Littman Metcalf systems which are the dominant design in continuously tunable laser systems.

We go on to develop mode-locked EC QCL systems which are the basis of future

spectroscopic schemes such as multi-heterodyne spectroscopy and may, in some applications, replace other short pulse systems which are largely limited to the visible spectrum. This is achieved using an active gain modulation scheme, driven by a number of bespoke electrical modulators which modulate the laser's driving current at the cavity round trip frequency. The increased path length of ECs reduces pulse repetition rates into the radio frequency range, reducing the complexity of the required electronics compared to mode-locked ridge type QCLs which have round trip frequencies in excess of 10 GHz. The ERC has been suggested as a potentially robust platform for mode-locking of QCLs where a unidirectional regime would suppress SHB which has been shown to distort and destabilise mode-locked pulses emitted from actively modulated QCLs.

1.1.1 Mid-Infrared Sources

The first solid state lasers suitable for spectroscopic tasks were based on lead salts. These heterojunction devices were first demonstrated in 1963[4] and are based on IV-VI semiconductors. Using standard growth techniques, such as molecular beam epitaxy (MBE), these material systems offer some considerable design freedom as far as bandgap tailoring is concerned. PbSe and PbTe have significantly different lattice constants but fairly similar band gap energies, doping these materials with elements such as Cd, Sn, Eu and Yb can alter the band gap without much associated shift in the lattice constant. This gives good flexibility when used to create ternary and quaternary alloys such as PbEuSeTe. This has allowed the realization of devices with emission wavelengths from 3 to over 20 μm, covering most of the mid-infrared. Unlike III-V semiconductors, they possess four direct band gap minima at the L-point. This gives these materials a two orders of magnitude reduction in Auger recombination over their III-V counterparts, especially significant at longer wavelengths where the Auger process is most significant. It's suggested that recombination through impurity and defect states is the dominant non-radiative relaxation mechanism in lead salt materials meaning better material and growth are needed to reduce threshold currents.

Thermally, these devices are problematic with continuous-wave emission demonstrated up to -80 °C and low duty cycle pulsed emission possible to around 80°C.

These materials have poor thermal conductivity, which limits the device's cooling, and are extremely soft. This means lead salt devices have to be much thicker than typical semiconductor heterojunction lasers, further compounding the thermal issues by increasing the thermal path length to the substrate, hindering heat extraction. Beyond this, the inhomogeneous gain profile quickly leads to spectral hole burning which limits the gain at the lasing wavelength, instead promoting threshold gain across the entire bandwidth[5]. This regime is highly inefficient at providing gain to the main lasing mode. This saturation effect limits the low temperature performance. Additional pumping leads to increased losses through free carrier absorption which dominate at high temperature. The net result of these limitations are devices that emit only a few mW of optical power. This may be suitable for spectroscopic tasks but the need for cryogenic cooling for CW performance make these devices unattractive.

Interband Cascade Lasers (ICLs) and Quantum Cascade Lasers (QCLs) are related designs with ICLs being somewhere between, and sharing some characteristics with, interband lasers and QCLs. ICLs were invented around 1994[6], the same year that QCLs were demonstrated for the first time. In ICLs the cascading principle was a means of connecting quantum wells (QWs) in series which meant injected carriers could be used to emit photons at each stage of a repeated structure. This increased the useful voltage which is poorly utilized in multi-quantum-well (MQW) structure where parasitics scale with the number of wells. This becomes increasingly important as wavelengths increase and photon energies become small compared to the parasitics.

ICLs are based on III-V semiconductor materials and are comprised of three different sections: the active quantum well, electron injector and hole injector. Current state of the art devices typically have 5 to 7 stages of this structure repeated. Active QWs are in a "W" configuration which is a symmetric arrangement with a central GaInSb hole QW surrounded by two InAs electron QWs then two AlSb barrier layers. This configuration creates a W shaped band diagram (see fig. 1.1) and has the effect of increasing the electron hole wave-function overlap despite their confinement being in separate layers. It also gives the scheme wavelength tunability as the bandgap in the active region is sensitive to the InAs electron QW thickness.

Semimetallic interfaces which separate the electron and hole injectors are the key to the design principle. These interfaces have a type II, or broken band alignment which means, at least under bias, the valance band maxima is above the adjacent conduction band minima. This allows the efficient promotion of valence band electrons in the hole injector into electron injector states through normal scattering processes.

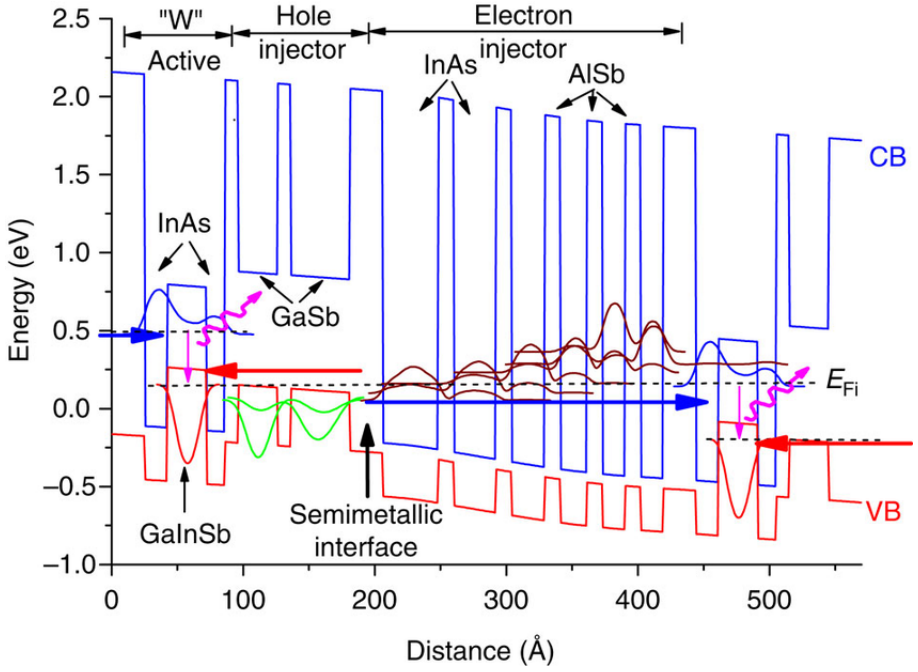

Figure 1.1: Band diagram of an interband cascade laser (ICL) showing one and a half complete stages of the active region[7].

These devices inherit many of the characteristics of interband lasers such as relatively long carrier lifetimes (∼1 ns)[8]. This means these devices lase with much reduced threshold currents and powers relative to their QCL counterparts. ICLs have been demonstrated with CW threshold currents as low as 106 Acm^{-2} and threshold powers as low as 29 mW[7] while still being capable of producing some hundreds of milliwatts of CW power at room temperature and maintaining CW output up to 118 °C. These performance figures are based on devices emitting in the 3 to 5.6 μm wavelength range where ICL performance is reaching some maturity. Clearly at these wavelengths ICLs are likely to be well suited for future handheld spectroscopic applications which require low input power and good thermal performance. Additionally the interband transition brings other differences such as sensitivity to TE

polarized light, which may be important in future vertical emission schemes, and high frequency opacity which QCLs don't suffer from.

Currently the limits of ICL technology aren't well understood with many suggesting that it may be possible to extend their success to increasingly long wavelengths. The role played by Auger recombination in non-radiative current loss is still a matter of debate[8]. This may have implications on future active designs which have shown some success in type I configurations which may improve performance. More research is required before the limits of ICLs will be understood.

QCLs, on the other hand, have received considerably more attention since their inception. These devices are typically built on the well-established InP material system. These, like ICLs, are comprised of a number of repeated subunits but are entirely electronic devices which lase on intersubband transitions. Each stage is made up of an active region and an electron injector. Here as many as 50 stages are used to produce optimal devices. Carrier lifetime associated with intersubband transitions are very short (∼1ps) due to rapid longitudinal optical (LO)-phonon assisted depopulation which is the dominant non-radiative mechanism in QCLs. This means QCLs require high threshold current densities (∼1 $kAcm^{-2}$) compared to interband lasers. While the increased number of stages does give QCLs increased slope efficiency, the high number of stages increases the voltage required to drive a QCL device. This high voltage and threshold current burden sees QCLs requiring a much greater threshold power, with even lower power devices requiring in excess of 1 W to lase. QCL characteristics such as their high slope efficiency, the favourable regrowth characteristics of InP and their naturally high characteristic temperature created by the absence of Auger recombination does allow for the realisation of higher powered devices. Room temperature CW emission as high as 5 W is possible, with pulsed broad area devices achieving over a hundred watts of peak power[9]. At these high powers it possible to achieve wall plug efficiencies of around 27%[10]. This high powered operation makes the QCL well suited for applications beyond spectroscopy which require high power levels such as infrared countermeasures and free space communications.

The real advantage of QCLs is the wavelength coverage that they provide, with high performance MIR devices demonstrated from 3 to 15 μm. This means they

cover the entire molecular fingerprint region with room temperature CW performance across most of this range. QCLs have been demonstrated emitting at much longer wavelengths (up to approx. 400 μm),where they are a prominent source of terahertz radiation.

Fig. 1.2 shows the emission wavelength bands that can be covered by the most common coherent mid-infrared sources. While DFG/OPO based systems can be engineered to emit over a broad band they are more complex systems. The light grey shading represents room temperature emission while the darker grey represents wavelengths that require cryogenic cooling. The room temperature emission of QCLs spans both of the atmospheric transparency windows making them well suited for mid-infrared spectroscopy.

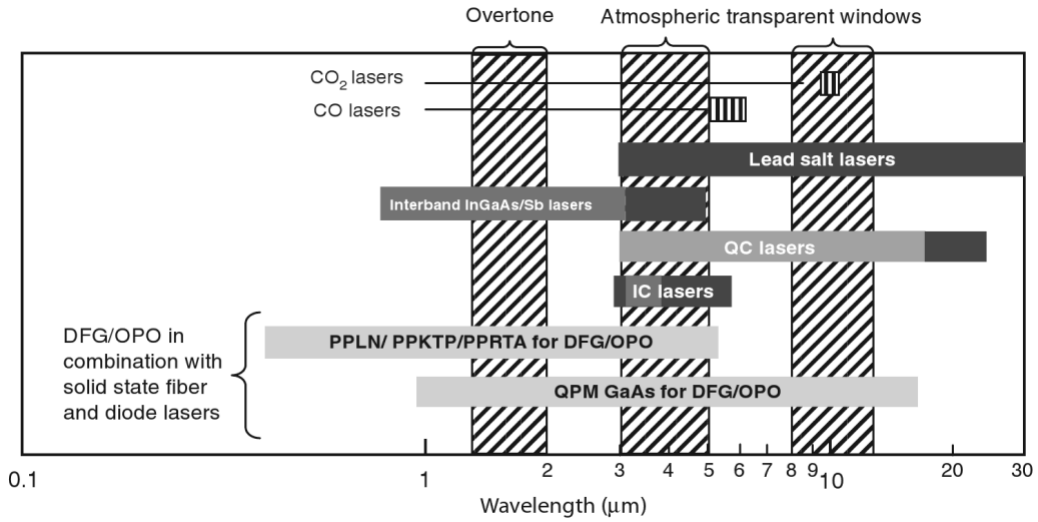

Figure 1.2: Wavelength coverage provided by various coherent mid-infrared sources[3].

1.2 Quantum Cascade Lasers (QCLs)

1.2.1 Introduction

The first work on Quantum Cascade Lasers (QCLs) began in 1971 when Kazarinov and Suris suggested the possibility of amplifying electromagnetic waves in a semiconductor super-lattice[11]. This followed on from Esaki and Tsu's work on the electronic properties of mono-crystalline super-lattices[12] the previous year. Here the composition of semiconductor materials is varied spatially in one dimension and repeated over many periods. One useful example of this is when two materials of differing bandgaps are abruptly alternated over a short period forming quantum wells. The higher bandgap materials form barriers while the lower ones become potential wells. Carriers experience confinement and have their energies modified by discretized well states. If the barrier thickness is sufficiently thin then tunnelling can readily occur between well states and they become coupled. A unipolar lasing scheme is markedly different from other semiconductor lasers, such as quantum well (QW) lasers which are exclusively bipolar, or band to band. In bipolar lasers photons are emitted when electrons in the conduction band recombine with holes in the valence band. In contrast QCLs emit photons when transitions between sub-bands of the conduction band occur. These processes are known as intersubband (ISB) transitions. Unlike interband lasers which have transition energies comprised of both confinement energy and the material bandgap, ISB transition energies don't depend on the material bandgap and are usually much lower. The ability to tailor structures for particular transition energies make QCLs attractive at wavelengths that are otherwise difficult to access. It also allows QCLs to be designed at wavelengths that precisely match the specific absorption features of a given analyte, allowing their deployment in a number of future sensors and spectroscopic platforms.

QCLs remained purely theoretical until 1994 when a device was realised by a group at Bell Laboratories[13] The device consisted of 25 active regions coupled by digitally graded injector regions. This structure was grown using molecular beam epitaxy (MBE) on the $Al_{0.48}In_{0.52}As$ / $Ga_{0.47}In_{0.53}As$ / InP material system and emitted at 4.2 μm in pulsed operation at cryogenic temperatures.

1.2.2 Intersubband (ISB) Transitions

Central to QCL operation, and the main distinction between it and other semiconductor lasers, is the fundamentally different mechanism of generating an inverted electronic population. Most solid state lasers emit light when an electron from the conduction band radiatively recombines with a hole from the valence band. This bipolar scheme is common to most classes of semiconductor lasers.

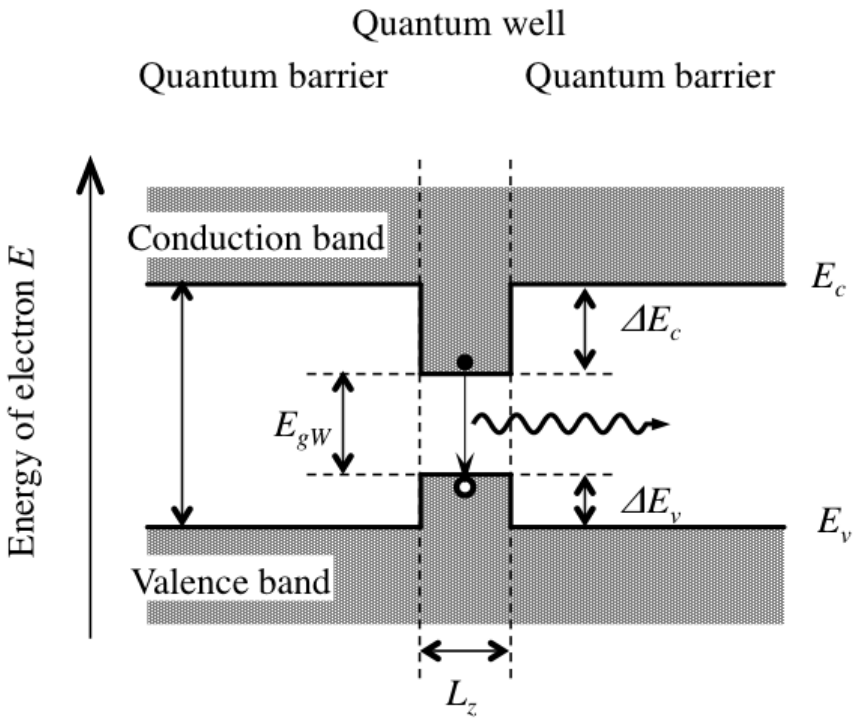

Figure 1.3: Band diagram of a single quantum well (QW) formed by sandwiching a lower bandgap semiconductor between two higher bandgap regions. Carriers of both types become trapped in the QW, allowing radiative recombination to occur in a spatially confined region of the device. In the case of a single quantum well Laser (SQWL) this sandwiching also has the benefit of providing optical confinement to the laser mode. This same scheme is used in many different types of heterojunction laser. LDS, (2017), Quantum Well Laser [ONLINE]. Available at: http://ldselection.com/tutorial/tag/emission/ [Accessed 6 November 2017].

Photons generated in this way will have an energy of:

$$E_{ph} = E_g + \Delta E_c + \Delta E_v \tag{1.1}$$

Where E_g is the band gap and ΔE_c and ΔE_v are, respectively, the conduction and valence band confinement energies. The E_g term dominates in this expression

meaning that potential lasing wavelengths are more a function of the chosen material system than epitaxial design. As higher gain and longer wavelengths are sought interband devices become less favourable. The lower energy transitions required to produce longer wavelengths utilize a decreasing fraction of the bias potential. This is exacerbated in multi-quantum well (MQW) devices which become very inefficient at long wavelengths. Additionally the Auger non-radiative recombination increases in interband devices as the wavelength is increased. While, as previously mentioned, ICLs mitigate these effects to some extent, a different scheme is needed to produce high powered devices at increasingly long wavelengths in the mid-infrared.

Unlike all band to band lasers, QCLs lase between confined electronic states. Fig.1.4 illustrates these types of transitions. Fig.1.4b. shows the in-plane dispersion of the two confined states which for ISB transitions share a similar parabolicity. This profoundly affects the gain profile of a QCL by ensuring that lasing transitions including small momentum transfers occur at similar energies. This leads to a delta-like gain profile in QCLs which is transparent on both sides of the transition energy. Interband transitions, on the other hand, are opaque on the high energy side where there is sufficient photon energy to create electron-hole pairs in the gain medium.

ISB transitions predominantly relax through non-radiative longitudinal optical (LO) phonon scattering which leads to very short state lifetimes ($\sim$ 1 ps) which is characteristic of QCLs in general.

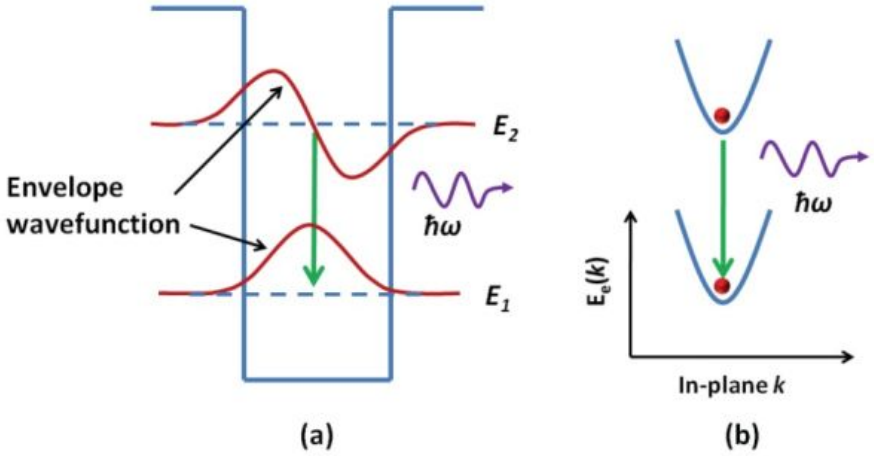

Figure 1.4: a)ISB transition in a type I aligned quantum well. b) In-plane dispersion between two confined electronic states within a quantum well.[14]

1.2.3 Resonant Tunnelling

One benefit to lasing between purely electronic states is the ability to *recycle* electrons. Unlike interband lasers which can only emit one phtoton for each injected electron-hole pair, QCLs can emit many for each electron that transits through the super lattice. This difference produces the high levels of differential gain typical to QCLs.

For electrons to be able to undergo this repeated radiative transition there must be some method of efficiently populating the upper laser level (ULL) and depopulating the lower laser level (LLL). This is achieved using resonant tunneling which is illustrated in fig.1.5. Applying an external bias to a superlattice structure has the effect of modfying the potential throughout the structure. Efficient tunneling occurs through the barriers when the energy of confined states in adjacent QWs is matched. This is the resonance condition which in QCLs allows tunneling both into the ULL and out of the LLL. Although real QCLs are more complex than a simple superlattice structure clearly these devices must be engineered in a way that means all the desired tunnelling transitions are resonant at the same external potential.

In real world QCL structures barriers of only a few monolayers thickness might be employed. In this limit electronic wavefunctions are no longer localized to a single QW but can spread across many. In finite Super-Lattices (SLs) these states form *minibands* which are seperated by *minigaps*.

1.2.4 Active Region

Practical active region designs are more complex than a simple SL structure. In addition to the active region which may be comprised of a small number of well-barrier pairs, injector regions sperate these active regions. One active region plus an injector can be considered the unit cell of the system which can be repeated a number of times ($\sim$10 - 100) to form a practical device. The design of the active region dictates the electronic wavefunctions of the states associated with lasing. In Faist's first demonstration (Fig.1.6), a three well active region gave rise to three localised states, one in each well. The laser transition occurs *diagonally* between the first and second well. The delocalized nature of this transition helps ensure a high non-radiative lifetime at the expense of the associated dipole matrix element.

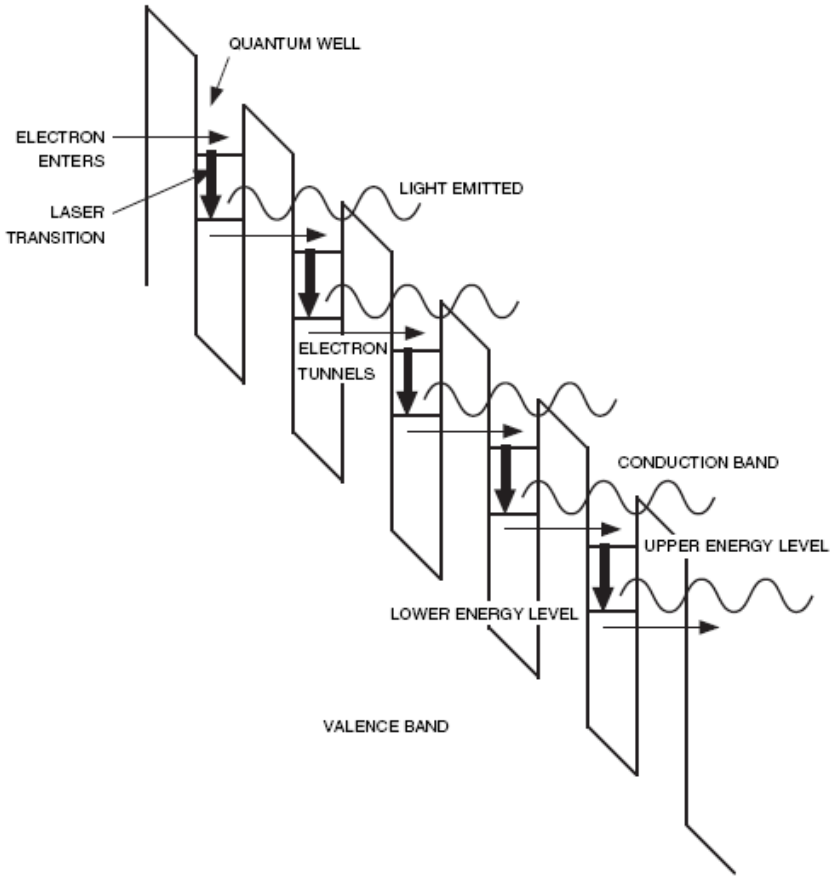

Figure 1.5: Simplified schematic showing carrier transport through the QCL structure. An external bias shifts the band allowing electrons to undergo repeated laser transitions by tunnelling through barriers to an excited state in the next stage.[15]

The injector region in Faist's design was achieved by creating a region of alternating well and barrier layers but with a ramped layer width ratio. This alloy graded region raises electron energies relative to the band edge and allows effiecient tunnelling into the next active region.

Since then other active region designs have utilized a *vertical* transition, that is where both laser states are localized within the same well. The first CW-QCL was demonstrated in 2002 and utilized a new 4-QW bound to continuum design where the LLLs were made up of a large number of closely spaced states forming a continuum. Here the active region operated in a similar fashion as previous designs but now the injector region is designed differently. These digitally graded SLs are designed so that injector states are coupled between wells. Pauli exclusion now applies which forces the formation of a miniband. This band has significant bandwidth and

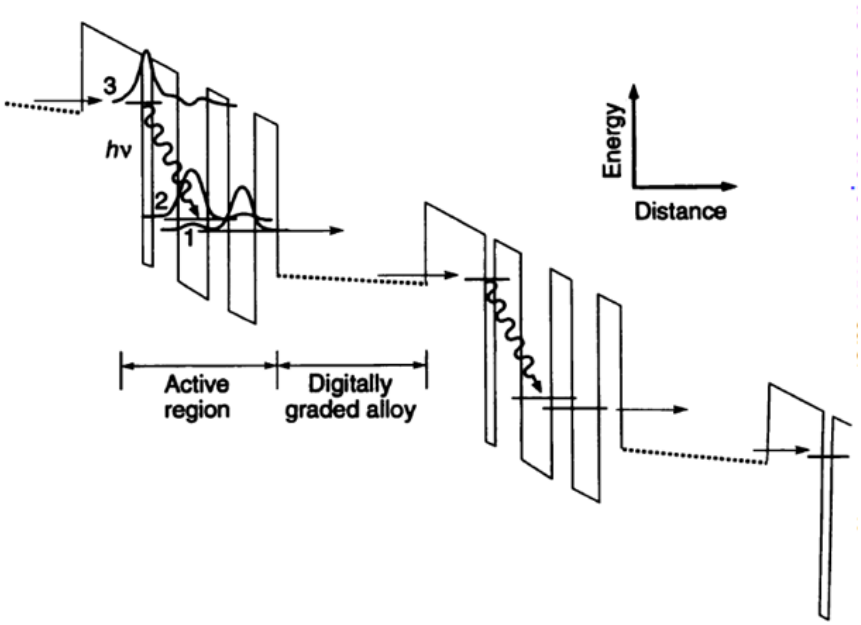

Figure 1.6: Band diagram of the first demonstrated QCL. This structure 3 well design lased in pulsed mode at 4.2 μm. It could produce 10 mW of peak power when cooled to 10K cryogenically. [13]

allows for both the efficient extraction of electrons from all the LLLs and injection into the ULL. This tailoring of electron wavefunctions is known as *band structure engineering* and gives designers the ability to create continously variable wavefunctions by simply altering well\barrier thicknesses. Designing QCL cores then becomes an optimization task which invariably relies on computational methods.

1.2.5 Waveguiding

For a laser device to function, in addition to the optical gain created by the inverted population, there has to be some means of providing optical feedback. That is some means of confining the field in the vicinity of the gain medium. This is achieved using some form of optical waveguide. These can vary but dielectric slab or *rib waveguides* are the most basic practical form employed in semiconductor lasers. While these structures are easily fabricated using standard techniques, the waveguide is formed from cladding material which must have low optical losses at the lasing wavelength to be effective. Waveguide losses reduce the net device gain so must be minimized to achieve high performance. Cleaving the device produces a pair of highly uniform and parallel facets on the cladding material which together form an optical resonator.

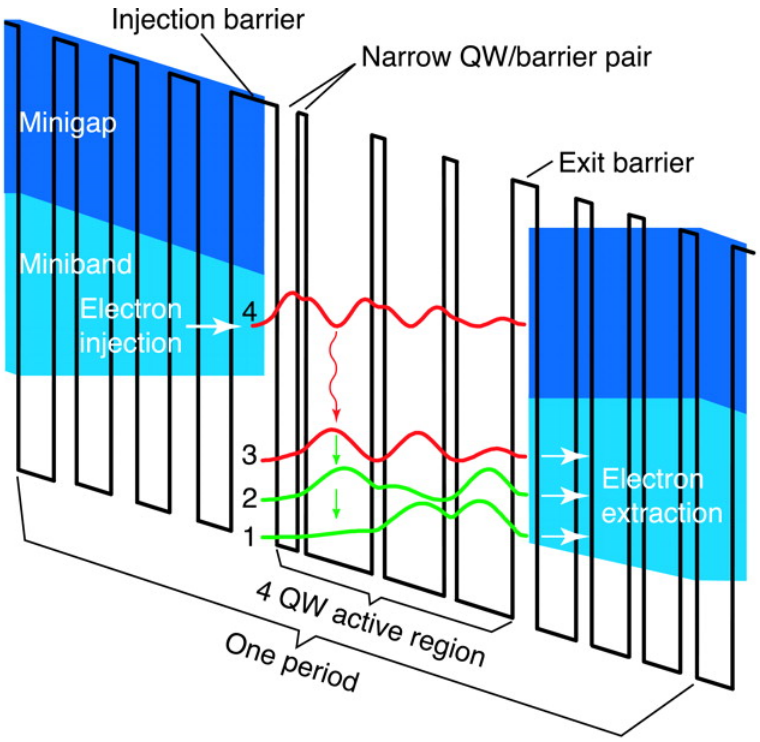

Figure 1.7: Band diagram of the first continuous-wave QCL device. Beck's 2002 design relied on a 4-QW double phonon resonant active region. Output powers in the mW range were produced up to 312K using this design processed into a buried structure device[16].

These partly reflective internal surfaces allow some part of the field to be internally reflected while allowing some part to transmit. This transmitted component acts as the laser's output.

At a basic level, waveguides exploit *total internal reflection* (TIR) to confine light within its structure. In dielectric waveguiding this is usually achieved by sandwiching a relatively high refractive index material between two lower index materials. To understand this mechanism, following here[3], we consider the two-dimensional case. Starting from Maxwells source-free equations in a dielectric medium;

$$\nabla \times \mathbf{H} = i\omega\epsilon_0 n_i^2 \mathbf{E} \tag{1.2a}$$

$$\nabla \times \mathbf{E} = -i\omega\mu_0 \mathbf{H} \tag{1.2b}$$

Where $\mathbf{E}$ and $\mathbf{H}$ are the electric and magnetic fields, ϵ_0, n_i and μ_0 are the vacuum permitivity, refractive indices and the vacuum permeability respectively. Due to the

constant index within each region it's possible to eliminate one of the fields to yield the Helmholtz wave equation

$$\left(\nabla^2 + \frac{n_i^2\omega^2}{c^2}\right)(\mathbf{H}, \mathbf{E}) = 0 \tag{1.3a}$$

The solutions are plane waves which propagate in the x-z plane

$$\mathbf{E} = \mathbf{E}_m e^{-ik_z z} e^{i(\omega t - \beta_m y)} \tag{1.4a}$$

$$\mathbf{H} = \mathbf{H}_m e^{-ik_z z} e^{i(\omega t - \beta_m y)} \tag{1.4b}$$

Where m is the mode index, k_z is the z component of the wave vector and β_m is the propogation constant on the mth mode. Substituting these solutions into 1.3a yields the propagation constant

$$\beta^2 + k_z^2 = \frac{\omega^2 n_i^2}{c^2} \tag{1.5}$$

We anticipate that the guided mode will propagate in the guiding layer but will vanish in the cladding layers. To this end we look for values β which make k_z real in the guided layer but imaginary in the cladding layers, i.e that exponentially decay in the cladding layers.

In general waveguides are able to support two polarizations, transverse electric (TE) and transverse magnetic (TM). These are defined by the field which has some component in the propagating direction. Importantly, the boundary conditions which apply at the interfaces are different for the two polarization states. In the case of intersubband transitions in QCLs, only components of the electric field parallel to the growth direction produce non-zero elements in the optical dipole matrix. This is due to z-dependent electron wavefunctions in the one band model. This phenomenon is well confirmed by experiment and means that only TM light is resonant with the QCL gain medium. For simplicity's sake, we will proceed for the case of TM light in a symmetric waveguide, that being one where both cladding regions have the same refractive index. A general solution exists under these circumstances, and can be written as

$$H_m(z) = \begin{cases} Asin(hz) + Bcos(hz) & -\frac{1}{2}d < z < \frac{1}{2}d, \\ Ce^{-qz} & z > \frac{1}{2}d, \\ De^{qz} & z < -\frac{1}{2}d. \end{cases} \tag{1.6}$$

From 1.11, $h = \sqrt{(\frac{n_2\omega}{c})^2 - \beta^2}$ and $q = \sqrt{\beta^2 - (\frac{n_2\omega}{c})^2}$. For TM polarized light the boundary conditions call for the continuity of $n_i^2\mathbf{E_z}$ and $\frac{\partial \mathbf{E_z}}{\partial z}$. Applying these condition leads to a set of equations:

$$Asin(h\frac{d}{2}) + Bcos(h\frac{d}{2}) = Ce^{-q\frac{d}{2}} \tag{1.7a}$$

$$-Asin(h\frac{d}{2}) + Bcos(h\frac{d}{2}) = De^{q\frac{d}{2}} \tag{1.7b}$$

$$Ahcos(h\frac{d}{2}) + Bhsin(h\frac{d}{2}) = -\bar{q}Ce^{-q\frac{d}{2}} \tag{1.7c}$$

$$-Ahcos(h\frac{d}{2}) + Bhsin(h\frac{d}{2}) = \bar{q}De^{q\frac{d}{2}} \tag{1.7d}$$

Where $\bar{q} = qn_1^2/n_2^2$. The coefficients can be eliminated to produce a transcendental equation

$$tan(hd) = \frac{2h\bar{q}}{h^2 - \bar{q}^2} \tag{1.8}$$

with an *effective modal index*

$$n_{eff} = \frac{\beta}{\omega/c} \tag{1.9}$$

The treatment so far has been restricted to the two-dimensional case where the field is confined along the z-axis and propagates along the y-axis. The z-axis is taken to be the growth direction which is likely to have good dimensional tolerances and abrupt interfacial surfaces, making the approximation a good one. In reality, rib waveguides are three-dimensional, having an extent in the x-direction. While other processes exist, QCL devices fabricated in Sheffield would have this dimension defined using photolithography and wet chemical etching which is a less dimensionally precise process that epitaxial growth. Nevertheless, we model the rib waveguide as

a rectangular body. In this situation the x-axis can be treated in a similar way to the z-axis. Now the fields have the form;

$$\mathbf{E} = \mathbf{E}_m e^{-ik_x x} e^{-ik_z z} e^{i(\omega t - \beta_m y)} \tag{1.10a}$$

$$\mathbf{H} = \mathbf{H}_m e^{-ik_x x} e^{-ik_z z} e^{i(\omega t - \beta_m y)} \tag{1.10b}$$

and the propagation constant can be found from

$$\beta^2 + k_z^2 + k_x^2 = \frac{\omega^2 n_i^2}{c^2} \tag{1.11}$$

Clearly, the symmetry between the z- and x-axis means the field dependence along the x-axis will have the same functional form as the z-axis, i.e. sinusoidal functions within the guided layer. The x and z components of the wavevector are quantized and have the form of standing waves. Physically, this quantization can be understood as the k-vectors for which internally reflected light interferes constructively. This is known as the *transverse resonance condition* and is responsible for the formation of the resonator's *spatial modes*.

For normal ridge laser devices the *as-cleaved* facets are partially reflective and form the laser resonator. While the length of the ridge is likely to be orders of magnitude greater than the transverse extent, the component of the wave-vector associated with the y-axis is also quantized. These are known as the *longitudinal modes* and are separated by a half wavelength in a similar fashion to the other axis.

If, on the other hand, anti-reflective (AR) coatings are applied to the facets and the device is aligned into an external cavity the longitudinal modes of the ridge laser will be suppressed. In this situation the longitudinal mode structure is dictated by the external cavity. These are referred to as the *external cavity modes.*

Layers needed to achieve good confinement would lead to poor thermal and electrical performance. One method of increasing performance in these devices is by employing highly doped cladding layers. In these layers free carrier effects can be used to create a low index layers which can be used to increase the optical confinement. These are known as *Plasmon Enhanced Waveguides*.

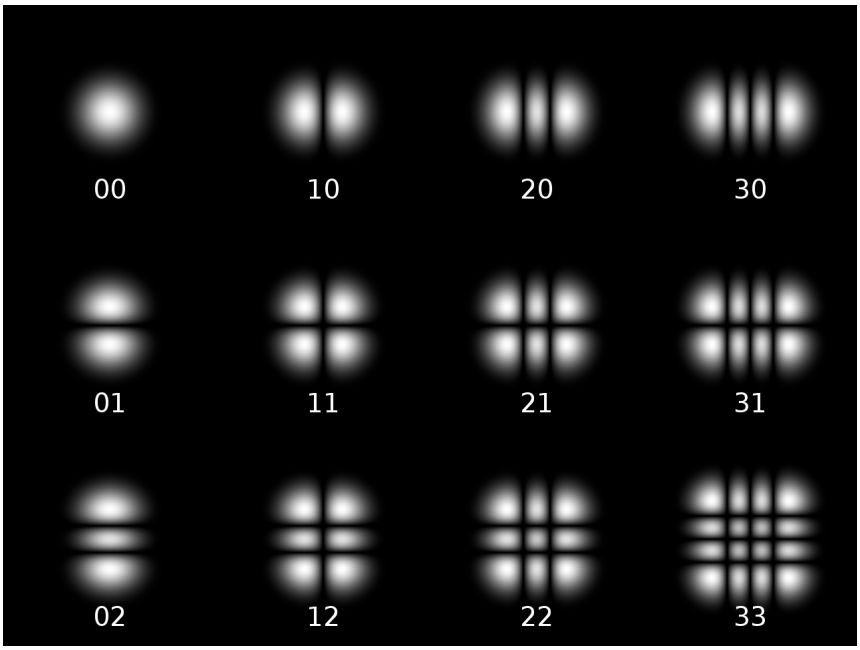

Figure 1.8: Representation of the low order spatial modes of a rectangular resonator. Dr Bob, (2017), Hermite-gaussian [ONLINE]. Available at: `https://en.wikipedia.org/wiki/Transverse_mode/media/File:Hermite-gaussian.png` [Accessed 24 October 2017].

Fig.1.8 shows a number of the lowest order far-field spatial mode profiles of a rectangular resonator, similar to the waveguide of a typical semiconductor laser. Here each spot or *lobe* represents an intensity maximum and, in the case of a collimated beam, these patterns would represent the beam cross-section. As waveguide lateral and vertical dimensions increase it becomes likely that a device will support a growing number of these spatial modes. It's also possible for some devices to lase on a number of these spatial modes simultaneously. Some buried structure QCLs have been shown to have three spatial modes with similar threshold currents[17]. Around these thresholds the beam intensity profile would be the superposition of these spatial modes. These higher order spatial modes will be seen to be of significance later in Chapter 5 where a comparison is made between a single and multi-mode buried structure under resonant modulation.

1.2.6 Maxwell - Bloch Equations

Mathematically modelling the dynamic behaviour of external cavity laser systems can be achieved using a number of approaches. The most basic model that captures

the interaction of a propagating electric field and an inverted population is that of Lang – Kobayashi (LK). These types of models are known as delayed differential equations (DDEs) as an inversion rate equation interacts with a time delayed field equation, the time delay being the time taken for light to traverse the external cavity. With these models being implemented computationally the delay is achieved simply by storing emission amplitudes for a large number of time steps. The returning field equation takes account of coupling efficiency using a simple coefficient and phase by using a complex amplitude based on the cavity length and frequency. This model neglects the spatial distribution of the field entirely, giving only a sample of the slowly varying field component in the time domain. This means that all effects dependent on spatial coordinates are neglected, including the finite length of the gain medium. This limits its use to the case of relatively long cavities. Additionally, the lack of polarization or spatial treatment makes it unsuitable for modelling anything other than the case of a device lasing on a single mode. It does, however, permit steady state analysis to be performed which results in the continuous-wave solutions. In the LK model these are called the external cavity modes (ECMs).

The Travelling-Wave (TW) model provides spatio-temporal treatment to the field distributions both inside a finite length device and also in the external section of the resonator. Through a system of coupled partial differential equations this model describes the evolution of two slowly varying counter propagating fields interacting with an inverted population. Although the spatial-temporal treatment allows for modelling distributed feedback (DFB) lasers, with a spatially varying index, this model still treats the inverted population as an average across the device, or at least a section of the device. An average field intensity interacts with an average carrier density. This means that during modelling the device must be discretized into sections sufficiently small as to capture any fast dynamics. Nevertheless, where effects due to spatially inhomogeneous carrier distributions are important, the TW model needs significant modification to allow variations of carrier density within each section. This feature will be shown to be important to this work in the theory section of chapter 3. The TW model also takes no account of material polarization which becomes important when the system has the ability to lase on a number of different longitudinal modes, or where emission is dictated by material properties rather

than the geometric properties of the waveguide. Systems like these are dependent on gain dispersion which is manifested through the material polarization. While it is possible to add these effects to the TW model, in the case of external cavity QCLs it's more appropriate, and common, to employ a treatment based on Maxwell – Bloch equations.

The form of Maxwell-Bloch equations used to model optical semiconductor devices depends largely on the significance of quantum noise fluctuations in the system. Spontaneous emission and amplified spontaneous emission are both manifestations of quantum noise. This makes their treatment vital in devices where the output is dominated by electroluminescence (EL) and super electroluminescence (SEL) such as superluminescent diodes and ultra low threshold semiconductor lasers. It can also be significant in gain guided and broad area devices where similar processes can have a deterministic effect on the spatial coherence of the output. Even in normal semiconductor laser devices the quantum noise within the dipole and light fields becomes significant around threshold, or in situations where different laser modes compete. In these situations, where EL and SEL are a significant component of the field, a model based on Quantum Maxwell-Bloch equations (QMBEs) is needed. In chapters 5 and 6 a broad emission regime is observed while resonantly pumping an external ring and linear external cavity QCL. It's suggested this is the result of EL and SEL processes. Producing a model for this resonantly pumped external cavity QCLs based on QMBE would be a significant undertaking, unnecessary to further the main aim of this work.

Here, like in the majority of theoretical work for QCLs and semiconductor laser devices in general, we employ a model based on the semi classical Maxwell-Bloch equations. Here the evolution of the dipole moment and inversion are described by the Bloch equations which are essentially that of a two level atom or system. These quantities are usually dealt with statistically by casting them into a density matrix form. This two state system is allowed to interact with a classical electromagnetic field. In the limit where the optical modes are at a high intensity, the quantized nature of the light field can be neglected and this classical description of the lasing mode is justifiable.

To find the field equation we begin with Maxwell's equation for the curl of the

electric and magnetic fields and the associated material equations

$$\nabla \times \mathbf{H} = \mathbf{j} + \partial_t \mathbf{D} \tag{1.12a}$$

$$\nabla \times \mathbf{E} = -\partial_t \mathbf{B} \tag{1.12b}$$

$$\mathbf{D} = \epsilon_0 \mathbf{E} + \mathbf{P} \tag{1.12c}$$

$$\mathbf{B} = \mu_0 \mathbf{H} + \mathbf{M} \tag{1.12d}$$

Where $\mathbf{E}$ is the electric field, $\mathbf{B}$ is the magnetic flux, $\mathbf{D}$ is the dielectric flux, $\mathbf{P}$ is the polarization, $\mathbf{H}$ is the magnetic field, $\mathbf{j}$ is the current density of free carriers and $\mathbf{M}$ is the magnetization. Taking the curl of eqn.1.12b, using the vector field identity $\nabla \times (\nabla \times \mathbf{A}) = \nabla(\nabla \mathbf{A}) - \Delta \mathbf{E}$ and substituting in eqns.1.12c & 1.12d leads to

$$\Delta \mathbf{E} - \mu_0 \partial_t (\mathbf{j} + \epsilon_0 \partial_t \mathbf{E} + \partial_t \mathbf{P}) = \partial_t \nabla \times \mathbf{M} + \nabla(\nabla \cdot \mathbf{E}) \tag{1.13}$$

In the dielectric, non magnetic material of a semiconductor laser there will be no free charges or currents due to free charges. This means that eqn.1.13 greatly simplifies to

$$\Big(\Delta - \frac{1}{c_0^2} \frac{\partial^2}{\partial t^2}\Big) \mathbf{E} = \mu_0 \frac{\partial^2}{\partial t^2} \mathbf{P} \tag{1.14}$$

This is a wave equation driven by the material polarization and is the first of the three Maxwell-Bloch equations. A further approximation is typically applied which will be seen later.

The remaining two equations are known as the Bloch equations. These are based on a two-level system with the state space spanned by energy eigenstates $|e\rangle$ and $|g\rangle$. The Hamiltonian of this system is given by

$$H_A = E_e|e\rangle\langle e| + E_g|g\rangle\langle g| \tag{1.15}$$

A possible choice of operator base is

$$\mathbf{1} = |e\rangle\langle e| + |g\rangle\langle g| \tag{1.16a}$$

$$\boldsymbol{\sigma_z} = |e\rangle\langle e| - |g\rangle\langle g| \tag{1.16b}$$

$$\boldsymbol{\sigma}^+ = |e\rangle\langle g| \tag{1.16c}$$

$$\boldsymbol{\sigma}^- = |g\rangle\langle e| \tag{1.16d}$$

States can be expressed as $\mathbb{C}^2$ vectors according to the rule

$$|\Psi\rangle = c_e|e\rangle + c_g|g\rangle \rightarrow \begin{pmatrix} c_e \\ c_g \end{pmatrix} \tag{1.17}$$

The operators can then be expressed in matrix format as

$$\mathbf{1} = \begin{pmatrix} 1 & 0 \\ 0 & 1 \end{pmatrix} \tag{1.18a}$$

$$\boldsymbol{\sigma_z} = \begin{pmatrix} 1 & 0 \\ 0 & -1 \end{pmatrix} \tag{1.18b}$$

$$\boldsymbol{\sigma}^+ = \begin{pmatrix} 0 & 1 \\ 0 & 0 \end{pmatrix} \tag{1.18c}$$

$$\boldsymbol{\sigma}^- = \begin{pmatrix} 0 & 0 \\ 1 & 0 \end{pmatrix} \tag{1.18d}$$

Acting on an arbitrary state $|\Psi\rangle = c_e|e\rangle + c_g|g\rangle$ shows that $\boldsymbol{\sigma}^+$ and $\boldsymbol{\sigma}^-$ have the effect of generating transitions from ground to excited and excited to ground states respectively. $\boldsymbol{\sigma}_z$ is a Hermitian operator and its expectation value

$$\langle\Psi|\boldsymbol{\sigma}_z|\Psi\rangle = |c_e|^2 - |c_g|^2 = w \tag{1.19}$$

which is the inversion of the system, where $|c_e|^2$ and $|c_g|^2$ represent the probabilities of finding the system in states $|e\rangle$ and $|g\rangle$ respectively.

Manipulating eqn.1.15 leads to a Hamiltonian of the form

$$H_A = \frac{1}{2}\hbar\omega_{eg}\boldsymbol{\sigma}_z \tag{1.20}$$

where $\omega_{eg} = \frac{1}{\hbar}(E_e - E_g)$. Now for eqns.1.16b -1.16d there are commutator

relations

$$[\boldsymbol{\sigma}^+, \boldsymbol{\sigma}^-] = \boldsymbol{\sigma}_z \tag{1.21a}$$

$$[\boldsymbol{\sigma}^+, \boldsymbol{\sigma}_z] = -2\boldsymbol{\sigma}^+ \tag{1.21b}$$

$$[\boldsymbol{\sigma}^-, \boldsymbol{\sigma}_z] = 2\boldsymbol{\sigma}^- \tag{1.21c}$$

To take account of the atomic systems interaction with the external field we introduce the dipole moment operator

$$\vec{\mathbf{p}} = -e_0\vec{\mathbf{x}} \tag{1.22}$$

The expectation value of the dipole moment of a state in the form of the left hand side of eqn.1.17 is

$$\langle\Psi|\vec{\mathbf{p}}|\Psi\rangle = -e_0\Big(|c_e|^2\langle e|\vec{\mathbf{x}}|e\rangle + c_e c_g^*\langle g|\vec{\mathbf{x}}|e\rangle + c_g c_e^*\langle e|\vec{\mathbf{x}}|g\rangle + |c_g|^2\langle g|\vec{\mathbf{x}}|g\rangle\Big) \tag{1.23}$$

In energy eigenstates the atomic system possess inversion symmetry meaning it has no permanent dipole moment, i.e. $\langle e|\vec{\mathbf{x}}|e\rangle = \langle g|\vec{\mathbf{x}}|g\rangle = 0$. This simplifies eqn.1.25 to

$$\langle\Psi|\vec{\mathbf{p}}|\Psi\rangle = -e_0\Big(c_e c_g^*\langle g|\vec{\mathbf{x}}|e\rangle + c_g c_e^*\langle e|\vec{\mathbf{x}}|g\rangle\Big) \tag{1.24}$$

With the dipole matrix elements $\vec{M} = e_0\langle g|\vec{\mathbf{x}}|e\rangle$ eqn.1.24 can be written

$$\langle\Psi|\vec{\mathbf{p}}|\Psi\rangle = -\Big(c_e c_g^*\vec{M} + c_g c_e^*\vec{M}\Big) = -\langle\Psi|\Big(\boldsymbol{\sigma}^+\vec{M}^* + \boldsymbol{\sigma}^-\vec{M}\Big)|\Psi\rangle \tag{1.25}$$

The energy of an electric dipole in an electric field is given by

$$H_{A-F} = -\vec{\boldsymbol{p}} \cdot \vec{E}(\vec{x}_A, t) \tag{1.26}$$

The electric field can be written as

$$\vec{E}(\vec{x}_A, t) = \frac{1}{2}\Big(\vec{E}(t)^{(+)} + \vec{E}(t)^{(-)}\Big) = \frac{1}{2}\Big(\hat{\vec{E}}(t)^{(+)} e^{j\omega t} + \hat{\vec{E}}(t)^{(-)} e^{-j\omega t}\Big) \tag{1.27}$$

Here the hat of $\hat{\vec{E}}(t)^{(+)}$ and $\hat{\vec{E}}(t)^{(-)}$ represents only the slowly varying electric field envelope. In the Rotating-Wave Approximation (RWA) only these slowly varying parts are included in the interaction Hamiltonian.

$$H_{A-F} \approx H_{A-F}^{RWA} = \frac{1}{2}\vec{M}^* \vec{E}(t)^{(-)} \boldsymbol{\sigma}^+ + h.c.. \tag{1.28}$$

Then the Schrödinger Equation for a two level system in a classical field is given by

$$j\hbar \frac{d}{dt}|\Psi\rangle = (H_A + H_{A-F})|\Psi\rangle \approx (H_A + H_{A-F}^{RWA})|\Psi\rangle \tag{1.29}$$

Later we will wish to add dissipative processes to the model which makes it useful to change from a deterministic wave function approach to a statistical one. To this end we introduce the density operator which for a pure state is defined as

$$\boldsymbol{\rho} = |\Psi\rangle\langle\Psi| \tag{1.30}$$

or in matrix form

$$\boldsymbol{\rho} = \begin{pmatrix} \rho_{ee} & \rho_{eg} \\ \rho_{ge} & \rho_{gg} \end{pmatrix} \tag{1.31}$$

which for a pure state is

$$\boldsymbol{\rho} = \begin{pmatrix} c_e c_e^* & c_e c_g^* \\ c_g c_e^* & c_g c_g^* \end{pmatrix} \tag{1.32}$$

In this representation each element has some physical significance. The main diagonal elements are the population probabilities of the two levels. The off-diagonals are the expectation values of the positive and negative components of the dipole moment of the system, i.e. its contribution to the polarization of the medium.

From eqn.1.29 we can derive the von Neumann equation, which is the equation of motion of the density operator.

$$\dot{\boldsymbol{\rho}} = \frac{d}{dt}|\Psi\rangle\langle\Psi| + h.c. = \frac{1}{j\hbar}H|\Psi\rangle\langle\Psi| - \frac{1}{j\hbar}|\Psi\rangle\langle\Psi|H = \frac{1}{j\hbar}[H, \boldsymbol{\rho}] \tag{1.33}$$

which in the case of a two-level system can be written

$$\dot{\boldsymbol{\rho}} = \frac{1}{j\hbar}[H, \boldsymbol{\rho}] = -\frac{1}{2}j\omega_{eg}[\boldsymbol{\sigma}_z, \boldsymbol{\rho}] \tag{1.34}$$

Using eqn.1.34 with commutator eqns.1.21a - 1.21c we find that dynamics of an isolated two-level system to be

$$\dot{\rho}_{ee} = 0 \tag{1.35a}$$

$$\dot{\rho}_{gg} = 0 \tag{1.35b}$$

$$\dot{\rho}_{eg} = -j\omega_{eg}\rho_{eg} \tag{1.35c}$$

$$\dot{\rho}_{ge} = j\omega_{eg}\rho_{ge} \tag{1.35d}$$

This is unlike a radiating systems which must have a Hamiltonian of the form

$$H = H_A + H_F + H_{A-F} \tag{1.36}$$

H_F is the Hamiltonian of the free field. The free field is responsible for spontaneous emission and absorption and leads to a change in the populations according to

$$\frac{d}{dt}\rho_{ee} = -\Gamma_e\rho_{ee} + \Gamma_a\rho_{gg} \tag{1.37}$$

where

$$\Gamma_e = \frac{1}{\tau_{sp}}(n_{th}+1) \tag{1.38a}$$

$$\Gamma_a = \frac{1}{\tau_{sp}}n_{th} \tag{1.38b}$$

$n_{th} = 1/(e^{\frac{\hbar\omega_{eg}}{kT}}-1)$ is the number of thermally excited photons of frequency ω_{eg} at temperature T. Because we know that the total probability of being in the ground or excited state remains the same we can also say

$$\frac{d}{dt}\rho_{gg} = -\frac{d}{dt}\rho_{ee} = \Gamma_e\rho_{ee} - \Gamma_a\rho_{gg} \tag{1.39}$$

The polarization decays with the populations making both absorption and emission process destructive to the polarization according to

$$\frac{d}{dt}\rho_{ge} = j\omega_{eg}\rho_{eg} - \frac{\Gamma_e+\Gamma_a}{2}\rho_{ge} \tag{1.40}$$

Taking account of the coherent (eqns.1.35a - 1.35d) and incoherent processes (eqns.1.39 - 1.40) allows the dynamics of the normalized average dipole moment d

and inversion w to be written

$$\dot{d} = \dot{\rho}_{ge} = (j\omega_{eg} - \frac{1}{T_2})d \tag{1.41a}$$

$$\dot{w} = \dot{\rho}_{ee} - \dot{\rho}_{gg} = -\frac{w - w_0}{T_1} \tag{1.41b}$$

Where T_1 and T_2 are the energy and phase relaxation time respectively, and are related to the incoherent processes such that

$$\frac{1}{T_1} = \frac{2}{T_2} = \Gamma_e + \Gamma_a = \frac{2n_{th} + 1}{\tau_{sp}} \tag{1.42}$$

and the equilibrium inversion w_0, the inversion due to thermal excitation is given by

$$w_0 = \frac{\Gamma_a - \Gamma_e}{\Gamma_a + \Gamma_e} = \frac{-1}{2n_{th} + 1} = -\tanh\left(\frac{\hbar\omega_{eg}}{2kT}\right) \tag{1.43}$$

To complete these equations for the average dipole moment and inversion we must add terms which take account of the external field. Taking H_{A-F} (eqn. 1.28)into account leads to additional terms in the von Neumann equation

$$\dot{\boldsymbol{\rho}}|_E = \frac{1}{j\hbar}[H_E, \boldsymbol{\rho}] = \frac{1}{2j\hbar}\vec{M}^*\vec{E}(t)^{(-)}[\boldsymbol{\sigma}^+, \boldsymbol{\rho}] + h.c. \tag{1.44}$$

or

$$\dot{\rho}_{ee}|_E = \frac{1}{2j\hbar}\vec{M}^*\vec{E}(t)^{(-)}\rho_{ge} + c.c. \tag{1.45a}$$

$$\dot{\rho}_{ge}|_E = \frac{1}{2j\hbar}\vec{M}\vec{E}(t)^{(+)}(\rho_{ee} - \rho_{gg}) \tag{1.45b}$$

$$\dot{\rho}_{gg}|_E = -\frac{1}{2j\hbar}\vec{M}^*\vec{E}(t)^{(-)}\rho_{ge} + c.c. \tag{1.45c}$$

This is the evolution of the dipole moment and inversion due to an external field. Adding this to the atomic and heat-bath terms yields

$$\dot{d} = -(\frac{1}{T_2} - j\omega_{eg})d - \frac{1}{2j\hbar})\vec{M}\vec{E}^{(+)} \tag{1.46a}$$

$$\dot{w} = -\frac{w - w_0}{T_1} + \frac{1}{j\hbar}(\vec{M}^*\vec{E}^{(-)}d - \vec{M}\vec{E}^{(+)}d^*) \tag{1.46b}$$

These are known as the Bloch equations. Along with eqn.1.14 these make up the Maxwell-Bloch equations. To arrive at their most standard form we substitute in to eqns.1.14,1.46a-1.46b the following set of ansatzs:

$$\begin{aligned} E(z,t) = &\frac{1}{2}[E_+^*(z,t)e^{-(i\omega t - kz)} + E_+(z,t)e^{-i(\omega t - kz)}] \\ &+ \frac{1}{2}[E_-^*(z,t)e^{-(i\omega t + kz)} + E_-(z,t)e^{-i(\omega t + kz)}] \end{aligned} \tag{1.47a}$$

$$d(z,t) = P_+(z,t)e^{i(\omega t - kz)} + P_-(z,t)e^{i(\omega t + kz)} \tag{1.47b}$$

$$w(z,t) = D_0(z,t) \tag{1.47c}$$

Where +(-) subscript represents waves travelling in the positive (negative) z direction. The slowly varying envelope approximation (SVEA) is applied which

assumes the wave envelope varies slowly compared to the wavelength or period, removing the second order differentials from the wave equation, producing

$$\frac{n}{c}\partial_t E_\pm = \partial_z E_\pm - i\frac{kN\vec{M}\Gamma}{2\epsilon_0 n^2}P_\pm - \frac{1}{2}l(E_+, E_-)E_\pm \tag{1.48a}$$

$$\partial_t P_\pm = \frac{i\vec{M}}{2\hbar}\boldsymbol{DE} - \frac{P_\pm}{T_2} \tag{1.48b}$$

$$\partial_t \boldsymbol{D} = \frac{D_p - \boldsymbol{D}}{T_1} + \frac{i\vec{M}}{\hbar}(E_+^* P_+ + E_-^* P_- - c.c.) \tag{1.48c}$$

N represents the number density of two-level systems, which is related to the doping density and Γ is the overlap between the optical mode and the gain medium. Dropping all the terms with negative subscripts allows the Maxwell-Bloch equations to be written in the their most compact and general form

$$\frac{n}{c}\partial_t \boldsymbol{E} = -\partial_z \boldsymbol{E} - i\frac{kN\vec{M}\Gamma}{2\epsilon_0 n^2}\boldsymbol{P} - \frac{1}{2}l_0\boldsymbol{E} \tag{1.49a}$$

$$\partial_t \boldsymbol{P} = \frac{i\vec{M}}{2\hbar}\boldsymbol{DE} - \frac{\boldsymbol{P}}{T_2} \tag{1.49b}$$

$$\partial_t \boldsymbol{D} = \frac{D_p - \boldsymbol{D}}{T_1} + \frac{i\vec{M}}{\hbar}(\boldsymbol{E}^*\boldsymbol{P} - c.c.) \tag{1.49c}$$

Where l_0 and D_p is the linear loss and the steady state inversion at $\boldsymbol{E} = 0$. One further substitution allows eqn. 1.49a to be written in a more meaningful way

$$\frac{n}{c}\partial_t \boldsymbol{E} = -\partial_z \boldsymbol{E} - \frac{i\vec{M}}{\hbar l_0 D_{th}}\boldsymbol{P} - \frac{1}{2}l_0\boldsymbol{E} \tag{1.50}$$

where D_{th} is the threshold inversion and is equal to

$$D_{th} = \frac{2\hbar l_0 \epsilon_0 n^2}{kN\mu^2\Gamma T_2} \tag{1.51}$$

These three equations (1.50, 1.49b & 1.49c) are the most standardised form of the Maxwell Bloch equations and are used extensively in QCL modelling. These

equations will form the basis of an analysis on the stability of EC- & ERC-QCL systems under continuous-wave operation later on in chapter 3.

1.3 External Cavity Lasers

1.3.1 General Principles

While QCLs clearly possess the performance characteristic and wavelength coverage needed for MIR gas spectroscopy, a more complex system must be formed to allow emission to be tuned over the device's full gain bandwidth. In a simple sense, it's impossible to act upon light which only exists within the dielectric waveguide of the QCL.

An External Cavity (EC) is one which is partially free-air-coupled. The simplest way to achieve this practically is by the addition of a collimating lens and external mirror. Applying a High-Reflectivity (HR) coating to the back facet and an Anti-Reflective (AR) coating to the front creates a high finesse external cavity while suppressing the FP modes of the ridge cavity. In this arrangement the QCL acts as a *gain medium* rather than a laser. Photons traversing the cavity will experience high levels of loss and gain in the gain medium but little interaction in the free-air region. This gives rise to an increase average photon lifetime which reduces both phase noise and emission linewidths. While these characteristics might be desirable for applications such as high-resolution gas spectroscopy, a system with only an external mirror has little practical value. The main motivation for ECs is the ability to introduce dispersive feedback elements as a means of tuning the emission wavelength. The simplest method of doing this is to replace the external mirror with a diffraction grating. Unlike a metallic mirror which can be expected to have a largely flat reflectivity response across the bandwidth of the QCL, diffraction gratings can be used to diffract only a small spectral component back towards the gain medium. In other words, high/complete losses can be introduced into all but a narrow spectral region. This effectively selects the system's emission wavelength. In the MIR region this is usually done with a blazed ruled diffraction grating. Blazed gratings maximise the efficiency into the first order, reducing the losses into other orders. Efficiencies of around 90% are attainable.

The two most well known examples of this type of tunable external cavity system are the Littrow and Littman Metcalf configurations. Fig.1.9 shows the Littrow configuration schematically. Often, depending on the cavity length, the grating pivot point can be some distance away from the grating. This is usually achieved using a rigid arm on which the grating is mounted. The additional mirror attached to the same arm, labelled 4 in the diagram, prevents output beam walk off as the grating is rotated.

Another option, sometimes called the quasi-Littrow, is to take the output from the opposite side of the laser chip. This ensures a stationary output beam and can be used to realise more compact designs.

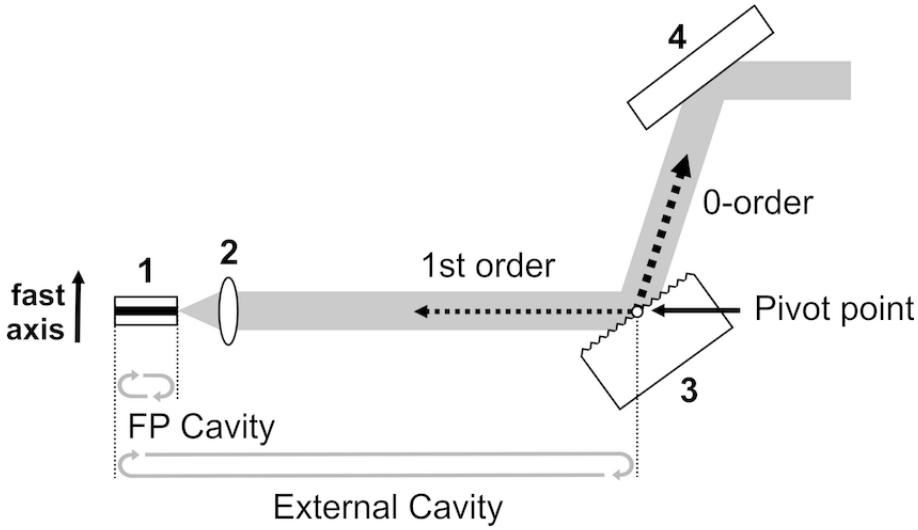

Figure 1.9: Schematic of Littrow configuration[18].

Fig.1.10 is an example of a simple Littrow system, sold by Thorlabs. A laser diode module has its beam collimated by a single lens. A linear actuator drives a spring loaded arm which supports the grating, thus altering the grating angle.

Additionally, the free-air nature of the cavity allows further optical components to be added to the beam path, allowing more complex systems to be constructed. The number of outputs and optical elements in these systems is only limited by the optical losses they introduce.

One further benefit of EC systems is the reduction in the round-trip frequency. Ridge type lasers with cavities only a few mm long typically have round-trip frequencies in the 10 to 20 GHz region. ECs allow this to be reduced to Radio-Frequencies

Figure 1.10: Thorlabs TLK-L780M Littrow tunable laser kit. Thorlabs, (2017), TLK-L780M [ONLINE]. Available at: `https://www.thorlabs.com/navigation.cfm?guide_id=34` [Accessed 9 October 2017].

(RF) which is more readily accessed using current electronics. This is of particular importance in Mode-Locking which will be discussed later in this thesis.

1.3.2 External Ring Cavities

ERCs are similar to ECs in the sense they use collimating lenses and external mirrors to form a cavity but have a fundamentally different geometry. Sometimes called a *Bow-Tie Resonator*, these four mirrored cavities allow light to circulate around a closed path rather than moving back and forth along a linear path. The result of this is the decoupling of the two propagation directions which in the linear EC

would form standing waves in the gain medium. This can in turn lead to an effect called Spatial-Hole-Burning (SHB), discussed in chapter 3, which can destabilize the desired lasing mode. ERCs, in principle, should be able to produce more stable emission by supressing SHB.

1.3.3 Motivation

Prior to this work QCL based high resolution mid-infrared spectroscopy platforms were limited to linear cavity configurations. This work develops the ring cavity configuration as an improved alternative by demonstrating, for the first time, that room temperature wavelength tunable emission can be generated from a ring cavity operating in a favourable unidirectional regime. With further development similar systems could be used to produce gas sensing systems with superior selectivity and lower detection limits. Previously, demonstrations of QCL mode-locking were limited to ridge type devices which required microwave frequency modulation and suffered from SHB. This made their pulses unsuitable for future applications which call for highly stable pulse trains. This work shows that external ring cavities can be used to produce unidirectional mode-locked pulse trains with radio frequency repetition rates.

1.4 Previous Work on EC-QCLs

The ability to generate mid-infrared radiation in the technologically important molecular fingerprint region has led to external cavity quantum cascade lasers (EC-QCLs) receiving a great deal of attention in the literature. External cavities have provided a means of exploiting the naturally broad gain bandwidth of the QCL which is highly desirable in a region of the electromagnetic spectrum which is otherwise difficult to access. This research, having now achieved commercialisation, focused on developing the wavelength tuning performance characteristics needed for various types of mid-infrared spectroscopy.

As mid-infrared QCL devices approached continuous-wave performance at temperatures achievable using thermoelectric cooling the development of tunable EC-QCLs gained pace. In 2005 Wysocki's group[19] demonstrated a EC-QCL system

based on a Littrow type configuration which was capable of coarsely tuning 35 cm^{-1} with a mode-hop-free tuning range of 1.2 cm^{-1} by employing a piezoelectric actuator. This early work included an analytical study based on a coupled cavity model which established the response of the system to changes in grating angle, cavity length and drive current. This coupled cavity approach was needed to correctly model the parasitic FP cavity which was significant at a time when anti-reflection (AR) coatings lacked the durability achieved using today's room-temperature buried structures. Not only did this work outline most of the electronic, mechanical and optical considerations involved in constructing Littrow type tunable EC-QCLs, it used the system to demonstrate the detection of Nitric Oxide (NO).

Similar approaches have been used since which have taken advantage of the steadily increasing performance of CW QCLs. Littrow type systems are in principle capable of tuning over very wide bandwidths, many times that of a typical QCLs gain bandwidth. Maulini's group extended[20] the broad gain bandwidth of bound-to-continuum QCLs by using a core design with two distinct types of stages, in this case centred at 8.4 μm and 9.6 μm, each with 20 repetitions. This early extended wavelength QCL didn't achieve CW performance but could be grating tuned from 8.4 to 10.4 μm (265 cm^{-1}) in pulsed mode at 253K. A later effort by a different group[21] used a similar principle making use of five distinct stages. These where arranged symmetrically with higher energy stages sandwiched between increasingly lower energy ones. This was done to optimize confinement and reduce cross absorption between sections. This system employed a similar Littrow configuration to previous efforts, using a 150 grooves per mm diffraction grating. This system achieved a tuning range of 432 cm^{-1}. Again, due to the immature QCL core design, the system could only achieve such an impressive tuning range when operating in a pulsed mode at low duty cycles (1.5%).

Many examples exist of the successful use of Littrow type EC-QCL as a source for gas detection using schemes such as photo-acoustic spectroscopy[22], Faraday rotation spectroscopy[23] and cavity ring down spectroscopy[24].

EC-QCLs have also seen success beyond the traditional configurations such as Littrow and Littmann Metcalf. A need for faster tuning speeds has led to the development of a number of novel EC-QCL systems. In reference[25] an entirely electronic

scheme to tune the emission of an EC-QCL is developed. This was done by attaching a piezoelectric actuator to an optical crystal. This meant that RF signals could be used to induce acoustic waves in the crystal, creating a phase grating that could be used to diffract the laser beam in a similar fashion to a normal diffraction grating. Using this acousto-optic modulation (AOM) scheme meant that tuning could be achieved rapidly by varying the driving frequency of the piezoelectric actuator. In this case varying the AOM drive frequency between 41 and 49 MHz led to a laser tuning range between 8.5 μm and 9.8 μm. This system did, however, cause instantaneous linewidths of 4.7 cm^{-1}. Other work seeks to miniaturize the EC-QCL configuration using Micro-Opto-Electro-Mechanical (MOEMS) systems. Grahmanns's group[26] achieved Kilohertz scanning frequencies using this miniaturized approach.

The suppression of spatial hole burning (SHB) should in principle give the ERCs an advantage over linear EC-QCLs in tasks requiring stable sources such as gas sensing. Despite this, external ring cavity quantum cascade lasers (ERC-QCLs) have received little attention in this regard. The first significant experimental work on ERC-QCLs was performed by a group at Harvard in 2013[27]. Here the authors study the characteristics of a 1.7 m ERC-QCL by comparing a number of measurements taken to those of the uncoated FP QCL prior to its deployment in the ERC. The main outcome of this study was the demonstration of ERC-QCLs tendency to lase in a directional regime, with one propagating direction becoming dominant during emission. Their results showed the transition from bidirectional to directional regime at some current above threshold. They support this using simulations based on Maxwell-Bloch equations which take account of some small facet reflectivity from imperfect facet AR coatings as well as some small loss imbalance in the two propagating directions. Their simulations suggest that a bidirectional regime exists for some range of current above threshold which eventually gives way to a directional regime. While in the higher current directional regime they observed a switching behaviour with the dominant propagation direction suddenly changing at certain driving currents. While this behaviour isn't accounted for by their model, they suggested it may relate to a current dependent loss term which wasn't included in their study.

They go on to focus on the comparison between the uncoated FP-QCL and the

ERC-QCL in a highly directional regime (10:1). Time-resolved spectral measurements were performed for both cases which show that the suppression of SHB leads to the system tending toward single longitudinal mode operation. The FP device, over the same number of round trips (2×10^5) favours a broad emission regime which the authors suggest is the result of mode proliferation caused by SHB. Finally the authors show the absorption caused by water vapour along the beam path demonstrating, in a basic fashion, the suitability of the system for intracavity absorption spectroscopy.

When this PhD programme started in 2013, the vast majority of interest in the ERC-QCL, and QCLs in general, centred around frequency combs and short pulse generation by mode-locking. These were considered a significant outstanding goal of QCL research.

Initially, QCL mode-locking started using ridge devices. The first reported demonstrations came in 2000 when Paiella et al published articles on both the active mode-locking (AML)[28] and self mode-locking (SML)[29] of ridge QCLs. In both of these cases broad optical spectra measured by FTIR and narrow RF linewidths measured by a fast quantum well infrared photodetector (QWIP) were taken as an indication that pulses of good modulation depth and phase stability were present over some operating range. These demonstrations based on early QCL material used 3.5 mm long devices which lead to a reported pulse repetition rate of around 13 GHz. Active modulation was suggested as a route to mode-locking in QCLs which aren't expected to form short pulses through passive techniques due to the fast gain recovery. This early self-mode-locking claim seemed to suggest passive techniques could lead to short isolated pulses. The authors suggest the SML effect observed may be due to a Kerr soft lensing effect which increases the confinement for high intensity components, reducing the modal overlap with the lossy metal contact. These devices operated at cryogenic temperatures and differ substantially from modern, high performance structures which are known not to emit short pulses passively.

In 2004 the AML was reported using a broadband QCL device[30]. This device, like other broadband QCL devices, was composed of a number of dissimilar stages. In this case the device had 5 different stage designs with centre wavelengths from 6.9 to 7.9 μm. The hope here was that a broader gain bandwidth would support

shorter pulses, an idea derived from the time-bandwidth product. This fundamental principle dictates that an optical pulse of increasingly short duration must have an increasingly broad spectrum. For a given device gain bandwidth, a minimum pulse duration exists. An increased number of phase locked modes should produce a shorter, more intense pulse. This device, without modulation, tended to lase CW at a single wavelength or two wavelengths at an increased current. This system had improved electronics compared to previous active modulation setups with impedance matching being maintained right up to the QCL device and special efforts being made to reduce the QCLs parasitic capacitance. When RF power at frequencies close to the devices free spectral range (FSR) at 14.3 GHz was applied the CW peaks broadened to include a number of adjacent FP modes. Again a fast QWIP detector signal was measured using a microwave spectrum analyser. The spectral broadening was followed by a broadening of the RF photocurrent which the group attributed to the poor phase locking of the additional FP modes. In this work there's an assumption that short pulses are formed with an estimated duration of 2.8 to 4.8 ps. Again, due to limitations with second harmonic generating (SHG) crystals in the MIR, the interferometric autocorrelation (IAC) needed to prove the formation of short isolated pulses was absent from this work. The field autocorrelation measurements provided by the FTIR spectrometers lack the ability to resolve phases, meaning some forms of broadband emission can be mistaken for phase locked pulse trains.

Indeed, later investigation, when a second order IAC was available, confirmed that all of these early measurements weren't the result of single mode-locked isolated pulses. Others[31] suggested that the broad emission regimes were the result of multi-mode instabilities caused by SHB and the Risken-Nummedal-Graham-Haken (RNGH) instability.

Current research which aims to develop the QCL as an emitter of broadband frequency combs is focusing on frequency modulated (FM) combs which are created through a constant power mode-locked condition which QCLs favour due to their fast reverse saturable absorption characteristics[32]. Mode proliferation due to the strong four-wave-mixing processes are inherited through the high second and third order non-linear susceptibility of the intersubband transitions. The modes naturally

arrange their phases such that a constant power output is achieved. In one experiment[33] it was found that this effect can be enhanced by the addition of some small amount of RF power at the lasers FSR. It may be the case that some component of these early broad emission regimes was in fact the formation of FM type combs enhanced by the addition of resonant RF power.

Unambiguous demonstration of short isolated pulses came in 2009[31] when active modulation was used to drive specially made sectioned QCL devices. These devices were 2.6 mm in length with a section of 120 and 160 um at one end which could be biased independently. This allowed RF power to be delivered to a more spatially isolated region of the device. The devices were also engineered to have a longer gain recovery time than conventional QCL devices. A diagonal transition meant that the upper state had a phonon limited lifetime of around 50 ps. This was comparable to the cavity round trip time which, according to conventional mode-locking theory, allows for better AML conditions. Subsequent theoretical studies have shown that AML in this fashion is still possible with short gain recovery devices[34]. The small section was driven with around 35 dBm of power at the round trip frequency of around 17.8 GHz.

Second order IAC confirmed that, with the unmodulated section at certain bias levels above CW threshold, short isolated pulses of around 6 ps duration could be formed with energies of around 0.5 pJ. These experimental results compared reasonably well with numerical simulations at low DC levels. The authors accepted that the pulses didn't likely have a simple form, instead having some structure which they claim is the result of the SHB instability. This pulse distorting effect has been the main driving force behind ERC-QCL work. The unidirectional regimes achievable in ERCs should allow the formation of stable pulses, free of SHB.

This first compelling evidence of the destructive role that SHB plays in actively mode-locked QCLs reinforced the suggestion that ERC-QCLs would serve as the ideal platform for short MIR pulses from QCLs. The first serious step toward short mode-locked pulses from ERC-QCLs came in 2013[35]. This comprehensive theoretical study was based on a Maxwell-Bloch treatment. This computational model was based on parameters which would be realistic for a high performance device. A 1 mm long gain medium was chosen, presumably this led to shorter pulses than with typical

device lengths (2.5 to 4.5 mm). The short gain recovery characteristics of typical high performance devices were used here. A 100 cm cavity was simulated, driven by both a harmonic tone, similar to the modulation used in previous ridge mode locking experiments, and Gaussian pulses. The result of this study was to show that under both modulation schemes pulses with a duration of 4 – 5 ps could be generated by an ERC-QCL, composed of many thousands of phase-locked longitudinal modes with a bandwidth of around 20 cm^{-1}. It also found that simulations where longer gain relaxation times were used led to asymmetric pulse distortion occurred at lower field intensities, suggesting that current high performance structures are well suited for mode-locking in this fashion.

1.5 Thesis Overview

The second chapter focuses on the initial deployment of Fabry-Perot QCL into external ring cavities. This early work, using Sheffield made QCL devices, illustrates the dynamic temporal behaviour seen when as-cleaved QCL devices are exposed to the additional external feedback of an external ring cavity. Driving these devices with square current pulses of varying lengths reveals the interplay between the FP cavity of the QCL and the external ring cavity. Time-resolved spectral measurements are taken to understand the effect that the additional external feedback has on the spectral evolution of such systems during start-up.

The third chapter builds on the second by developing the system into a tunable source potentially suited to high resolution gas spectroscopy. This is achieved by using higher performance continuous-wave QCLs which have been anti-reflection coated on both facets to supress the natural FP action of the device, leading to a system which lases on modes belonging entirely to the external cavity. We demonstrate the tendency of external ring cavities to emit in a unidirectional regime. Spectral comparisons are made between free running systems in a linear and ring external cavity configuration. The wavelength tunability of the external ring cavity system is demonstrated by replacing one of the external mirrors with a diffraction grating. Adjusting the grating angle is shown to tune the systems emission wavelength across the entire gain bandwidth of the QCL.

The fourth chapter details the initial work towards the realisation of an actively mode-locked external ring cavity system. An electrical modulation scheme is developed based on a number of bespoke electrical modulators and power amplifiers which are capable of modulating the QCLs drive current at the external ring cavity's round-trip frequency. Some initial data is presented showing the response of the cavity to electrical modulation. An improved system is developed which relies on a custom made RF amplifier and an aluminium nitride laser mount which includes a bias-tee used to couple the RF power into the QCL.

In the fifth chapter we employ the improved modulation system from chapter four to demonstrate the active mode-locking of the external ring cavity using two higher performance, double anti-reflection coated QCLs. The data presented shows the tendency of these systems to emit pulses in an asymmetric fashion. A comparison is made between these two devices under resonant modulation, the difference being that one emits on a single spatial mode while the other supports a number of higher order modes. Spectral measurements provided by FTIR along with the detected RF spectra indicate the emission of pulse trains which remain stable over many thousands of round trips.

In the final chapter we use the same electrical modulation scheme to study the response of a linear external cavity to electrical modulation at the round trip frequency. A number of higher performance Sheffield made devices are anti-reflection coated on one facet while being high-reflectivity coated on the other. This allows for the formation of an external linear cavity with the addition of a single external mirror. It's suggested that the spatial hole burning instability can hinder the formation of stable pulses when in a linear cavity configuration. This is investigated firstly at the cavity's fundamental round trip frequency before going on to pump the linear cavity at multiples of the round trip frequency, resulting in up to 18 individual pulses propagating within the cavity. Similar spectral measurements as in the case of the external ring cavity reveal that stable mode-locking conditions can be attained in a linear configuration.

Bibliography

[1] O Cathabard, R Teissier, J Devenson, JC Moreno, and AN Baranov. Quantum cascade lasers emitting near 2.6 μ m. *Applied Physics Letters*, 96(14):141110, 2010.

[2] A Wade, G Fedorov, D Smirnov, S Kumar, BS Williams, Q Hu, and JL Reno. Magnetic-field-assisted terahertz quantum cascade laser operating up to 225 k. *Nature Photonics*, 3(1):41–45, 2009.

[3] Jerome Faist, Federico Capasso, Deborah L Sivco, Carlo Sirtori, Albert L Hutchinson, Alfred Y Cho, et al. Quantum cascade laser. *Science-AAAS-Weekly Paper Edition-including Guide to Scientific Information*, 264(5158):553–555, 1994.

[4] JF Butler, AR Calawa, RJ Phelan Jr, TC Harman, AJ Strauss, and RH Rediker. Pbte diode laser. *Applied Physics Letters*, 5(4):75–77, 1964.

[5] Maurus Tacke. Lead–salt lasers. *Philosophical Transactions of the Royal Society of London A: Mathematical, Physical and Engineering Sciences*, 359(1780):547–566, 2001.

[6] Rui Q Yang. Infrared laser based on intersubband transitions in quantum wells. *Superlattices and Microstructures*, 17(1):77–83, 1995.

[7] I Vurgaftman, WW Bewley, CL Canedy, CS Kim, M Kim, CD Merritt, J Abell, JR Lindle, and JR Meyer. Rebalancing of internally generated carriers for mid-infrared interband cascade lasers with very low power consumption. *Nature communications*, 2:585, 2011.

[8] I Vurgaftman, R Weih, M Kamp, JR Meyer, CL Canedy, CS Kim, M Kim, WW Bewley, CD Merritt, J Abell, et al. Interband cascade lasers. *Journal of Physics D: Applied Physics*, 48(12):123001, 2015.

[9] Y Bai, S Slivken, SR Darvish, A Haddadi, B Gokden, and M Razeghi. High power broad area quantum cascade lasers. *Applied Physics Letters*, 95(22):221104, 2009.

[10] Y Bai, N Bandyopadhyay, Slivken Tsao, S Slivken, and M Razeghi. Room temperature quantum cascade lasers with 27% wall plug efficiency. *Applied Physics Letters*, 98(18):181102, 2011.

[11] RF Kazarinov and RA Sui-is. Possibility of the amplification of electromagnetic waves in a. *Soviet Physics-Semiconductors*, 5(4), 1971.

[12] Leo Esaki and Ray Tsu. Superlattice and negative differential conductivity in semiconductors. *IBM Journal of Research and Development*, 14(1):61–65, 1970.

[13] Jerome Faist, Federico Capasso, Deborah L Sivco, Carlo Sirtori, Albert L Hutchinson, and Alfred Y Cho. Quantum cascade laser. *Science*, 264(5158):553–556, 1994.

[14] Greg Sun. The intersubband approach to si-based lasers. In *Advances in Lasers and Electro Optics*. InTech, 2010.

[15] Jeff Hecht. *Understanding lasers: an entry-level guide*, volume 21. John Wiley & Sons, 2011.

[16] Mattias Beck, Daniel Hofstetter, Thierry Aellen, Jérôme Faist, Ursula Oesterle, Marc Ilegems, Emilio Gini, and Hans Melchior. Continuous wave operation of a mid-infrared semiconductor laser at room temperature. *Science*, 295(5553):301–305, 2002.

[17] Aleksander K Wójcik, Nanfang Yu, Laurent Diehl, Federico Capasso, and Alexey Belyanin. Self-synchronization of laser modes and multistability in quantum cascade lasers. *Physical review letters*, 106(13):133902, 2011.

[18] N Ruhnke, A Müller, B Eppich, M Maiwald, B Sumpf, G Erbert, and G Tränkle. 400 mw external cavity diode laser with narrowband emission at 445 nm. *Optics letters*, 39(13):3794–3797, 2014.

[19] Gerard Wysocki, Robert F Curl, Frank K Tittel, Richard Maulini, Jean-Marc Bulliard, and Jérôme Faist. Widely tunable mode-hop free external cavity quantum cascade laser for high resolution spectroscopic applications. *Applied Physics B*, 81(6):769–777, 2005.

[20] Richard Maulini, Arun Mohan, Marcella Giovannini, Jérôme Faist, and Emilio Gini. External cavity quantum-cascade laser tunable from 8.2 to 10.4 μ m using a gain element with a heterogeneous cascade. *Applied physics letters*, 88(20):201113, 2006.

[21] Andreas Hugi, Romain Terazzi, Yargo Bonetti, Andreas Wittmann, Milan Fischer, Mattias Beck, Jérôme Faist, and Emilio Gini. External cavity quantum cascade laser tunable from 7.6 to 11.4 μ m. *Applied Physics Letters*, 95(6):061103, 2009.

[22] V Spagnolo, AA Kosterev, L Dong, R Lewicki, and FK Tittel. No trace gas sensor based on quartz-enhanced photoacoustic spectroscopy and external cavity quantum cascade laser. *Applied Physics B: Lasers and Optics*, 100(1):125–130, 2010.

[23] Rafał Lewicki, James H Doty, Robert F Curl, Frank K Tittel, and Gerard Wysocki. Ultrasensitive detection of nitric oxide at 5.33 μm by using external cavity quantum cascade laser-based faraday rotation spectroscopy. *Proceedings of the national academy of sciences*, 106(31):12587–12592, 2009.

[24] Anatoliy A Kosterev, Alexander L Malinovsky, Frank K Tittel, Claire Gmachl, Federico Capasso, Deborah L Sivco, James N Baillargeon, Albert L Hutchinson, and Alfred Y Cho. Cavity ringdown spectroscopic detection of nitric oxide with a continuous-wave quantum-cascade laser. *Applied optics*, 40(30):5522–5529, 2001.

[25] Arkadiy Lyakh, Rodolfo Barron-Jimenez, Ilya Dunayevskiy, Rowel Go, and C Kumar N Patel. External cavity quantum cascade lasers with ultra rapid acousto-optic tuning. *Applied Physics Letters*, 106(14):141101, 2015.

[26] Jan Grahmann, André Merten, Andreas Herrmann, Ralf Ostendorf, Daniela Bleh, Christian Drabe, and Jörg Kamenz. Large moems diffraction grating results providing an ec-qcl wavelength scan of 20%. In *MOEMS and Miniaturized Systems XIV*, volume 9375, page 93750W. International Society for Optics and Photonics, 2015.

[27] Pietro Malara, Romain Blanchard, Tobias S Mansuripur, Aleksander K Wojcik, Alexey Belyanin, Kazuue Fujita, Tadataka Edamura, Shinichi Furuta, Masamichi Yamanishi, Paolo de Natale, et al. External ring-cavity quantum cascade lasers. *Applied Physics Letters*, 102(14):141105, 2013.

[28] Roberto Paiella, Federico Capasso, Claire Gmachl, Harold Y Hwang, Deborah L Sivco, Albert L Hutchinson, Alfred Y Cho, and HC Liu. Monolithic active mode locking of quantum cascade lasers. *Applied Physics Letters*, 77(2):169–171, 2000.

[29] Roberto Paiella, Federico Capasso, Claire Gmachl, Deborah L Sivco, James N Baillargeon, Albert L Hutchinson, Alfred Y Cho, and HC Liu. Self-mode-locking of quantum cascade lasers with giant ultrafast optical nonlinearities. *Science*, 290(5497):1739–1742, 2000.

[30] Alexander Soibel, Federico Capasso, Claire Gmachl, Milton L Peabody, A Michael Sergent, Roberto Paiella, Harold Y Hwang, Deborah L Sivco, Alfred Y Cho, HC Liu, et al. Active mode locking of broadband quantum cascade lasers. *IEEE journal of quantum electronics*, 40(7):844–851, 2004.

[31] Christine Y Wang, Lyuba Kuznetsova, VM Gkortsas, Laurent Diehl, Franz X Kaertner, Mikhail A Belkin, Alexey Belyanin, Xiaofeng Li, Donhee Ham, Harald Schneider, et al. Mode-locked pulses from mid-infrared quantum cascade lasers. *Optics Express*, 17(15):12929–12943, 2009.

[32] JB Khurgin, Yamac Dikmelik, Andreas Hugi, and Jerome Faist. Coherent frequency combs produced by self frequency modulation in quantum cascade lasers. *Applied Physics Letters*, 104(8):081118, 2014.

[33] Andreas Hugi, Gustavo Villares, Stéphane Blaser, HC Liu, and Jérôme Faist. Mid-infrared frequency comb based on a quantum cascade laser. *Nature*, 492(7428):229–233, 2012.

[34] Yongrui Wang and Alexey Belyanin. Active mode-locking of mid-infrared quantum cascade lasers with short gain recovery time. *Optics express*, 23(4):4173–4185, 2015.

[35] Aleksander K Wójcik, Pietro Malara, Romain Blanchard, Tobias S Mansuripur, Federico Capasso, and Alexey Belyanin. Generation of picosecond pulses and frequency combs in actively mode locked external ring cavity quantum cascade lasers. *Applied Physics Letters*, 103(23):231102, 2013.

Chapter 2

Pulsed External Ring Cavity QCLs

2.1 Introduction

Work on the external ring cavity (ERC) QCL was conducted as part of the Quantatec project, an EU funded collaboration between the University of Sheffield, Radboud University, Sensor Sense and M Squared Lasers. The aim of the project was to develop the ERC-QCL as a source for high-resolution gas spectroscopy.

In this chapter the initial ERC-QCL systems are discussed. This includes the first system that was borrowed as well as the second system that was built subsequently. These early setups led to the development of the continuous-wave system which is the subject of chapter 3. Some initial measurements are presented that show the temporal characteristics of ERC-QCLs using an: as-cleaved Fabry-Perot QCL, forming a composite cavity; and a double anti-reflection coated QCL, leaving only external cavity effects. By measuring the evolution of the systems intensity for varying current pulse lengths (100 ns – 1 ms), a comparison is made between the two cases. Finally, time-resolved measurements are presented for the AR coated ERC-QCL system which shows its spectral evolution during the first millisecond of start-up.

2.2 Initial Setup

The first ERC system that I worked on was an initial prototype from M Squared Lasers. This standalone ERC-QCL system was mounted on a small optical bread-board and included all the elements needed to observe emission. The cavity was approx. 40 cm in length and formed of four small (10 mm diameter) planar metallic mirrors which had received a dielectric coating to increase their reflectivity at the design wavelength of the system (around 8 μm). Lens positioning was achieved using a pair of xyz translators, each comprised of three linear stages. A dedicated Avtech AVOZ-DF1-B pulse generator was used to pump the QCL with pulses of around 50 – 75 ns at a repetition rate of around 1 kHz. Emission was coupled out of the cavity using an uncoated CaF_2 window which was positioned at the half way point, on the opposite side to the QCL. Emission was detected using a Vigo systems PVI-2TE-8 MCT detector. The QCL used in this system was one manufactured in Sheffield at the national III-V centre, which emitted at around 8 μm in a pulsed regime only.

The interesting feature of these QCLs was the waveguide geometry. These had been processed with angled facets. The goal here was to suppress the Fabry-Perot (FP) modes of the QCL without the need for anti-reflection (AR) coatings. Study of this system was highly limited. The QCL had poor thermal performance, limiting the pulse duration, and very poor coupling efficiency into the external cavity. Reduction in threshold voltage was taken to be a measure of the coupling from the cavity and, using these 8 μm QCLs, very little reduction was achieved (1 – 5%). Observing the pulse amplitude as small adjustments were made to mirror alignments was the limit of the initial experimentation. This poor coupling efficiency was likely due to a combination of the QCLs waveguide design and the type of lenses used.

2.3 Setup Development

The poor performance of the long wavelength system prompted the development of a second system which was tailored to make use of Sheffield's higher performing, shorter wavelength QCLs.

A simple post mountable laser submount holder was produced which allowed the QCL to be mounted between a pair of moulded aspheric high numerical aperture lenses. These were mounted in a pair of lens mounts which provided xyz translation, though it was later found to be more stable and repeatable when linear stages were used instead of the holder's z stage which adjusted the focus. Fig. 2.1 shows the laser mount and lens holder assembly. Uncoated planar metallic mirrors were found to provide good feedback across a broad wavelength range. Two red diode lasers were also used to aid with alignment.

Experimentation across a broad set of QCL devices was pursued to help identify which device characteristics were important to the cavity's operation. The Aspheric lenses were broadband anti-reflection coated from 3 to 5 μm and had reasonable performance up to about 5.5 μm. This allowed the test of devices made in Sheffield with design wavelengths from 3.3 to 5.4 μm.

Unlike in a true ERC-QCL system, these devices had uncoated facets which meant their FP modes were unsuppressed. This affects the system in a number of ways. Firstly, and advantageously, these devices would lase without any additional

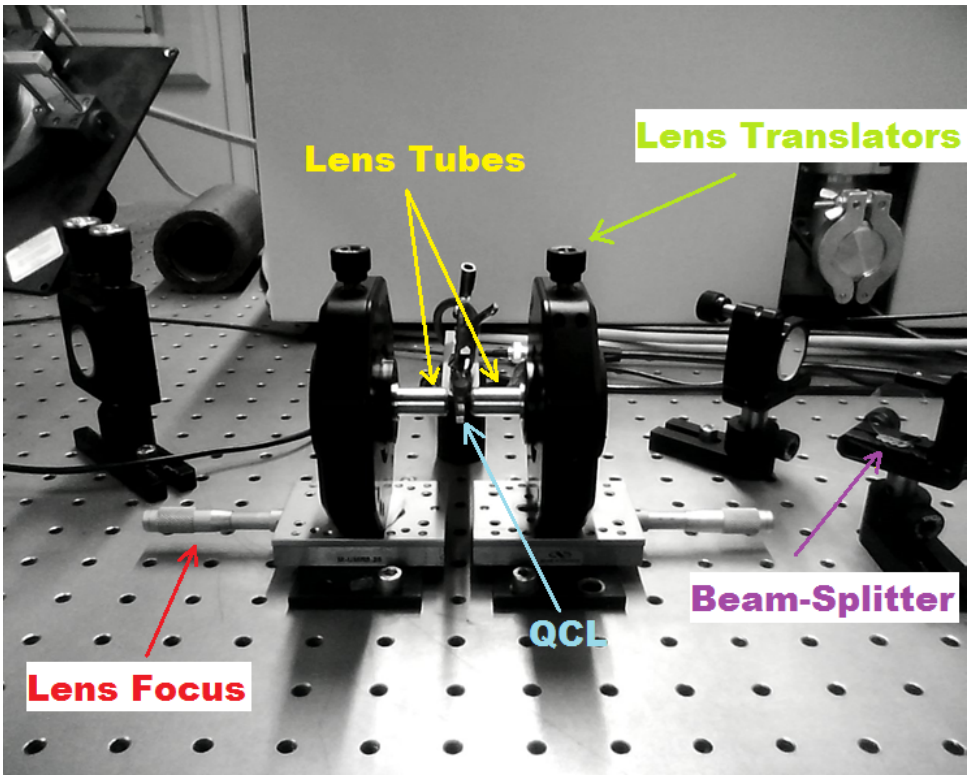

Figure 2.1: Laser and lens mounting assembly used for early pulsed devices. Each of the lens holders provides x-y translation to the lenses. The pair of lower stages provides z-axis (focus) translation. A piece of plate aluminium is necked to the width of the QCL submount and is post mounted.

external feedback. This made the alignment of the cavities easier as the driving pulse current could be set above the FP threshold while the system was being aligned and this would produce a very strong signal that could be tracked by moving the detector around. This was particularly helpful given that the cavities had a much greater path-length than had been the case with the M Squared setup. This was partly due to the bulky lens holders which meant it was impossible to create ERCs with path-lengths below around 90 cm. It was also deemed to be of interest to see what the limits were, as well as good alignment practice. Fig. 2.2 shows a typical ERC aligned with a path-length of approx. 2.9 m. It also meant, from theory, that the cavity would lase on an FP mode rather than an external cavity mode (ECM), which would be the case if the facets were coated. FP devices deployed in the way are essentially operating in a coupled cavity regime which in the single mode steady state limit would lase on a mode in the close vicinity of both an FP and EC mode. For a 3 mm InP QCL in a 3 m ERC the FP mode spacing would be around 15 GHz (0.5 cm^{-1})

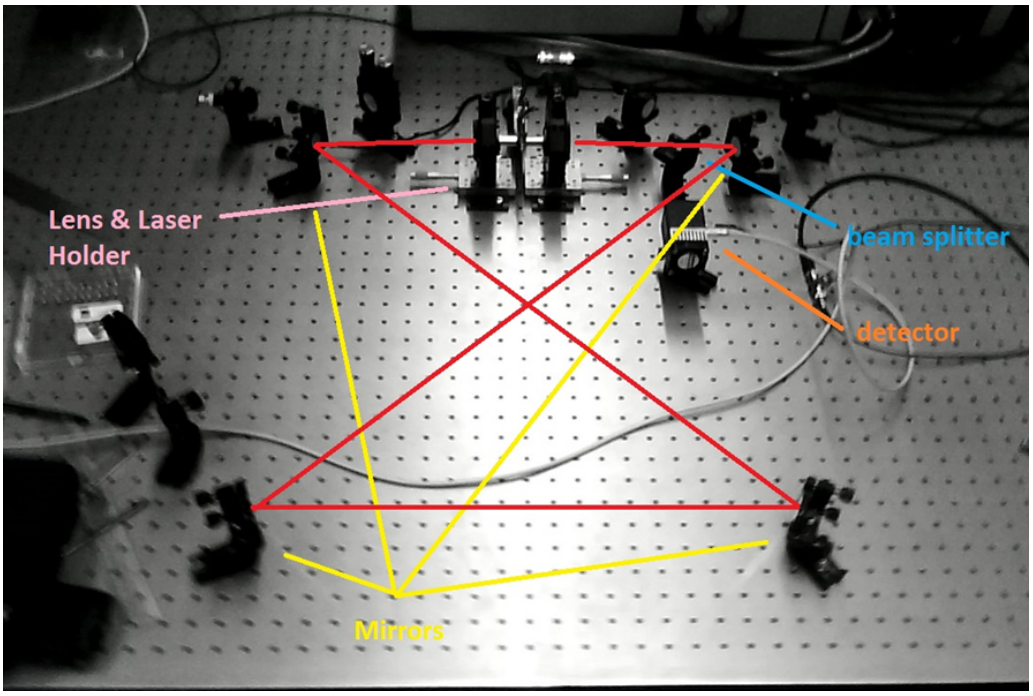

Figure 2.2: Aligned 2.9 m pulsed ERC system. The red line indicates the path of the beam.

and the ECM spacing would be approx. 100 MHz (0.0033 cm^{-1}). This fine spacing makes it easy for the system to find an ECM in the close vicinity of an FP mode, allowing the system to largely satisfy both resonant conditions simultaneously. As will be explained later, investigation in the spectral domain showed that the external cavity and QCL ridge weren't the only elements producing etalon mode structures.

2.3.1 FP-ERC-QCL

The first interesting observations were made when the cavity reached a length which brought the round trip frequency below the bandwidth of the new fast MCT detectors ($\sim$ 300 MHz). This was first observed for a 3 m cavity and is shown in Fig. 2.3.

Here the temporal response of the cavity to a 110 ns current pulse shows a strong resonant behaviour. In the blocked cavity response (fig.2.3b), where some opaque object is introduced into the cavity to block external feedback, the device operates as a normal FP laser. This device had a FP threshold of 176 mA and the current pulse was set at around 190 mA, just under 8 % above threshold. Around 40 ns passes from the current pulse reaching this threshold before emission rapidly climbs.

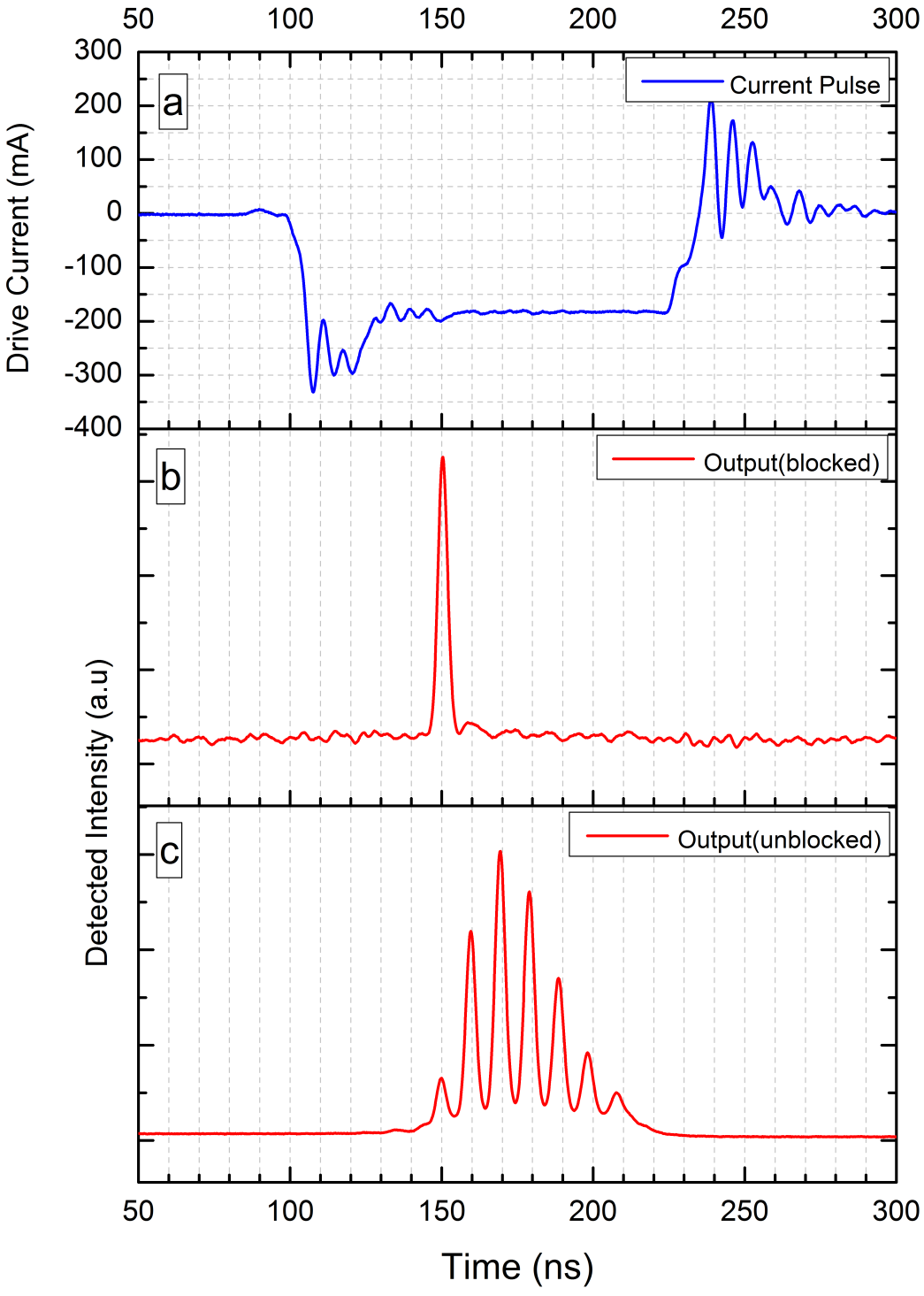

Figure 2.3: Current pulse and resulting detected emission of an ERC system with a 3 mm long QCL with a centre wavelength of approx. 5 μm in a blocked and unblocked state.

The pulse dies away just as rapidly despite the electrical pulse being sustained for a further 70 ns. This is purely due to thermal effects with the device rapidly heating, reducing gain through the thermal scattering of carriers inside the gain region.

Unblocking the cavity (fig.2.3c) with all other variables remaining fixed reveals an interesting response. Now after the initial pulse is emitted, related to the FP feedback, there are a number of *echo* pulses which arrive at a frequency corresponding to the cavity round trip time. This would suggest that the initial FP pulse is propagating around the cavity and is able to access some net gain over a number of round trips. It should be noted that the two outputs (fig.2.3b & c) aren't to scale. The blocked pulse and the first unblocked pulse have *similar* amplitudes. There are however a number of strange phenomenon which require some explanation.

In the unblocked case (fig.2.3c) there appears to be some emission features before the first pulse which aren't present in the blocked case. This is likely related to the electroluminescent (EL) emission which in the blocked case would have never arrived back at the gain medium. Even though some time (40 ns) passes before laser emission is seen in the blocked case, some amount of EL will have been emitted from the start of the current pulse. In the unblocked case some portion of these EL photons would have been allowed to propagate around the cavity and arrive back at the gain medium where they are amplified in a super EL fashion. This means that, in the unblocked case, there are 4 round trips over which the EL in the ERC builds up. This could be responsible for the features before the initial pulse, the slight but significant difference in the initial pulse amplitudes and it may also be responsible for the fact that the pulses aren't entirely isolated in the unblocked case, with some emission persisting between the pulses.

Another point which seems counterintuitive is the apparent increase in available gain. In the blocked case the emission collapsing in a few nanoseconds would suggest no net gain is available after the 150 ns mark whereas in the unblocked case some net gain must exist until at least the 170 ns mark, evidenced by the growing pulses. This may again relate to the circulating EL which may reduce device heating by depopulating carriers through radiative rather than non-radiative transitions.

This distinctive pattern is characteristic of FP-ERC-QCLs and was observed with similar form across all devices tested. Cavities were aligned with lengths of

1.8, 3 and 3.6 m. In each case the observed pulses had separations corresponding to round trip times of 6, 10 and 12 ns respectively, confirming that the pulses were echoing in the way described. The characteristic shape shown in Fig. 2.3 is only the first part of a longer characteristic shape observed when pumping FP-ERC-QCLs with square current pulses.

Fig. 2.4 shows the emission measured when the cavity is pumped with a pulse of some hundreds of nanoseconds. In this case the cavity has a better level of alignment than in the previous figure. Here the coupling into the ERC is as high as possible. This general form of emission is seen from all FP-ERC-QCLs, regardless of alignment quality. The initial oscillations are followed by a number of smaller sets. These oscillations settle after around 300 ns although there can be some small round trip frequency component in the remainder of the pulse, depending upon the laser, alignment, etc. Some time after, in this case around the 450 ns mark, the emission amplitude reaches a maximum. This shows that the increased feedback provided by the external cavity allows gain to be sustained for a longer period. From this point the emission dies away gradually. It was possible to drive some devices with pulses as long as a millisecond but measuring the output using AC coupled detectors produces an emission pulse that returns to the baseline over a few microseconds despite emission still being present. Noise in the signal as well as an associated negative swing indicates that emission was sustained despite the detector signal having returned to zero volts.

2.3.2 AR Coated ERC-QCL

A true ERC system which lases on pure ECMs requires the suppression of the gain medium's FP modes. Like in the previous case, an uncoated device leads to a situation where two cavities, with their respective mode-structures, compete in a coupled cavity regime. In the long run this scheme is undesirable as it not only makes wavelength tuning difficult by giving the system a set of preferred emission wavelengths, but prevents unidirectional emission by coupling one propagating direction into the other. These facet reflections destroy the circular boundary condition that makes the ERC an attractive platform.

To this end, a number of higher performance, Sheffield made devices were AR

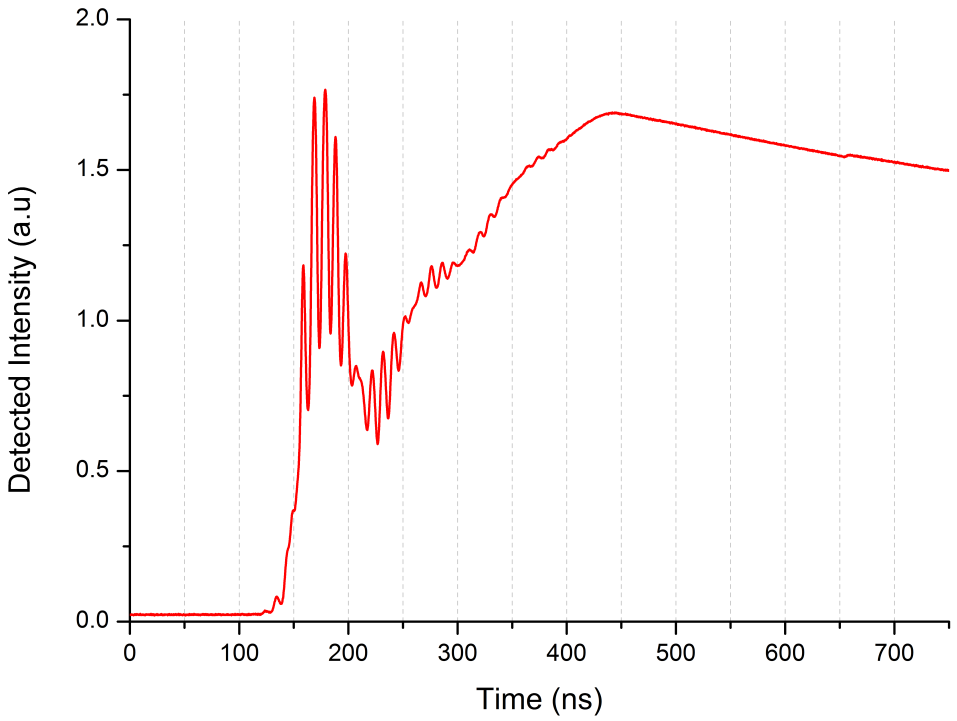

Figure 2.4: Detected start-up emission from a 2.9 m FP-ERC-QCL pumped with longer current pulses.

coated on both facets by Helia Photonics. Further details of the AR coating process are provided in section 3.3. Despite being coated it is expected that some residual reflectance would remain. This is more so the case when using non-buried structures where the facet doesn't extend beyond the ridge. This leads to edge effects during the coating process. This poor quality region around the edge wouldn't make much difference to the fundamental spatial mode but may coincide strongly with higher order or plasmonic components of the guided mode. Some upper limit can be placed on the residual reflectance by measuring the device's output outside of an external cavity. In principle an AR coated device should lack the feedback needed to lase if a good quality coating has been achieved. In our case no laser emission was observed from any device when driven with pulses right up to the device's respective roll-over currents, indicating at least a reasonably low residual reflectance across the set.

It was anticipated that working with AR coated devices would complicate the alignment task by suppressing lasing up until the point the cavity was aligned. This

turned out not to be overly problematic. With the devices pumped at levels that would have otherwise caused them to lase, the electroluminescent output was clearly detectable by our MCT detectors. This meant the laser beam could be collimated in a similar way with only a little more care needed during the initial stages.

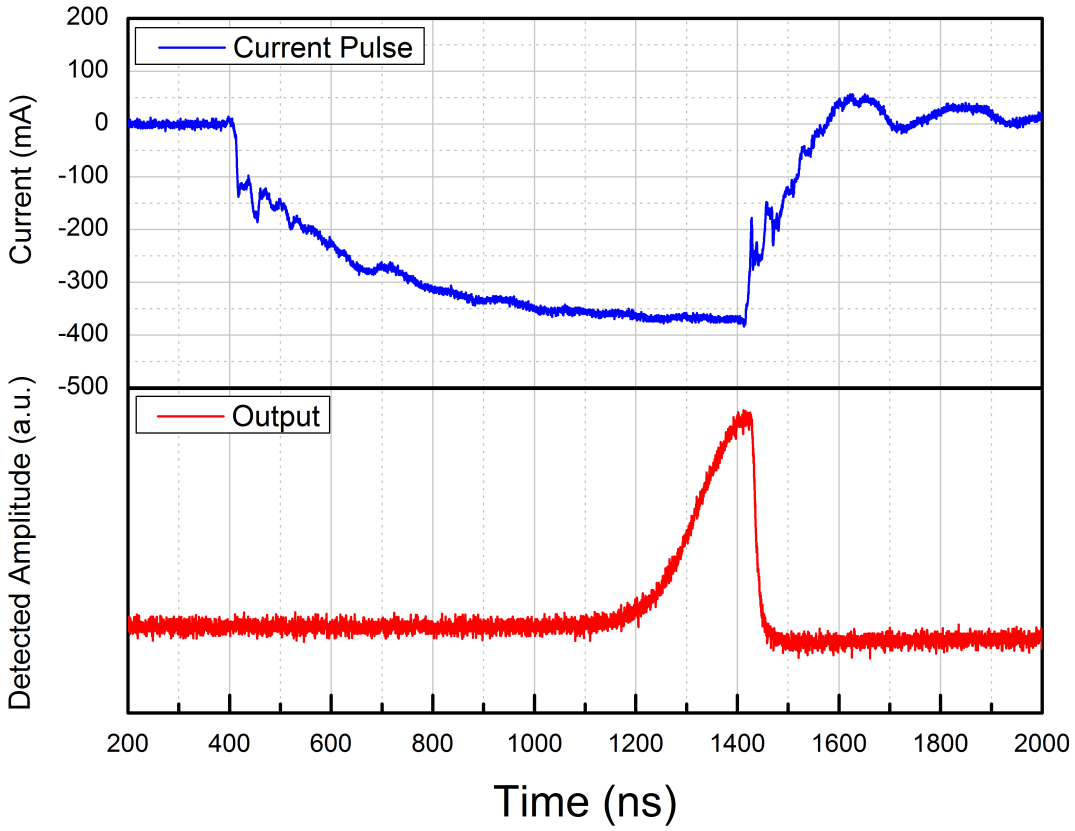

Figure 2.5: Current pulse and resulting detected emission from a 3 m ERC-QCL. A 1 μs pulse drives a double AR coated buried structure QCL. The non-uniform current pulse is caused by a less than ideal termination setting of the pulse generator. The resulting current pulse shape doesn't achieve threshold until around 1000 ns, causing the observed delay.

Fig. 2.5 shows the output characteristic of AR-coated ERC-QCLs pumped with square pulses. Here, compared to the previous case, the complex features present during start-up are entirely absent. Instead emission builds up in a slow and gradual fashion.

Fig. 2.6 shows a pulse of longer duration. Note that, due to the AC nature of the detector and current probe, the baseline of the signal drifts on a microsecond timescale. Over longer periods, the step in the signal at the end of the pulse indicates

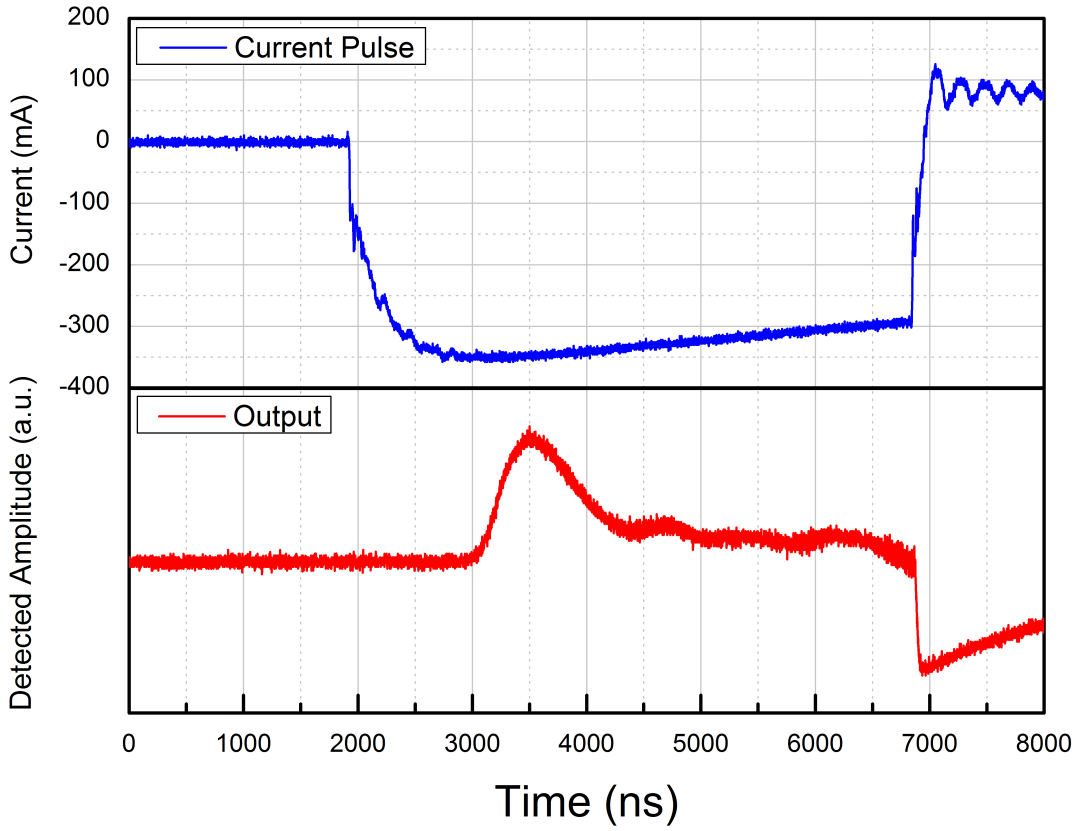

Figure 2.6: Current pulse and resulting detected emission from a 3 m ERC-QCL. A 5 μs pulse drives a double AR coated buried structure QCL.

that emission was still present. Also the current pulses appear softer than in the FP-ERC case due to a different setting being used on the Avtech pulse generator. Comparing the longer pulses of the FP and AR-coated systems, fig.2.4 and fig.2.6, would seem to provide support for the idea that the "hand-like" features are a result of FP action, as suggested. It's also clear that in most cases, after a certain duration the outputs of coated and uncoated systems look very similar, with both reaching some peak intensity then slowly decreasing. This, of course, is true for the pulsed devices that were used here. Better quality continuous-wave devices would instead achieve some equilibrium intensity which would be reached asymptotically after some initially high intensity emission.

To measure the spectral behaviour of these pulsed systems during start-up, time-resolved spectra were measured at a number of temporal positions of a 1 millisecond pulse. The measurement of time-resolved spectra required a number of changes to be

made to the system. For most spectral measurements the FTIR would be equipped with a sensitive but slow MCT detector. This had a response time of around 4 μs. For time-resolved measurements this was replaced by a fast MCT detector with a response of around 3 ns. With the laser being driven with current pulses at a repetition rate in the range 1 to 10 KHz the FTIR would be set in step scan mode. Rather than allowing the FTIR to measure the average intensity, as would be the case in CW measurements, the output from the detector was connected to an oscilloscope. This meant that auto-correlated pulse shapes could be observed on the oscilloscope as the FTIR varied the optical path difference using its moving mirror. In this way a single temporal section of the pulse could be gated on the oscilloscope. The oscilloscope acted as analogue to digital converter, sending the gated reading back to the FTIR for each successive step of its mirror. This task was accomplished using a specially made Labview script which only required the gate position to be adjusted using the oscilloscope cursors.

Fig. 2.7 shows a spectral evolution that is in good agreement with other studies[1]. The difference being that in this case, rather than averaging over the entire pulse up to each time interval, this time-resolved setup allowed for the gating of signals in such a way that meant instantaneous spectra could be recorded at each time interval. This gives a more accurate picture of the spectral evolution than a system using large time interval averages which would likely be distorted by amplitude fluctuations over the course of a long pulse.

This difference doesn't significantly affect the overall result which shows the tendency of these systems to begin lasing broadly, across a number of longitudinal modes. Over some period of time the emission bandwidth narrows with single mode emission been presumably achieved as a steady state is approached. This phenomenon is related to gain competition, which sees one dominant longitudinal mode win out against the others by consuming, and therefore depriving others of, the available gain. This stochastic process also occurs in ridge devices where it promotes single mode emission in a similar way. It's likely the timescales involved are related to the cavity length with a given device requiring so many round trips before a single mode becomes dominant.

One striking feature of the time-resolved spectra, particularly at short time

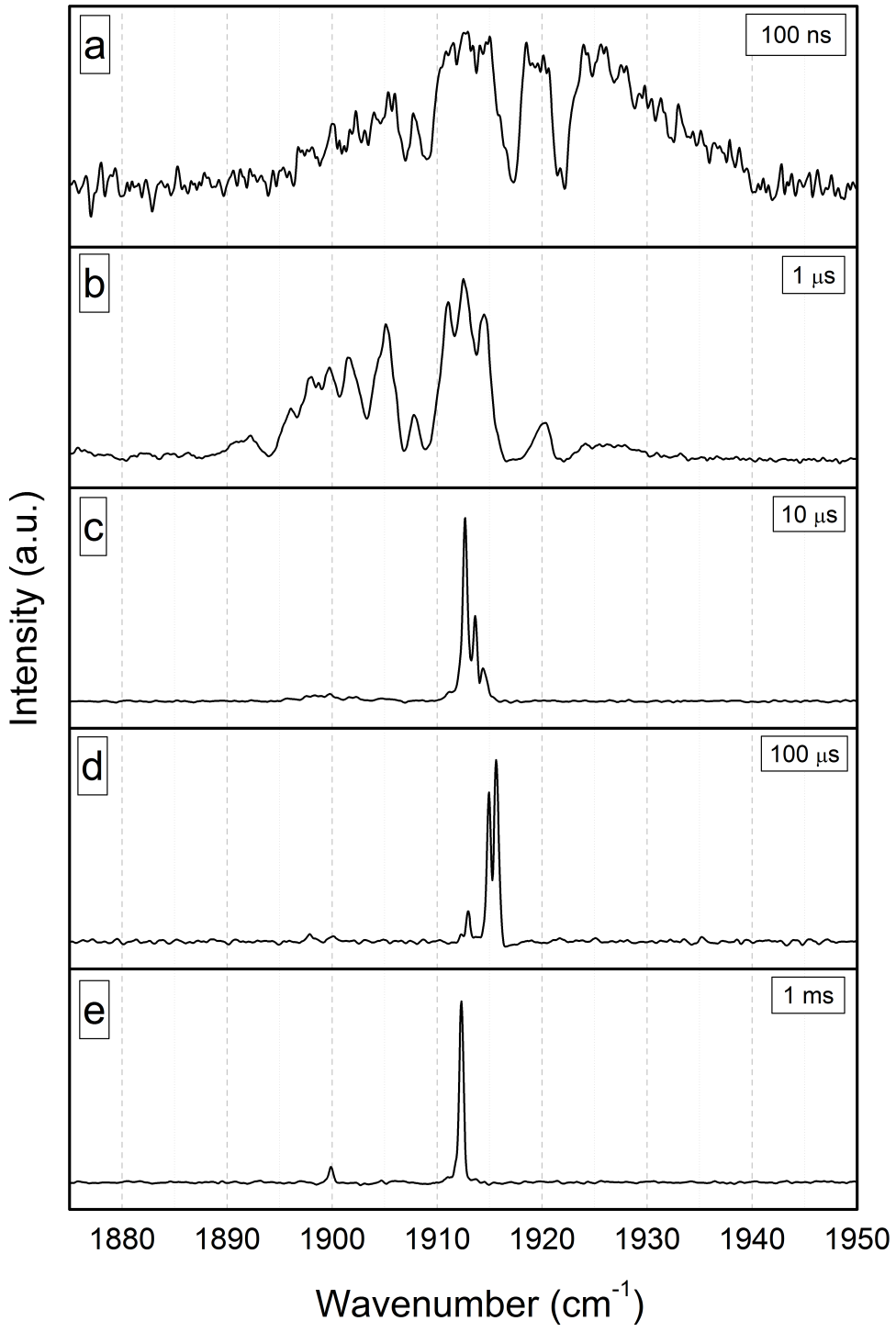

Figure 2.7: Time-resolved spectral measurements of an ERC-QCL driven with 1 ms pulses. Gating of the pulse at certain temporal positions provides instantaneous spectral measurements.

scales, is the comb like emission structure. This doesn't correspond to the FP modes which should have a mode spacing of around 0.5 cm^{-1}, their absence from any measured spectra demonstrates that these modes are sufficiently suppressed by the AR coatings. This mode structure is being created by the parasitic etalon effects of the 2 mm thick CaF_2 window that's used as a beam-splitter. The 45° AOI leads to a reflectance of 6.85 % for light which is s-polarized and a mode spacing of around 2 cm^{-1}, in line with observations. Essentially the beam-splitter acts as a spectral filter which, despite its low finesse, can have a dominant effect on the system during the highly sensitive start-up period. From this point forward it was realised that some method of suppressing this etalon effect must be used to achieve uncoloured behaviour. To this end a number of CaF_2 windows were AR coated on one side. This leaves only one side reflective, allowing for emission to be coupled out, without the etalon effect caused by internal reflections.

2.4 Discussion

The alignment procedure developed here would be employed in all subsequent systems, irrespective of the final intended pumping mode. Using uncoated QCLs has allowed the demonstration of external feedback effects in a clear way. Realigning the cavity using a good number of different Sheffield made QCL devices helped to identify those most suitable for AR coating. These coated devices which were used to create a true ERC-QCL system, albeit limited to a pulsed regime.

Time-resolved spectral measurements are presented which show the general tendency of the system to spectrally narrow from start-up, in good agreement with previous studies[1]. These measurements also demonstrated the need to suppress parasitic etalon effects created by additional optical elements in the system's beam path.

Bibliography

[1] Pietro Malara, Romain Blanchard, Tobias S Mansuripur, Aleksander K Wojcik, Alexey Belyanin, Kazuue Fujita, Tadataka Edamura, Shinichi Furuta, Masamichi Yamanishi, Paolo de Natale, et al. External ring-cavity quantum cascade lasers. *Applied Physics Letters*, 102(14):141105, 2013.

Chapter 3

Wavelength Tunable Room Temperature Continous-Wave External Ring Cavity QCLs

Currently, wavelength-tunable MIR continuous-wave sources used for high resolution gas spectroscopy are exclusively based on linear external cavities. These Littrow type systems use diffraction gratings to continuously tune the emission wavelength. This allows these systems to act as a source for the detection of organic compounds through various gas detection schemes. One shortcoming of these systems comes as a result of the spatial hole burning (SHB) instability that is common to all linear laser resonators. This can have the effect of destabilising the system's emission, creating amplitude and frequency noise which is detrimental to most detection schemes.

External ring cavities, and ring geometries in general, are able to support unidirectional emission, light which propagates around the ring in only one direction. Unidirectional emission exists as a travelling wave as opposed to the standing waves patterns of linear laser resonators. In the absence of this standing wave pattern the SHB effect is avoided. This means, in principle, a tunable MIR source based on a unidirectional ring geometry should have lower intrinsic noise levels than its linear counterparts, owing to the suppression of SHB.

In this chapter we take the first steps toward realising a wavelength-tunable room-temperature continuous-wave source potentially suitable for high resolution gas spectroscopy based on an external ring cavity QCL. Firstly, a comparison is made between the continuous-wave performance of linear and ring cavities without employing a tuning element. Then, by introducing a diffraction grating in place of an external mirror, we demonstrate a basic scheme for tuning the emission of an external ring cavity QCL. Finally, measurements are presented which demonstrate an interesting self-phase-locking regime observed while driving the ERC-QCL under the same bias conditions used for continuous-wave emission.

3.1 Introduction

Laser systems which are capable of operating in a continuous-wave (CW) regime have a number of advantages over systems limited to pulsed emission. This is particularly true in gas sensing/monitoring where wavelength sweeps may be required to cycle continuously to provide the necessary response. In high resolution systems

the narrow linewidths needed to provide the high spectral selectivity may only be possible under CW conditions. The laser/gain medium in pulsed or low duty cycle systems is limited by thermal effects which begin to reduce the gain from the instant the laser is driven. Even high efficiency QCL devices dissipate most of electrical energy as heat. For a given device driven with square current pulses there will be a heating of the laser core with an average thermal power;

$$P_{th} = VId - L = VIt_p r - L \tag{3.1}$$

Where V and I are pulse voltage and current, d is the duty cycle, t_p and r are pulse duration and repetition rate and L is the power of the emitted light.

In reality the heating occurs rapidly during the current pulse and has the effect of shutting the pulse down. The heating of the core produces a number of effects such as thermal backfilling and continuum state scattering which reduce the effective gain and shift the effective threshold to higher currents. The total effect of heating can then be considered as two components, the average described in equation 3.1 and a rapidly varying or cyclic component caused by switching. The temperature rise caused by the first component is dependent on the thermal impedance of the laser mount and can be reduced using standard heatsinking methods or by using active cooling such as thermoelectric coolers (TECs). The effect of the second term is governed almost entirely by the laser core and ridge design. Here the high energy densities deposited in the active region of the QCL must be extracted into the surrounding semiconductor material and into the substrate. Historically, this has been one of the struggles in developing good quality QCLs.

In some QCL based systems this heating effect can be utilized to chirp the emission wavelength in a predictable way. DFB QCLs, for example, have a temperature dependent emission wavelength which can be made to sweep across some small band (≈ 2 cm^{-1}) by driving the devices with ramped current pulses. The addition of some sub-threshold d.c. between the pulses as well as varying the duty cycle gives some additional degrees of freedom to achieve the desired frequency response. This type of operation is limited to the case of QCLs with DFB gratings which limits the laser to a very narrow emission band which in the case of spectroscopy make it suitable for targeting only a single analyte. Without the wavelength selective grating of a DFB

laser, temperature effects invariably lead to chaotic and unstable behaviour during laser start-up. This, as well as other switching effects, such as electrical ringing, can cause instabilities, multi-mode emission, mode-hopping, etc which are significant for the first few hundred nanoseconds but can continue into the seconds where the thermal equilibrium of the system as a whole has been significantly affected.

Current high resolution gas spectroscopy techniques call for a single, low linewidth, broadly tunable emission peak. Noise of any type can interfere with most detection schemes and reduces the system's sensitivity, while a broader line or the presence of multiple lines, could compromise the system's selectivity. CW sources don't suffer from any switching transient effects and after some short period of time can be considered to be in a steady state. It's usually the case that modal competition leads to a single longitudinal mode lasing. While noise is still present in CW EC-QCL systems linewidths below1 kHz can be achieved[1], allowing even very closely spaced molecular spectral features to be resolved.

3.2 Theory

The potential benefit of using an ERC-QCL system as a tunable source for high resolution gas spectroscopy lie in its ability to lase in a unidirectional regime. This should allow for more stable emission by suppressing the spatial hole burning (SHB) instability. SHB, and other instabilities, can be modelled using the appropriate form of Maxwell-Bloch equations. This type of analysis will lead to an analytical solution for the onset of instabilities relevant to EC- and ERC-QCLs operating in a continuous-wave regime.

We proceed from the standard Maxwell-Bloch equations derived in section 1.2.6.

$$\partial_t \mathbf{E} = -\frac{c}{n}\partial_z \mathbf{E} - \frac{c}{n}\frac{i\vec{M}\mathbf{P}}{\hbar l_0 D_{th}} - \frac{c}{2n} l_0 \mathbf{E} \tag{3.2a}$$

$$\partial_t \mathbf{P} = \frac{i\vec{M}}{2\hbar}\mathbf{D}\mathbf{E} - \frac{\mathbf{P}}{T_2} \tag{3.2b}$$

$$\partial_t \mathbf{D} = \frac{D_p - \mathbf{D}}{T_1} + \frac{i\vec{M}}{\hbar}(\mathbf{E}^*\mathbf{P} - c.c.) \tag{3.2c}$$

These equations describe the propagation of a classical external field in an inverted two level system. To build an accurate model of the QCL, both as a ridge laser or in an EC configuration, a number of other effects must be taken into account. Models including the effects of spatial hole burning (SHB) and saturable absorption (SA) on CW QCL emission have been studied extensively and more recently models including self-phase modulation (SFM) and group velocity dispersion (GVD) have been used to model pulse propagation and mode-locking mechanisms. To build a model suitable for the analysis of CW EC-QCL systems we must take account of these effects where appropriate and analytically possible.

Because we are concerned with the characteristics of QCL CW emission, study of these systems of equations may provide insight into the different emission characteristics. From a spectroscopic perspective the most important characteristic is stability. Linear stability analysis of these equations could outline the differences in operating regions of linear vs ring geometry QCL systems. Analysis of the ring cavity is more straight forward than the ridge or linear cavity so we will begin there.

Firstly we include the saturable absorption effect by introducing a field dependence to the loss term in 3.2a

$$\partial_t \mathbf{E} = -\frac{c}{n}\partial_z \mathbf{E} - \frac{c}{n}\frac{i\vec{M}\mathbf{P}}{\hbar l_0 D_{th}} - \frac{c}{2n}(l_0 - \gamma|\mathbf{E}|^2)E \tag{3.3}$$

This saturable absorption effect can be interpreted as an intensity dependent loss. The mechanism most likely to account for this in QCLs is *Kerr soft lensing* which has the effect of focusing the spatial mode toward the centre of the waveguide.

Under high fields greater confinement causes the mode to overlap more with the gain region and less with the lossy waveguide cladding.

Proceeding in a fashion similar to reference[2], we define

$$\tilde{\mathbf{E}} \equiv \frac{\mathbf{E}\vec{M}}{\hbar} \tag{3.4a}$$

$$\tilde{\gamma} \equiv \frac{\hbar^2\gamma}{\vec{M}^2} \tag{3.4b}$$

$$\tilde{\mathbf{P}} \equiv \frac{l_0\mathbf{P}}{D_{th}T_2} \tag{3.4c}$$

$$\tilde{\mathbf{D}} \equiv \frac{l_0\mathbf{D}}{D_{th}T_2} \tag{3.4d}$$

This allows eqs. (3.2a–3.2c) to be rewritten in the more compact form

$$\frac{n}{c}\partial_t\tilde{\mathbf{E}} = -\partial_z\mathbf{E} - i\tilde{\mathbf{P}} - \frac{1}{2}(l_0 - \tilde{\gamma}|\tilde{\mathbf{E}}|^2)\tilde{\mathbf{E}} \tag{3.5a}$$

$$\partial_t\tilde{\mathbf{P}} = \frac{i\tilde{\mathbf{D}}}{2}\tilde{\mathbf{E}} - \frac{\tilde{\mathbf{P}}}{T_2} \tag{3.5b}$$

$$\partial_t\tilde{\mathbf{D}} = \frac{pl_0}{T_1T_2} - \frac{\tilde{\mathbf{D}}}{T_1} + i(\tilde{\mathbf{E}}^*\tilde{\mathbf{P}} - c.c.) \tag{3.5c}$$

We begin our analysis by finding a set of steady state solutions to eqs. (3.5a–3.5c) of the form $\tilde{\mathbf{E}} = \bar{\mathbf{E}}, \tilde{\mathbf{P}} = \bar{\mathbf{P}}, \tilde{\mathbf{D}} = \bar{\mathbf{D}}$. This is done by setting the time and space derivatives to zero.

After some manipulation we have

$$\bar{\mathbf{D}} = \frac{l_0}{T_2} - \frac{\tilde{\gamma}\bar{\mathbf{E}}^2}{T_2} \tag{3.6a}$$

$$\bar{\mathbf{P}} = \frac{i}{2}(l_0 - \tilde{\gamma}\bar{\mathbf{E}}^2)\bar{E} \tag{3.6b}$$

$$p + 1 = (1 - \frac{\tilde{\gamma}\bar{\mathbf{E}}^2}{l_0})(1 + \bar{\mathbf{E}}^2 T_1 T_2) \tag{3.6c}$$

We then rewrite eqs. (3.5a–3.5c) in terms of the steady state solutions plus a perturbation $\tilde{E} = \bar{E} + \delta\tilde{E}$, etc. Linearizing these equations with respect to the perturbations yield two sets of decoupled linear equations.

$$\partial_t \delta\tilde{\mathbf{P}}_I = \frac{1}{2}(\bar{\mathbf{D}}\delta\tilde{\mathbf{E}}_R + \delta\tilde{\mathbf{D}}\bar{\mathbf{E}}) - \frac{\delta\tilde{\mathbf{P}}_I}{T_2} \tag{3.7a}$$

$$\partial_t \delta\tilde{\mathbf{D}} = -T_2\bar{\mathbf{D}}\bar{\mathbf{E}}\delta\tilde{\mathbf{E}}_R - \bar{\mathbf{E}}\delta\tilde{\mathbf{P}}_I - \frac{\delta\tilde{\mathbf{D}}_I}{T_1} \tag{3.7b}$$

$$\frac{n}{c}\partial_t \delta\tilde{\mathbf{E}}_R = \partial_z \delta\tilde{\mathbf{E}}_R + \delta\tilde{\mathbf{P}}_I - (l_0 - 3\tilde{\gamma}\bar{\mathbf{E}}^2)\frac{\delta\tilde{\mathbf{E}}_R}{2} \tag{3.7c}$$

and

$$\partial_t \delta\tilde{\mathbf{P}}_R = \frac{1}{2}\bar{\mathbf{D}}\delta\tilde{\mathbf{E}}_I - \frac{\delta\tilde{\mathbf{P}}_R}{T_2} \tag{3.8a}$$

$$\frac{n}{c}\partial_t \delta\tilde{\mathbf{E}}_I = \partial_z \delta\tilde{\mathbf{E}}_I + \delta\tilde{\mathbf{P}}_R - (l_0 - 3\tilde{\gamma}\bar{\mathbf{E}}^2)\frac{\delta\tilde{\mathbf{E}}_I}{2} \tag{3.8b}$$

As well as being decoupled these are translationally invariant which suggests their eigenfunctions are plane waves i.e $\delta E_R(z,t) = \delta E_R(t)e^{ikz}$, etc. To determine the stability of the CW solution we calculate the Jacobian Matrix for the first set of equations

$$M = \begin{pmatrix} -T_2^{-1} & \frac{1}{2T_2}(l_0 - \tilde{\gamma}\bar{\mathbf{E}}^2) & \frac{1}{2}\bar{\mathbf{E}} \\ \frac{c}{n} & \frac{c}{n}(-\frac{1}{2}l_0 + \frac{3}{2}\tilde{\gamma}\bar{\mathbf{E}}^2 - ik) & 0 \\ -2\bar{\mathbf{E}} & \tilde{\gamma}\bar{\mathbf{E}}^3 - l_0\bar{\mathbf{E}} & -T_1^{-1} \end{pmatrix} \tag{3.9}$$

The CW solutions are stable if the real parts of all the eigenvalues are negative. To find an analytical solution we note that there are three frequency parameters T_1^{-1},T_2^{-1} and $\frac{c}{2n}(l_0 - 3\tilde{\gamma}\bar{\mathbf{E}}^2)$. Because the latter term is generally much smaller in typical QCLs we derive expressions, correct to the first order in l_0 and $\tilde{\gamma}$. With $l_0 = 0$ and $\tilde{\gamma} = 0$ the eigenvalue with the greatest real part is $\lambda_0(k) = -ick/n$. Putting $\lambda(k) = \lambda_0(k) + \lambda_1(k)$ back into the characteristic polynomial of M and equating the parts which are first order in l_0, $\tilde{\gamma}$ and λ_1 gives

$$\begin{aligned} \lambda_{max} = &- i\Omega - \frac{l_0 c}{2n}\frac{(\Omega T_1 + i)\Omega T_2 - 2(p-1)}{(\Omega T_1 + i)(\Omega T_2 + i) - (p-1)} \\ &+ \frac{(p-1)\tilde{\gamma}c}{2nT_1T_2}\frac{(\Omega T_1 + i)(3\Omega T_2 + 2i) - 4(p-1)}{(\Omega T_1 + i)(\Omega T_2 + i) - (p-1)} \end{aligned} \tag{3.10}$$

where $p = D_p/D_{th} - 1$ and $\Omega = kc/n$. Taking the real parts yields an expression for the parametric gain as a function of Ω which is the detuning from the lasing frequency.

$$\begin{aligned} g(\Omega) = &- \frac{l_0 c}{2n}\Re\Bigg[l_0\frac{(\Omega T_1 + i)\Omega T_2 - 2(p-1)}{(\Omega T_1 + 1)(\Omega T_2 + i) - (p-1)} \\ &+ \frac{\gamma\hbar^2)p-1)}{\vec{M}^2 T_1 T_2}\frac{(\Omega T_1 + i)(3\Omega T_2 + 2i) - 4(p-1)}{(\Omega T_1 + 1)(\Omega T_2 + i) - (p-1)}\Bigg] \end{aligned} \tag{3.11}$$

This function has a minimum at $\Omega = 0$ with maxima symmetric about it at

$$|\Omega_{max}| = \Omega_{Rabi}\sqrt[4]{\frac{2p}{p-1}} \tag{3.12}$$

where

$$\Omega_{Rabi} = \sqrt[4]{\frac{p-1}{T_1 T_2}} \tag{3.13}$$

The gain at this frequency is

$$g(\Omega_{max}) = \frac{l_0 c}{2n}\frac{T_2}{T_1}\left[3(p-1) - 2\sqrt{2p(p-1)}\right] + \frac{c\tilde{\gamma}(p-1)}{T_1 T_2} \tag{3.14}$$

Setting this to zero gives the instability threshold

$$p_{th} = 1 + 8\left[4\left(\frac{\hbar^2\gamma}{\vec{M}^2 T_2^2 l_0}\right)^2 + 12\frac{\hbar^2\gamma}{\vec{M}^2 T_2^2 l_0} + 1\right]^{-1} \tag{3.15}$$

This instability associated with the matrix M is present in all EC-QCL and is related to the Risken-Nummedal-Graham-Haken (RNGH) instability. RNGH is present even in the absence of a SA effect with an onset occurring at 9 times the lasers threshold current (see fig.3.1a). Real QCL devices can't be driven at such high levels. The effect of a SA is to reduce this instability threshold towards laser threshold (see fig.3.1b). This instability is characterised by the development of Rabi sidebands around the CW mode which are caused by rapid coupled oscillations between the population inversion and the material polarization[3].

For the case of the ridge laser, or the linear EC, equations equivalent to eqs. (3.5a–3.5c) are

$$\frac{n}{c}\partial_t \tilde{\mathbf{E}}_\pm = \mp\partial_z \mathbf{E}_\pm - i\tilde{\mathbf{P}}_\pm - \frac{1}{2}l_0\tilde{\mathbf{E}}_\pm \tag{3.16a}$$

$$\partial_t \tilde{\mathbf{P}}_\pm = \frac{i}{2}(\tilde{\mathbf{D}}_0\tilde{\mathbf{E}}_\pm + \tilde{\mathbf{D}}_2^\pm\tilde{\mathbf{E}}_\mp) - \frac{\tilde{\mathbf{P}}_\pm}{T_2} \tag{3.16b}$$

$$\partial_t \tilde{\mathbf{D}}_0 = \frac{\tilde{D}_p - \tilde{\mathbf{D}}_0}{T_1} + i(\tilde{\mathbf{E}}_+^*\tilde{\mathbf{P}}_+ + \tilde{\mathbf{E}}_-^*\tilde{\mathbf{P}}_- - c.c.) \tag{3.16c}$$

$$\partial_t \tilde{\mathbf{D}}_2^\pm = \pm i(\tilde{\mathbf{E}}_+^*\tilde{\mathbf{P}}_- + \tilde{\mathbf{P}}_+^*\tilde{\mathbf{E}}_-) - \frac{\tilde{\mathbf{D}}_2^\pm}{T_g} \tag{3.16d}$$

To account for the possibility of spatial hole burning we include $D_2^{\pm}$, where the superscript $\pm$ represents complex conjugate pair, which is the envelope of the inversion grating and is assumed to be of the form[1] $D_2(z,t) = D_2(t)e^{2ikz}$. T_g is introduced and is the lifetime of the gain grating which depends on carrier diffusion

$$T_g^{-1} = T_1^{-1} + 4k^2D \tag{3.17}$$

where D is a diffusion coefficient. The treatment follows the case of the ring cavity except now with perturbations for both propagation directions modelled explicitly. Once spilt into real and imaginary components the system can be described by seven equations. Again, there are two sets of decoupled equations. A generalized parity operator is defined which reflects the z-axis about the centre of the cavity and swaps the propagating directions for the quantities $\tilde{\mathbf{E}}, \tilde{\mathbf{P}}$ and $\tilde{\mathbf{D}}$

$$PX_{\pm}(z,t) = X_{\mp}(L-z,t) \tag{3.18}$$

Since the equations commute with P they can be expressed in eigenstates of P. In this case for each set of equations there is one non trivial solution which is assumed. This allows the equations to be reduced to one propagating direction. In this case two Jacobians are produced for stability analysis

$$M_1 = \begin{pmatrix} -T_2^{-1} & \frac{l_0}{2T_2} & \frac{1}{2}\bar{\mathbf{E}} & \frac{1}{2}\bar{\mathbf{E}} \\ \frac{c}{n} & \frac{c}{n}(-\frac{1}{2}l_0 - ik) & 0 & 0 \\ -4\bar{\mathbf{E}} & -2l_0\bar{\mathbf{E}} & -T_1^{-1} & 0 \\ -2\bar{\mathbf{E}} & -l_0\bar{\mathbf{E}} & 0 & -T_g^{-1} \end{pmatrix} \tag{3.19}$$

and

[1]Higher order term (e^{4ikz}, e^{6ikz}, etc) may also become significant in high fields but would make analysis difficult

$$M_2 = \begin{pmatrix} -T_2^{-1} & \frac{l_0}{2T_2} & \frac{1}{2}\bar{\mathbf{E}} \\ \frac{c}{n} & \frac{c}{n}(-\frac{1}{2}l_0 - ik) & 0 \\ -2\bar{\mathbf{E}} & -l_0\bar{\mathbf{E}} & -T_g^{-1} \end{pmatrix} \tag{3.20}$$

M_1 relates to the RNGH instability while M_2 relates to SHB. For the case where $T_g = T_1$ eq. (3.19) gives a threshold identical to eq. (3.14) without a SA effect ($\gamma = 0$). Solving eq. (3.20), as before, yields a parametric gain of

$$g(\Omega) = -\frac{l_0 c}{2n}\Re\left[1 + \frac{3i(i + \Omega T_1) - (p-1)}{3(i + \Omega T_2)(i + \Omega T_2) - (p-1)}\right] \tag{3.21}$$

This describes the parametric gain associated with SHB for $T_G = T_1$ which is the limit of zero carrier diffusion.

Fig. 3.1 shows a plot of the parametric gain associated with M_1, which is caused by the RNGH instability. Fig. 3.1b shows that the instability threshold is reduced when a saturable absorber (SA) term is included.

Modelling the dynamics of continuous-wave QCL systems in this way provides insight into the origins and behaviour of these well established instability mechanisms. What's clear from this approach is that instability mechanisms in QCL systems cannot be considered independently, as is shown for the case of SA effects on the RNGH instability. Previous experimental studies have observed the onset of an RNGH like instability occurring at thresholds well below those predicted by theory[2]. Accounting for this much reduced threshold would require significant SA effects to be present in the QCL device. While this might be possible in normal narrow ridge devices, this has also been observed in buried structures where the effect should be relatively small. This assumes Kerr soft lensing is the dominant SA mechanism which would be heavily dependent on modal overlap with the metallic contacts.

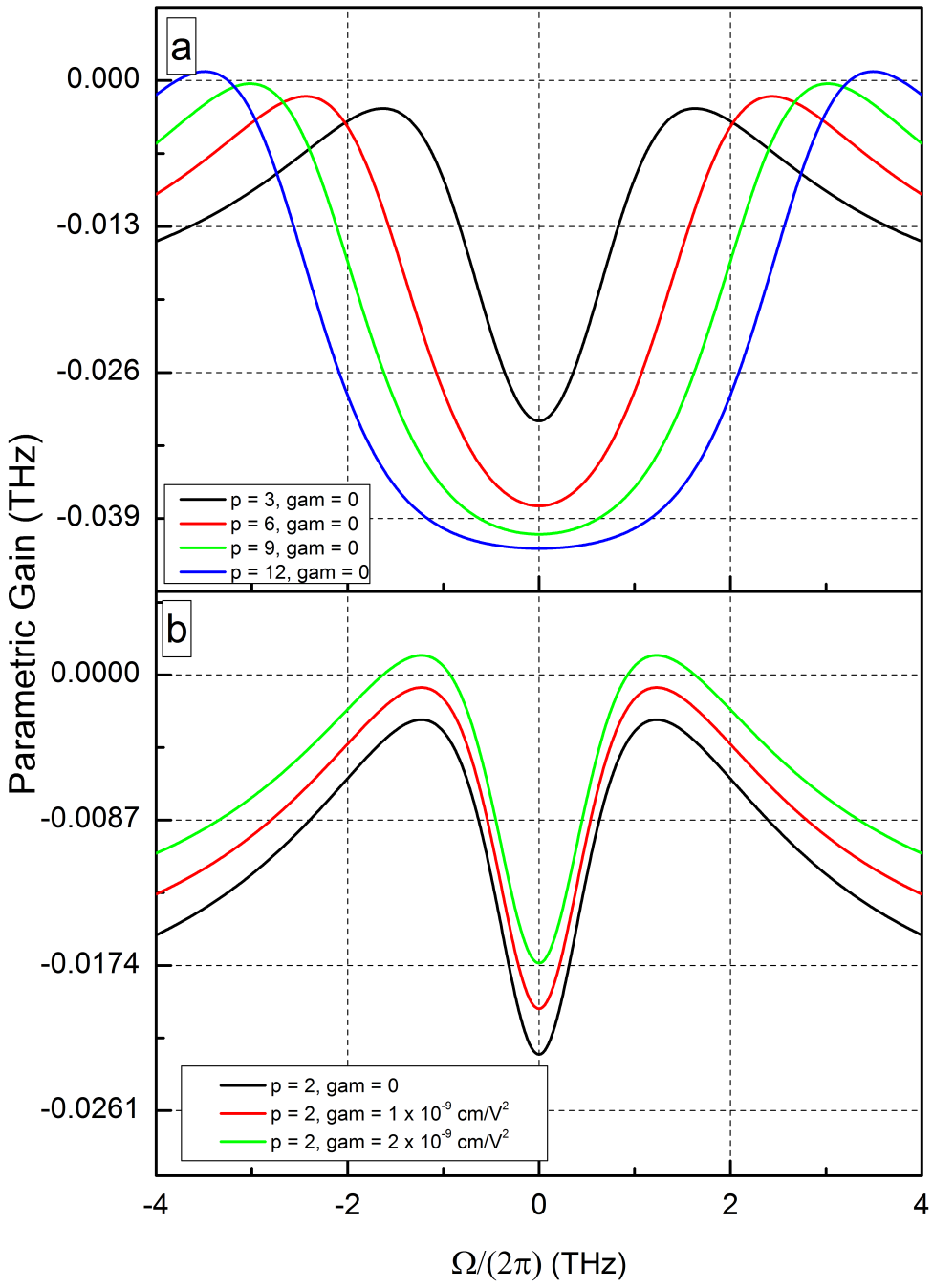

Figure 3.1: **a:** Parametric gain in the absence of SA effect. This is due to the RNGH instability with an onset at nine times the threshold pumping factor. **b:** The effect of a SA effect for a fixed pumping factor. Here the parametric gain is increased in a frequency independent fashion, lowering the instability threshold of the pumping factor nearer to lasing threshold.

Recent theoretical studies have drawn into question the established understanding of the RNGH instability in QCLs[3]. Their work suggests that SHB may be the dominant mechanism responsible for the *low threshold* RNGH onset. While there is more work to be done before the exact roles of these phenomena are understood, clearly the tendency is for these mechanisms to couple, reducing their respective onset thresholds and causing complex dynamic behaviour. Unlike other instabilities which are intrinsic to QCL devices, SHB can be suppressed using ring cavities. If these most recent studies are correct, developing ERC-QCLs would not only improve stability in continuous-wave QCL systems by suppressing SHB, but could also increase the observed low threshold RNGH instability outside the practical driving range of the device.

3.3 System

The continuous-wave system used for this work inherited much from the previous setup used for the pulsed measurements in chapter 2. This includes the planar mirrors, the beam splitters and the lens holding assembly. The major difference was the redesign of the laser mounting assembly to accommodate a thermoelectric cooler (TEC) module and water-block. These would be used to stabilize the temperature of the QCL. This was deemed necessary considering the additional heat dissipation that comes from the DC levels needed to sustain a continuous-wave regime. The key to room-temperature continuous-wave operation of an ERC-QCL is the QCL, or gain medium, itself. In this work a number of high performance buried structure QCL from Alpes Lasers are used. All of these devices had the same centre wavelength of 5.3 μm.

During fabrication buried structure QCLs have an additional iron doped indium phosphide (InP:Fe) regrowth phase after the ridge has been etched. This material covers the lateral walls of the waveguide and aids in heat extraction from the gain medium by providing a thermal bridge to the substrate. In normal ridge devices these walls are surrounded by ambient air, which is a relatively poor thermal conductor. The resulting reduction in thermal impedance between the ridge and the substrate greatly improves the device's thermal performance. This makes these types of QCLs ideal for use in a continuous-wave system. One further benefit of the regrowth is that it causes the facet to extend beyond the waveguide ridge. This is beneficial when applying anti-reflection coatings to the facet that would otherwise suffer from edge effects during deposition that can reduce the coatings effectiveness. The larger facet created by the regrowth ensures that ridge receives a uniform coating. Fig. 3.2 shows an SEM image of a buried structure QCL after a gas phase InP:Fe regrowth.

These devices were all AR coated on both facets to supress their FP action. The AR coatings, applied by Helia Photonics, are comprised of a 411 nm layer of Yttrium Flouride (YF_3) and a 180 nm layer of zinc selenide (ZnSe). A 5 nm layer of Yttrium oxide (Y_2O_3) is used as an adhesion layer between both the substrate and YF_3 and between the YF_3 and ZnSe.

These coatings are essential where unidirectional emission is sought as any resid-

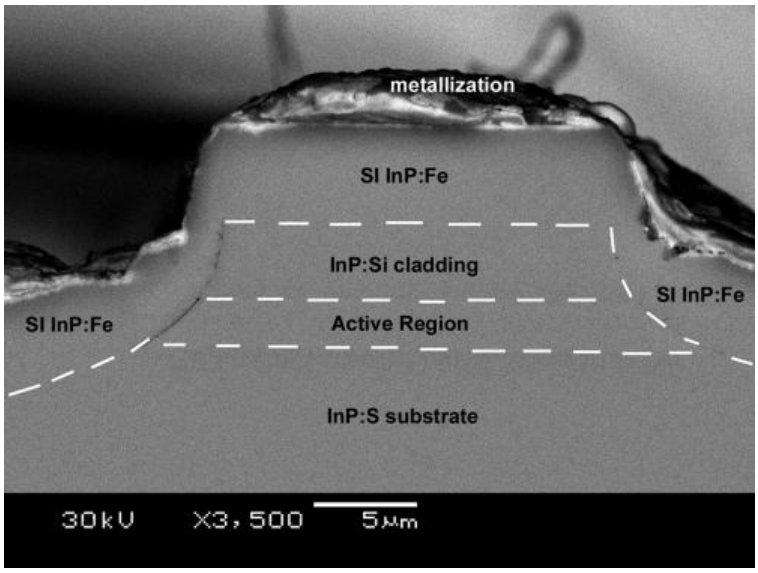

Figure 3.2: Scanning electron microscope image of a cleaved facet from a buried structure QCL[4]. Top contact metallization is alloyed into a highly doped upper cladding region, allowing efficient charge injection into the active region.

ual reflectance of the facets would cause coupling between the propagation directions by reflecting one into the other. Even small residuals can cause phase locking between the two propagation directions. This isn't particularly important if the residual is low enough to produce the level of decoupling needed to support unidirectional emission.

Fig. 3.3 shows the basic apparatus used to take measurements of the continuous-wave system. For clarity this is shown in a linear setup but the ring cavity case is otherwise similar. Unlike in the case of pulsed emission, continuous-wave work necessitates the use of an optical chopper. The AC coupling of the detector makes it impossible to measure continuous, constant intensity, emission which, without a chopper, would be indistinguishable from zero emission.

Fig. 3.4 illustrates the convention used to designate the two propagation directions when in a ring configuration. Clock-wise (CW) propagates through the QCL left to right, while counter-clock-wise (CCW) propagates through the QCL right to left. Rotating the beam-splitter 90 degrees would result in these outputs being reversed but the convention holds when the beams are described by the direction they travel through the QCL gain medium.

№	Name	Notes
1	QCL	Alpes Buried structure. 5.3 μm centre wavelength. Double AR coated. Indium soldered epi-layer up to a copper submount and wire bonded to a bonding pad.
2	Copper Mount	Supports submount while acting as a heatsink, thermal compound is applied between this and the submount.
3	Thermo-Electric Cooler (TEC)	40 x 40 mm^2 138 W generic module. Thermal compound is applied to both sides of the TEC module.
4	Waterblock	Cools TEC modules hot side. Connected to a passive heat exchanger.
5	Aspheric Lenses	Thorlabs Molded Black Diamond (C036TME-E) EFL: 4 mm, NA: 0.56, AR coated for 3 – 5 μm. Held in place by various X-Y-Z stage assemblies.
6	Mirrors	25 mm planar circular unprotected silver.
7	Beam Splitter	0.5 mm thick single-side AR coated CaF_2 window.
8	Detector	Vigo Systems 2 stage TEC cooled Fast MCT detector. 4 ns rise time, 300 MHz bandwidth.
9	Pulsed Laser Driver	Avtech AV-1011-C used for pulsed measurement and alignment.
10	Bench Supply	Provides the DC used to drive the laser CW. A similar supply is also used to drive the TEC module.
11	Oscilloscope	Techtronix TDS 3032C 300 MHz bandwidth, 2.5 GSPS.
12	Spectrum Analyzer	HP E4411B 1.5 GHz bandwidth.
13	FTIR	Brucker iFS 66v/s 0.25 cm^{-1} resolution.
14	Optical Chopper	Used to chop beam during CW measurements.

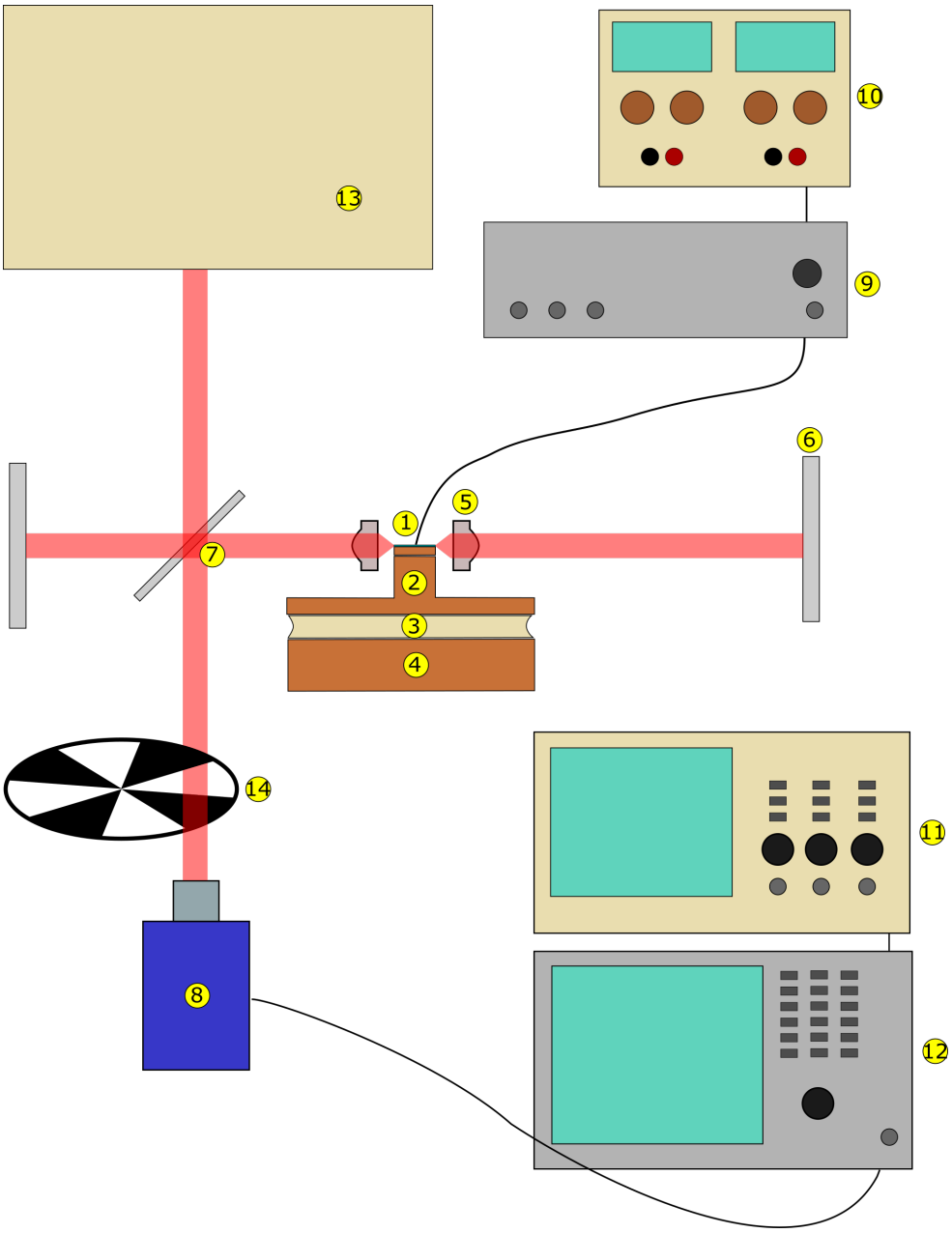

Figure 3.3: Schematic arrangment of appuratus for measurements of a Linear external cavity QCL.

3.4 I-V Characteristics

The I-V characteristics of EC-QCL systems are largely similar to ridge QCLs. The high impedance at low voltage gives way to a conductive region where the dependence is reasonably linear over the usable range of the device. This knee in the I-V curve is a consequence of super-lattice band alignment which is a key to QCL functionality. In contrast to ridge QCLs where, for a given temperature, a single I-V

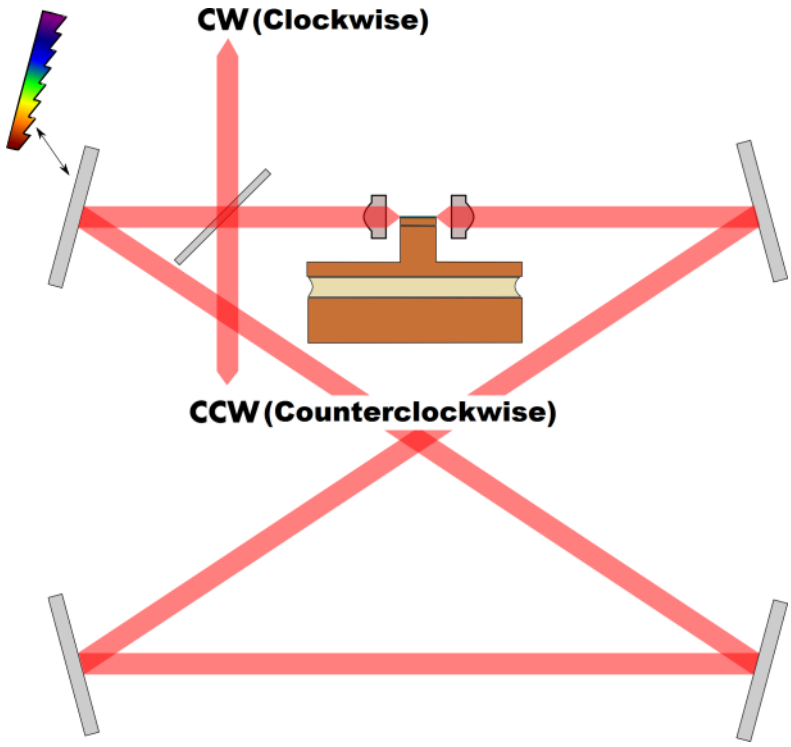

Figure 3.4: Ring cavity arrangement. All other test equipment is arranged similar to the previous linear setup. This shows the convention on designating propagation directions for the ring cavity. Also showing the placement of the diffraction grating used for the tuning measurements. The cavity is aligned with 4 planar mirrors and then the grating replaces the top left mirror.

curve describes the electrical characteristics of the system, external cavities allow an additional degree of freedom in the coupling. The difference between the case where the cavity is allowed to lase and one where the cavity is completely blocked is shown in fig.3.5. The conductance of the device is increased in the presence of a resonant laser field which modifies the electron transport properties of a biased device. Lifetimes of electrons in the upper laser state will depend upon resonant field intensities and will be reduced significantly when high optical fields exist within the waveguide. This behaviour is fully expected by all QCL transport models[5]. Steady state analysis of 3 or 4 level systems shows that the stimulated emission process depopulates the ULL at a rate proportional to the field intensity. In good quality QCL structures this mechanism can become dominant over non-radiative scattering of the ULL populations which are usually designed to be long lived (>5 ps). As would be expected this splitting begins at laser threshold, when the intra-cavity field becomes significant, and increases with intracavity power. Around the laser's

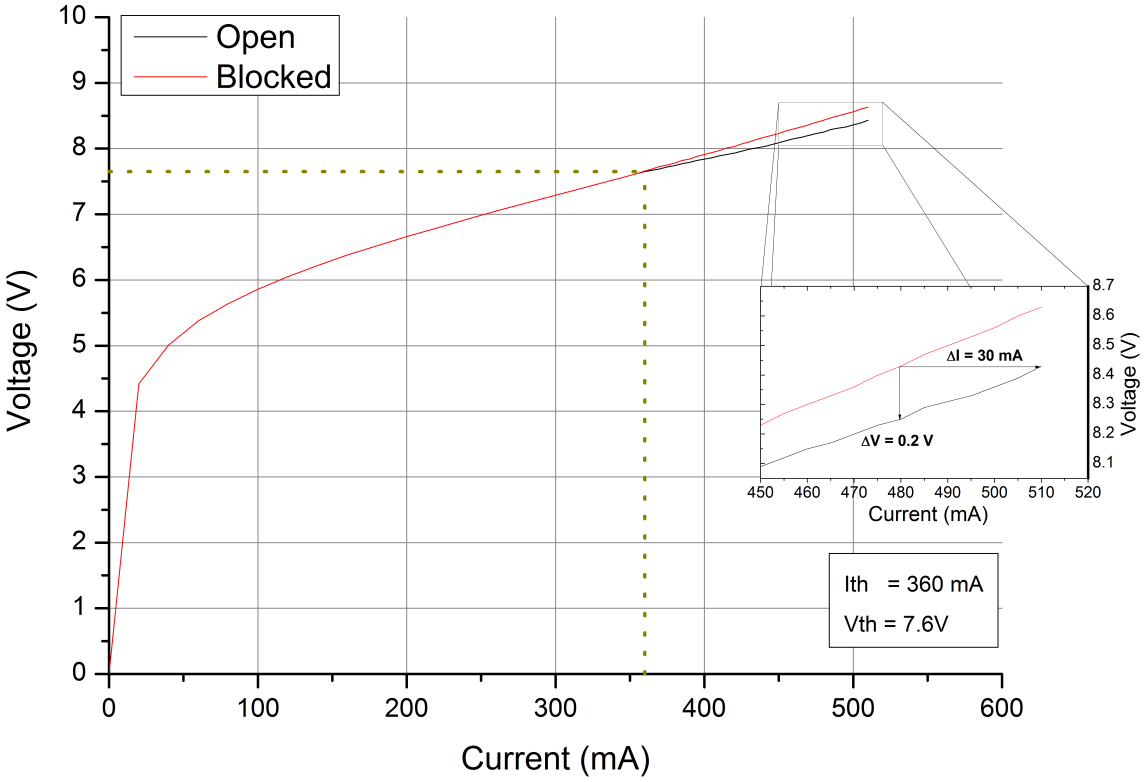

Figure 3.5: I-V curve of an external Linear cavity QCL. An Alpes single spatial mode buried structure with both facets anit-reflection coated shows the classic QCL non ohmic I-V dependance. Inset: The difference in voltage and current between the blocked an unblocked case.

normal operating point the difference is considerable(see inset fig. 3.5), around 30 mA or 0.2 V depending upon the driving source type. At these levels it conceivable that this effect could be utilized in a number of ways useful to QCL laser systems. Firstly driving the device with a constant current source would allow the voltage signal to be used as part of a self-alignment mechanism. If the intra-cavity beam was mechanically chopped an AC signal proportional to the field intensity would be generated that could be used to confirm lasing or set power levels. The advantage here is that no external detector is required to perform these operations. Generally, above threshold, the voltage required to maintain a constant current is dependent on cavity losses. High quality drive electronics may allow intra-cavity absorption to be monitored directly from the driving voltage.

More generally, this effect could be exploited in a way that allows the same

QCL device to act as both a source and a detector. The interest here being in the realisation of on-chip sensors made from a single substrate. Other groups[6] have developed bi-functional QCL structures which act as both a QCL in a biased state and a same frequency photo-detector in an unbiased state. What's proposed here is different in the sense that the QCL would both emit and detect in a biased state. This could be problematic due to the biased device emitting even when being used as a detector, although this could be mitigated using optical isolation or temporally separating the emission and detection phases using a long path length cavity.

One further novel use for this effect might be in the realisation of an opto-electronic oscillator(OEO). By integrating the QCL into an electrical resonant tank, or oscillator, and with a suitably sized external cavity, it should be possible to create stable coupled oscillations in both the optical and electrical domains. These type of oscillators generate their signals based on the transit time of light around some optical path. This optical basis makes them useful as high precision local oscillators due to their increased immunity from electrical interference. The system would be useful in its own right as an OEO, with only a single active device it would represent an improvement on other systems which rely on separate sources and detectors. In this case it might be possible to use the system as an industrial sensor which could simultaneously measure two quantities in real-time. The frequency of oscillation would provide a measure of the optical path length, this would reveal the refractive index of a gaseous or liquid medium, while the attenuation could be used to measure concentrations of a particular analyte.

3.5 Uni-directionality

The key characteristic of external ring cavity QCLs that makes them a promising mid-infrared source for high resolution gas spectroscopy is their ability to support unidirectional emission regimes. In a purely unidirectional regime, where light propagates around the ring in only one direction, emission exists as a travelling-wave as opposed to the standing-wave regimes of linear resonators. Operating in a travelling-wave regime avoids entirely the spatial hole burning (SHB) instability which can introduce noise into the output of laser systems based on linear cavity geometries.

A ERC system able to operate in a unidirectional regime should, in principle, have lower intrinsic noise levels than the linear Littrow type systems which are currently the standard.

3.5.1 Spatial Hole Burning

Spatial hole burning (SHB) is present to some extent in all linear laser resonators where the lasing mode is defined by a standing wave pattern. In a classic two mirrored resonator standing waves form the solutions of the resonator modes. Like all standing waves, they can be considered to be comprised of two counter-propagating fields, one in each direction along the longitudinal component of the lasing mode. The reflection that occurs at the boundary of the resonator couples one propagating direction into the other and, under steady state conditions, ensures a fixed phase relationship exists between them.

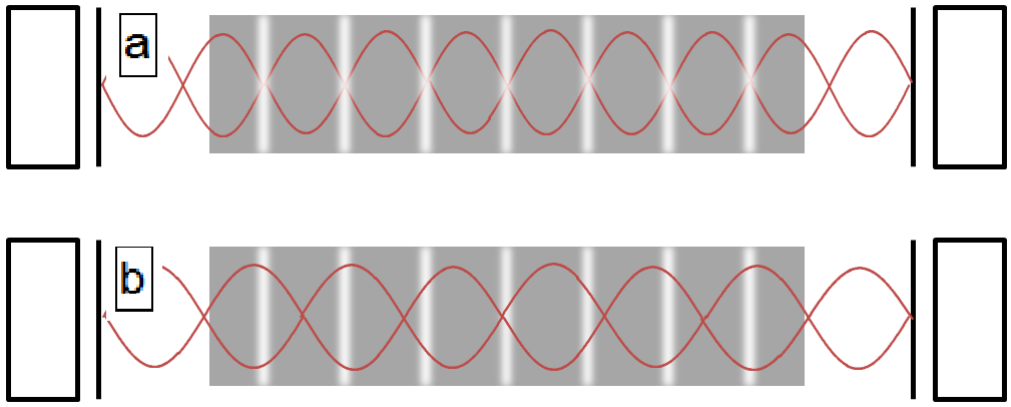

Figure 3.6: **a:** The preferred lasing mode creates a gain grating with the light coloured bands showing where gain remains undepleted at the nodes of the mode. **b:** An adjacent cavity mode is now able to access these areas of increased gain.

In Fabry-Perot lasers this mechanism gives rise to the longitudinal mode structure which is comprised of the solutions to the slab dielectric waveguide. In the case of an external linear resonator the same principle applies except the coupling from one propagating direction into the other occurs outside the gain medium. The nodes and antinodes of the standing wave, points of zero and maximum field intensity respectively, will remain stationary along the length of the resonator. This can lead to

spatially inhomogeneous carrier concentrations along the length of the gain medium. An ideal gain medium would have, amongst other things, a homogenous gain profile throughout the waveguide which remained constant even after a stimulated emission process had occurred. This would amplify the waves in a non-distorting fashion. In reality semiconductor lasers, including QCLs, operate with an inhomogeneous gain profile which affects the stability of the emission and can produce noise in the desired lasing mode. Unlike other sources of instability, the onset of SHB can occur at driving currents just above laser threshold[2].

A more realistic gain profile can be found by considering two counteracting mechanisms within the gain medium. Firstly, the laser field tends to consume the gain by resonantly depopulating the ULL through the stimulated emission process. This preferentially occurs at the antinodes of the standing waves where the field is at its highest intensity. The result of this is a population grating that shares its periodicity with the standing mode that created it. Carrier diffusion, on the other hand, tends to wash out this gain grating as ULL electrons migrate from the nodal regions, where their interaction with the field is minimal, into the depleted regions. Under steady state conditions the magnitude of the gain grating will depend on these two things and are characteristics of the device and the operating point.

The effect of the gain grating is to destabilise the lasing mode in two different ways. The foremost effect is due to the reduction in the modal gain. With the gain depleted regions coinciding exactly with the current lasing mode, adjacent cavity modes could potentially experience increased gain, causing them to lase. Additionally, because the waveguide region has developed this well-defined periodicity, the gain grating can cause the propagating wave to experience a back scattering in a way analogous to electrons in a crystal lattice.

Despite this, the consequence on real world QCL laser systems is, at worst, to introduce an additional source of noise. While it may be significant in some applications, many QCL based systems are successfully employed in high resolution gas spectroscopy without any mechanism to mitigate the effect of SHB. Clearly, where ultra-sensitive detection is sought, SHB suppression is technologically desirable. The advantage of ERC systems is their ability to support unidirectional emission which suppresses the SHB instability by avoiding the standing wave pattern that gives rise

to it. This means a system based on a ring geometry could, in principle, provide a source for high-resolution gas spectroscopy with lower noise (amplitude, phase, frequency) levels than its linear counterpart.

3.5.2 Travelling Waves

External ring cavities (ERCs), when compared to linear External cavities (ECs), are generally more difficult to align and maintain the alignment, suffer from greater cavity losses due to the increased number of mirrors and are more difficult to wavelength tune. The advantage, as far as sources for MIR spectroscopy is concerned, lies in the fundamentally different boundary conditions that are created in a ring geometry.

In a linear configuration, including as cleaved Fabry-Perot ridges, photons of one propagating direction are constantly being coupled into the opposite direction. This along with the associated phase shift that occurs at the mirror surface produces the standing wave pattern. This is not the case in a ring geometry. In an ideal sense, like in a good quality micro ring resonator or in an ERC where AR coatings entirely suppress reflections at the facet, the two propagating directions become decoupled. A photon propagating in one direction has no possibility of being reflected into the other. This decoupling destroys the fixed phase relation between the two directions. Even though no 'hard' fixed phase relation exists, two travelling waves of the same wavelength and spatial mode will create standing waves in the waveguide as they pass each other. These phases could, in principle, drift over some time scale but it's more likely that spurious reflections will phase lock the two directions regardless.

Real world AR facet coatings can have a residual reflectance of the order of 1% and this can also be true of other optical elements used in the ERC which would ideally be completely non-reflective. Parasitics of this order usually aren't sufficient to prohibit the effects of decoupling which allows for asymmetries to develop between the two propagating directions. A difference in amplitude in one of the directions will lead to a reduction in the standing wave ratio (SWR) of the laser field in the gain medium.

3.5.3 Asymmetry

The limit of propagating asymmetry is reached when the laser emission within a ring cavity becomes unidirectional, that is when one propagating direction is shut down entirely. One way to conceptualise this process is in a similar fashion to how free running lasers come to emit on single longitudinal mode. This occurs through a process of gain competition where a mode of even modestly greater amplitude has a higher probability of interacting with the gain medium and as a result consumes more gain, eventually "starving" other modes. This run-away process, seeded by noise, quickly selects modes and would account for unidirectionality when sufficiently decoupled. In modal competition, gain dispersion plays a significant role in selecting an emission wavelength, usually favouring a prefered band near the central peak of the gain bandwidth, where no tuning elements are present. In unidirectional lasing the system does seem to posses a prefered direction. Turning the gain medium around 180° switches this direction which suggests that the main source of this asymmetry is the QCL chip itself. The most likely explanation is a small difference in the level of residual reflectance seen at each facet. Despite favouring one direction, unidirectional lasing is usually observed in both directions, with a tendancy to switch suddenly[7]. This is particularly true during changes in driving current and adjustments to the system's alignment. Fig. 3.7 shows a typical response and is comprised of a region after threshold where the two propagating directions share a common power level. At around 415 mA the two directions begin to diverge and have a peak power ratio of around 20:1. In other data runs ratios as high as 100:1 were observed. The difficulty here lies in measuring this behaviour accurately when only one power meter can be utilized. This means one direction must be measured over the full current range followed by the other. The switching behaviour shown in this figure is a stochastic process which like other ERC characteristics is extremely sensitive to conditions such as temperature and mechanical stability. Additionally, the switching from the prefered to non prefered direction can be short lived (<1 s) which makes it difficult for the power meter to register an accurate reading. It's highly likely that if two ideal power meters could be used to measure simultaneously, both switching times and power would coincide perfectly. From the data gathered it would seem that the total output power follows a traditional linear light-current

dependence, seen from most semiconductor ridge lasers, except with the possibility that the power is divided unevenly between the directions. There also exist examples where at some current above the splitting point the two directions again become equal for some current range. The different forms and power ratios are largely alignment dependent. In these highly unidirectional states the majority of the laser field in the gain medium exists as a travelling wave. This sweeps through the waveguide rapidly and consumes the gain in a more uniform manner rather than at points centred around the modal antinodes. Being able to access, more readily, the gain available at the nodes of the standing waves likely forms part of the mechanism that promotes one direction over the other. A propagating direction with a smaller amplitude can be decomposed into only a standing wave component, whereas the greater amplitude direction can be decomposed into an equal standing wave component and some traveling wave component. It's this travelling wave component that can access the most fertile regions of the gain medium.

Unidirectionality, in this sense [2], doesn't offer any real control method over the power distribution and tends to spontaneously collapse into some level of asymmetry. For a system to operate with the full benefits of SHB free emission then a total shutdown of one propagating direction is desirable. In reality this is difficult to achieve. Some power will always be present in to non-prefered direction owing to spontaneous emission and parasitic reflectances. Electro-luminesence (EL) will be created randomly through spontaneous emission processes which produce some background power. However, this is an incoherent process and doesn't contribute to SHB. Parasitic reflectance, on the other hand, does contribute to standing waves by coupling highly coherent light from the prefered direction into the other. The most significant source of this is the residual facet reflectivity from imperfections in the AR coatings. The residual reflectance will dictate the miniumum amount of power present in the non-prefered direction and, as a consequence, the extent of the gain grating created in the gain medium. Where high levels of SHB supression are

[2]Unidirectional lasing can also be forcably achieved using an optical isolator. These devices, based on Verdet crystals, can be introduced into the cavity allowing the field to propagate in a prefered direction with only modest loses while introducing as much as 30 dB of attenuation in the non-prefered direction. This level of isolation is likely to be much greater than what is needed to ensure reliable unidirectional lasing.

sought, good quality AR coatings are likely to be the key.

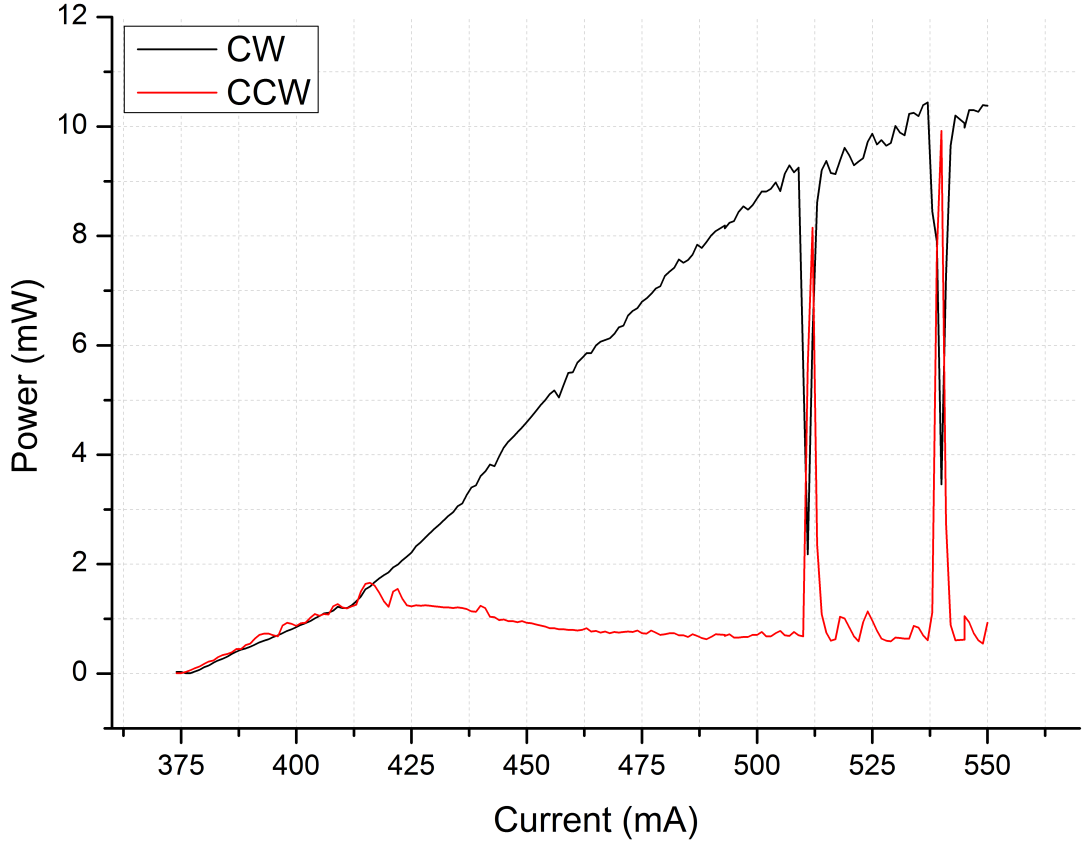

Figure 3.7: Light – Current dependence of an external ring cavity QCL. A double AR coated Alpes single spatial mode QCL with a centre wavelength of 5.3 μm is driven continuous-wave. A Labview program increments the driving current to the QCL while the output power is measured in both the clockwise (CW) and counter-clockwise (CCW) propagation directions by a thermopile detector.

3.6 Spectral Response

The spectral performance and control offered by external cavity QCL systems, when compared to ridge devices, increasingly drive their use in high resolution gas spectroscopy. Here we study the response of an untuned system, that is a system without any wavelength selective element, in both a linear and ring cavity configuration. No practical systems operate in this way but study here can help understand the under-

lying processes which QCL based systems are subject to. To gain any useful insight, a clear conceptual basis must be formed of the factors influencing the behaviour of these untuned systems. All lasing is based on regenerative noise amplification and as a result the spectral evolution of these systems is a deeply stochastic process. There can for a given laser, temperature, alignment,etc be a number of evolutionary paths the system is likely to access. Transient conditions exist during laser startup for up to a few milliseconds. The end point is a steady state that is arrived at when transient thermal effects have settled. The main contributors to the gain spectrum are:

1. **External cavity modes** – These dictate the allowed lasing wavelengths for a given cavity length. These allowed modes are the basic resonances of the external cavity which for most cavaties are very closely spaced. For example, the free spectral range (FSR) of a 1 m cavity is approx 300 MHz or 0.01 cm^{-1}. This is beyond the resolvable bandwidth of all but the biggest FTIRs.

2. **Gain Bandwidth/Dispersion** – This is the most significant factor in the wavelength selection of an untuned system. Generally, in QCLs, this function is a broad single peak which in high performance QCLs can be over 100 cm^{-1} in width. This characteristic makes QCLs appropriate as a tunable source, able to support lasing across a broad wavelength range. A real world QCL can have a more complex gain function, composed of sharp features around its central peak. While the tails of the bandwidth invaribly fade to zero gain, the central part can have a number of similar amplitude peaks.

3. **Etalon effects** – Imperfect AR coatings can produce etalon effects in a number of optical components. This essentially places other cavaties, albeit with a low finess, within the external cavity. These will produce a filtering effect which can have a significant bearing on the lasing evolution. The two most problematic examples are the QCL itself, which for a 4.5 mm QCL has a FSR of about 0.35 cm^{-1}, and the beam splitters. Uncoated windows such as CaF_2 can have a very strong etalon effect due to their high parallelism. With a reflectivity of 2 – 7 % these elements can have a dominant effect on emission. Even with a single side AR coated for a given angle it possible to leave some

residual effect. A 0.5 mm CaF_2 at 45° would have a FSR of approx 8 cm^{-1}. Imperfections in AR coatings are also likely to be highly dispersive meaning their finess will vary across the gain bandwidth of the laser. In complex systems with many optical elements this can cause strong features where the fringes from a number of etalons coincide.

4. **Atmospheric Absorption** – The free air coupled nature of EC systems introduces another influence on the emission wavelength of an untuned system. The large pathlength propagating through the air means atmospheric constituents with resonances in the the wavelength range of the gain bandwidth attenuate some spectral components of the beam. These can be very narrow absorption line through to broader features which can inhibit lasing over a significant band. In practical spectroscopic EC systems this problem is usually solved by enclosing the free air coupled parts in a purgable container. Inert gases such as N_2 are transparent over the Infrared region.

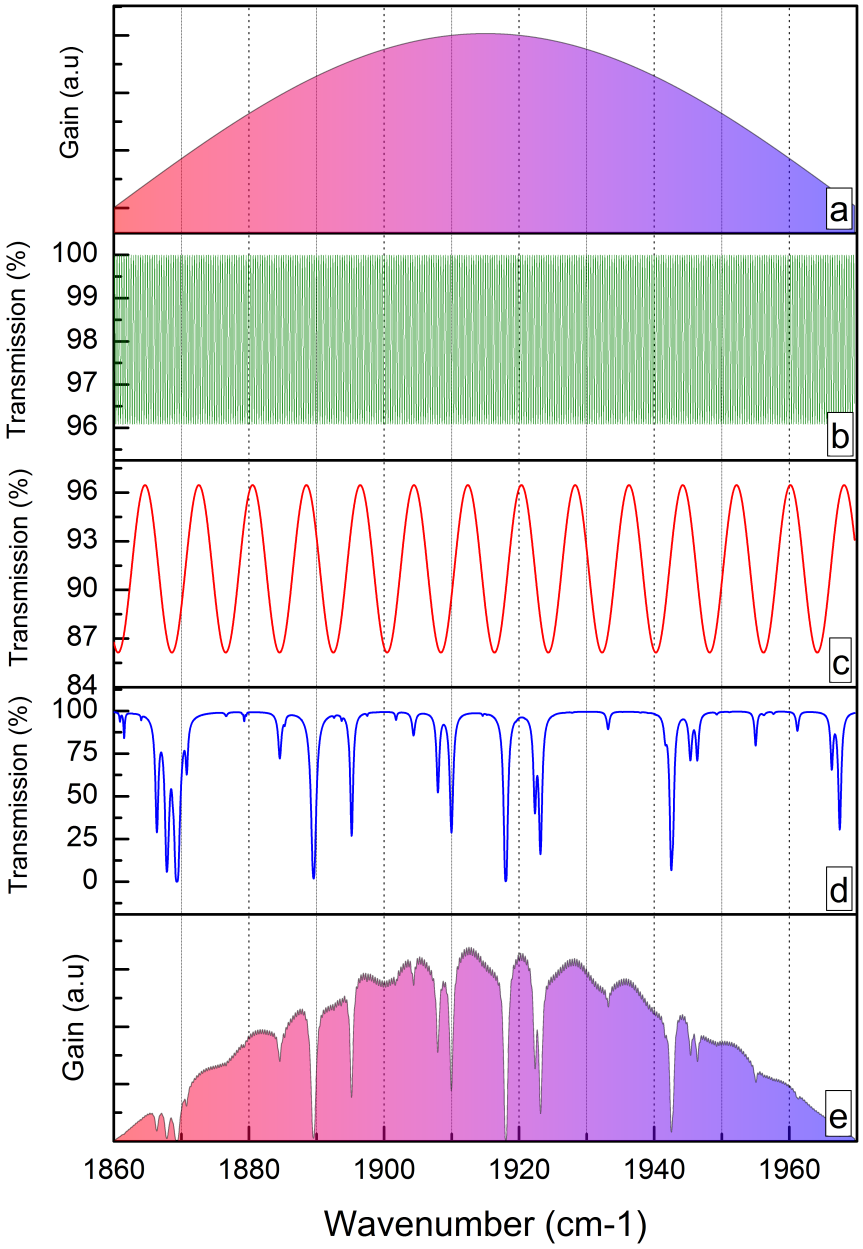

Figure 3.8: **a:** General form of the gain of a QCL centred around 5.3 um wavelength.**b:** Etalon effect caused by a residual facet reflectivity of 1% with a ridge length of 4.5 mm. FSR = 0.347 cm^{-1}. **c:** Etalon effect caused by a 1% residual reflectance of the AR coated side of a 0.5mm CaF_2 beam splitter at 45° AOI. FSR = 7.96 cm^{-1}. **d:** Approximate form of water transmission for a 220 cm ring cavity under standard atmospheric conditions. This is based on a simple lorentzian self-broadening of a line-list taken from the HITRAN database. **e:** The general form of the gain spectrum based on the previous factors.

Fig. 3.8 shows the calculated transmission functions for a number of effects present in our cavity. Fig. 3.8e gives a sense of the overall transmission function experienced by light traversing the cavity. The combination of these effects can be to produce a complex probabilistic emission spectrum. This randomised process occurs each time the laser has threshold gain but isn't already lasing. This is the case at startup, when the laser is first turned on. It also occurs if the beam is broken which has the effect of 'resetting' the system. If this is done repeatedly, a number of different evolutions can be observed, characterised by different emission amplitudes and wavelengths. The system shows high levels of hysteresis and when well stabalised can lase on the same single mode almost indefinately. If, on the other hand, there is some mechanical or thermal drift present in the system, the emission can be observed to hop periodically. This can be due to a change in ambient temperature or even the slightest movement of the optical stages. Only a very small difference is needed to shift the cavity mode positions and cause the overall gain function to change considerably, favouring a different wavelength. These behaviours are present in both EC and ERC-QCLs and are likely to begin when the lasing photon population is driven into a lossy condition. The difference between these two platforms is, as previously mentioned, the presence of SHB in linear type EC systems. Interactions between counter-propagating field components are increased in single spatial mode lasers. Buried structures which can support higher order spatial modes tend to have similar threshold levels across all spatial modes which can reduce the effect of SHB by reducing the spatial overlap between spatial modes in the waveguide. Fig 3.9 shows the case of a single spatial mode laser in a high coupling regime, conditions under which the effects of SHB are expected to be greatest.

Clearly some significant perturbing effect exists which leads to lasing on multiple wavelengths simultaneously over large parts of the driving current range. Where this occurs emission peaks have a broader base and noisier floor in the surrounding spectral region. This may be indicative of switching or instability rarther than emission in a steady state. At current values where a single peak exists, the peak appears narrow. This is the form of emission expected for a laser emitting on a single longitudonal mode. It's impossible to say whether or not the system lases on a single longitudonal cavity mode because the cavity mode spacing, which is 100 -

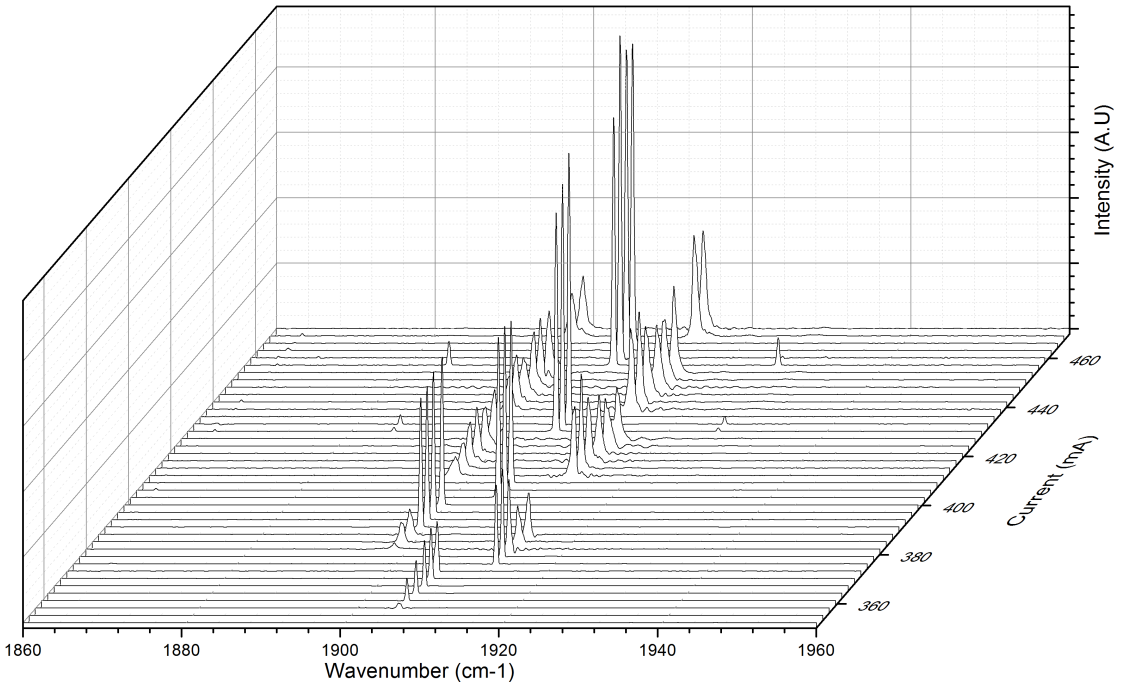

Figure 3.9: Spectral response at various CW driving currents of a Linear EC-QCL. A double AR coated Alpes single spatial mode QCL with a centre wavelength of 5.3 um provides gain to a cavity approx. 80cm in length. No wavelength tuning elements are present.

250 MHz, is well below the FTIR resolution of 7.5 GHz. Fig 3.10. gives a sense of this while showing the minimum detectable FWHM linewidth of emission that we observe using our FTIR. This is the resolution limited linewidth. In this example approx 90 external cavity modes are present within the measured FWHM linewidth of the CW emission.

This partial instability in an untuned EC arrangement seems to confirm that the effect of SHB is to generate noise which interferes with the established lasing mode. Fig 3.11 shows the same measurement performed on an ERC system where the effect of SHB is suppressed due to the travelling-wave nature of emission. Here the system maintains a single peak at a fixed position throughout the driving current range. All but one of the spectra has the distinctive resolution limited narrow single line shape. The spectrum taken at 415 mA resembles the form of the multi-mode peaks seen in the linear configuration. This would seem to coincide closely with the onset

of decoupling shown in fig 3.7. It would seem sensible to assume that the processes which give rise to the decoupling could also have some perturbative effect on the spectral response.

Comparing the spectral performance of the EC-QCL (fig. 3.9) and the ERC-QCL (fig. 3.11) would seem to validate the premise of this work by strongly supporting the suggestion that ERCs are capable of supporting more stable emission through the suppression of the spatial hole burning instability. While the requirement of continuous wavelength tuning must be met before ERC-QCLs reach the maturity needed for high-resolution gas spectroscopy, these findings would seem to confirm that, with respect to emission stability, these systems are fundamentally superior to their linear counterparts.

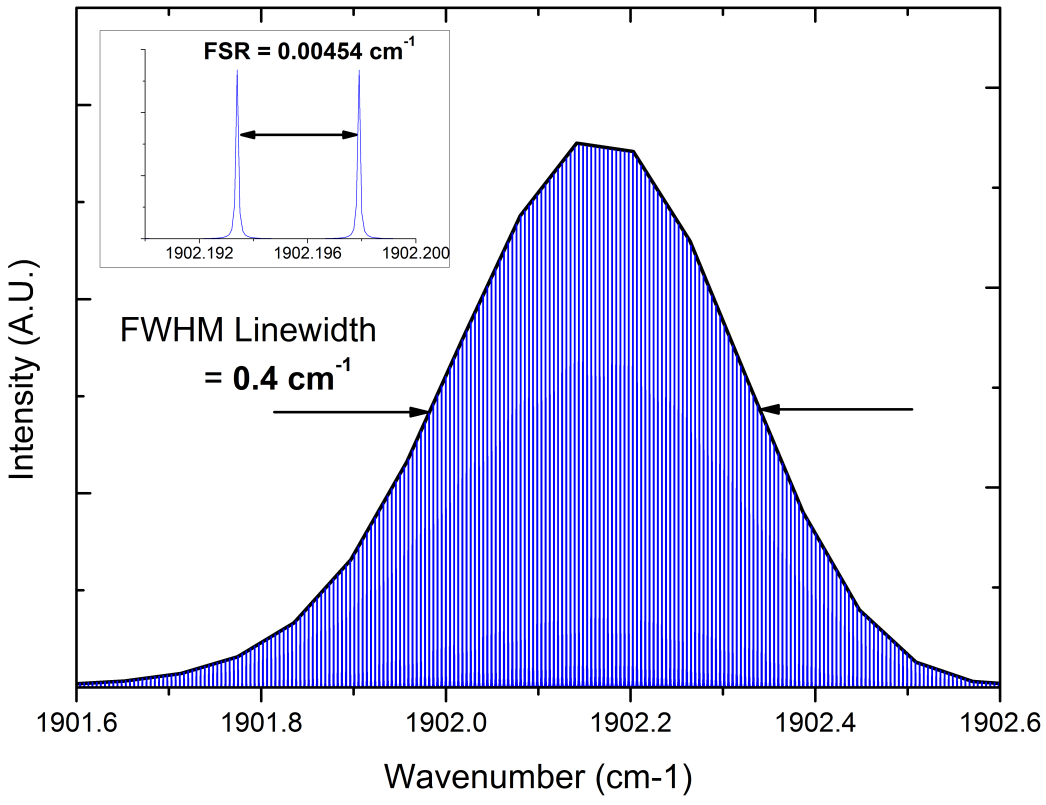

Figure 3.10: Resolution limited spectrum from 2.2m ERC-QCL measured at a CW driving current of 465 mA in a single emission peak regime. The black lined peak is measured from an FTIR while the blue lines represent the calculated external cavity modes of the system. A much higher resolution FTIR would be needed to resolve these individual cavity modes.

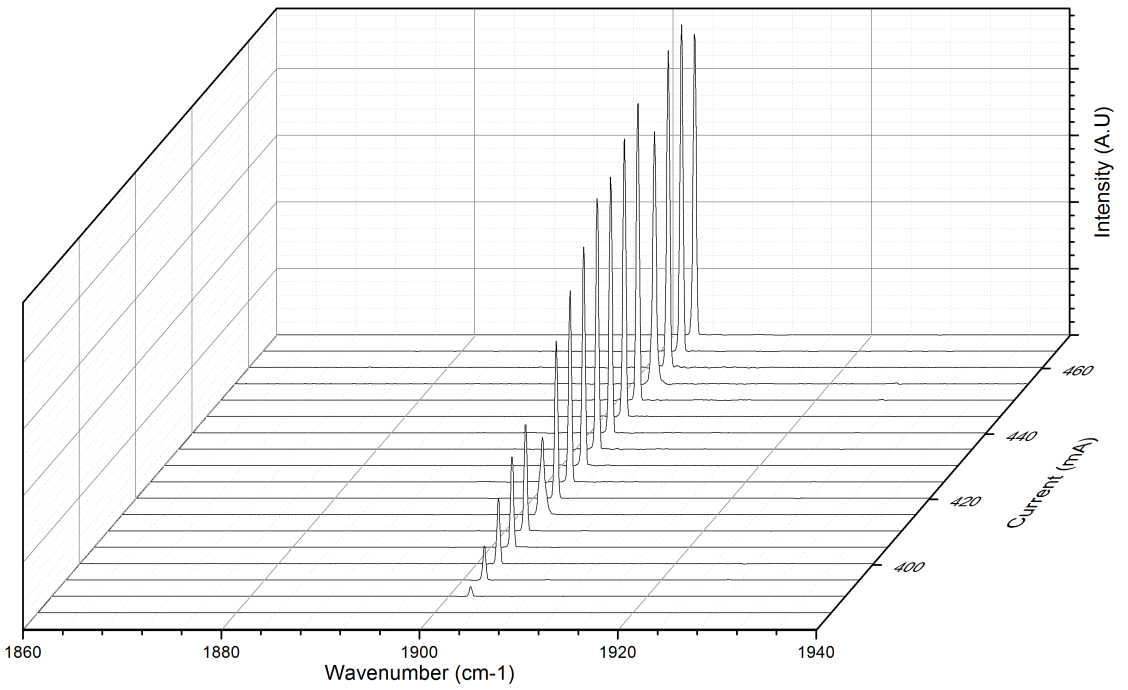

Figure 3.11: Spectral response at various CW driving currents of an ERC-QCL. A double AR coated Alpes single spatial mode QCL with a centre wavelength of 5.3 μm provides gain to a cavity approx. 220 cm in length. No wavelength tuning elements are present.

3.7 Tuning

The behaviour of EC-QCL systems detailed in the previous section, while insightful, doesn't provide any clear indication of system performance in real world applications. While DFB-QCLs may be useful for targeting single species, all tunable EC-QCL systems are arranged into some variant of the Littrow or Litmann-Metcalf configurations. This allows the system to be tuned over a wide range, usually limited by the gain bandwidth of the QCL. These tuning mechanisms change the gain landscape entirely, making the spectral measurements shown in the previous section a tool to help understand underlying processes rather than an indication of the characteristics or limitations of real world systems. Clearly a system that suffered from frequency noise on the scale of that observed in the untuned EC-QCL would

be entirely unsuitable for gas sensing. When a dispersive feedback element is used, such as a diffraction grating, this type of frequency switching becomes impossible. Light which is even a small fraction of a wavenumber away from the filter centre of the grating would suffer very high or even complete losses. In this case any destabilising effect, such as SHB, would likely manifest itself as amplitude noise. As mentioned before, linear EC-QCL systems in Littrow type configurations have shown great success in high resolution gas spectroscopy and commercially available units of this type are the gold standard in this field. This work attempts to advance the ring cavity as a broadly tunable source, comparable to the linear Littrow type configurations. In principle, a system based on a ring geometry should be able to produce more stable MIR light through the suppression of SHB.

To create broad tunability in the ring cavity system a familiar approach of replacing a cavity mirror with a diffraction grating is employed. This could be achieved by aligning the ring cavity in the normal fashion before replacing one of the mirrors with the grating. In our case this was the mirror immediately to the left of the QCL chip, though in principal this could be any of the mirrors. A number of factors influence the performance of gratings under these circumstances.

1. **Design Wavelength** – This is specific to the grating and care should be taken in matching the grating to the gain medium. Ruled blazed gratings are the standard at these wavelengths. There are a limited number of commercially available specifications from which a best choice must be made.

2. **Polarization** – QCLs produce highly TM (p-) polarized light. Ruled MIR diffraction gratings generally have higher efficiencies when used with TE (s-) polarized light. This can usually be easily addressed by correctly orienting the QCL and grating with respect to each other. It should be noted that conventionally the polarization is defined with respect to the lines of the grating, not the plane of incidence.

3. **Spot size** – Diffraction gratings efficiency generally increase with increasing spot size. This relates to the focus or collimation of the beam. The point here is to understand that once a mirror is replaced by the grating, a readjustment of the focus may yield better coupling.

4. **Angle of Incidence** – In addition to the grating angle there is now, unlike in Littrow type configurations, an additional angle of incidence. This depends on the relative orientation of components. In our experience, highest efficiency is achieved with a minimal AOI.

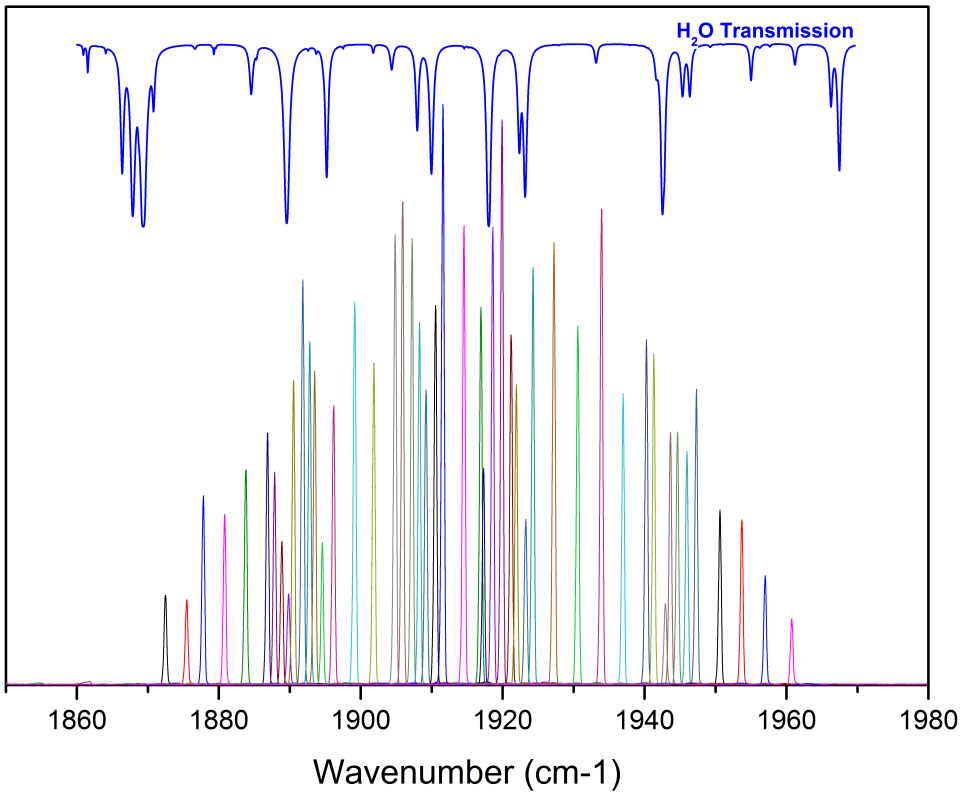

Figure 3.12: Multiple emission spectrums from a diffraction grating tuned ERC-QCL. Each emission peak corresponds to a scan taken with the grating set at a different angle. A 5.3 μm wavelength multi-spacial mode buried structure provides gain to an approx. 220 cm cavity. The driving current remains fixed with a I/I_{th} of around 1.5. The blue line shows the absorption features of atmospheric water vapour over the corresponding frequency range.

Fig 3.4 shows our tunable ERC-QCL system. In this arrangement almost 100 cm^{-1} of wavelength tuning was achieved by adjusting the grating angle by approx. 3°. This tuning range coincides well with the expected gain bandwidth of the QCL. This type of *hard* tuning resulted in a single, resolution limited emission peak at every grating angle. The intensity of emission follows the gain profile which is

expected to be a broad single peak. Fig 3.12 shows this response as well as an approximate transmission function of atmospheric water vapour calculated from line lists available on HITRANs online database. In this long path length free air coupled cavity, atmospheric water vapour can be expected to attenuate light resonant with its absorption features. This certainly appears to be this case, indeed, at lower driving currents the emission is shut down entirely in the vicinity of these features. An increased number of spectra were taken close to these features to try and expose their coincidence. This can't really be regarded as any type of spectroscopy but demonstrates nicely the resonant interaction of MIR laser emission with gas phase species.

This work was the first demonstration of a wavelength-tunable room-temperature continuous-wave ERC-QCL system potentially suitable for high-resolution gas spectroscopy. This was published in Applied Physics Letters[8] and was also the basis for an invited talk at the Conference on Lasers and Electro-Optics (CLEO) 2015[9].

3.8 Self-Phase-Locking

While much attention has been given to CW QCL systems that emit on a single longitudonal mode, under certain circustances there exists clear evidence that the systems emits on a number of adjacent cavity modes simultaneously. These can be refered to as supermodes.

Under the DC pumping used for CW emission the expectation would be that a steady state output would be observed. It's certainly the case that under most conditions constant emission amplitudes are observed. There are, however, instances where the system's emission amplitude begins to spontaneously oscillate. To measure this effect an RF spectrum is recorded as a function of the laser's DC driving current. This will clearly show any points at which the detected emission develops a significant frequency component, the expectation being that an ideal CW output would have a flat RF spectrum, with the only significant frequency component occurring at 0 Hz. It was clear from early observations that the system tends to oscillate very close to the round trip frequency.

Fig. 3.13 shows instances of this behaviour in a 2.1 m ERC-QCL system. While

this seems to occur randomly the effect can be initiated by adjusting the alignment or driving current. Sweeping through the drive current allows this stochastic phenomenon to be observed, in this case, at 5 different drive currents. At these points (circled in fig. 3.13) the frequency component of the emission amplitude at the FSR increases by as much as 60 dB. In the time domain, oscillations occur at these positions. The inset of fig. 3.13 shows an example oscilloscope trace of the detected emission while in an oscillating state. Once the system is oscillating it can remain in that state for a few seconds to a number of minutes. Each oscillating state has an oscillation amplitude which varies from a small fraction of the field amplitude to the full amplitude, i.e. forming isolated pulses. In the frequency domain this can be understood as the phase-locking of a pair of adjacent external cavity modes which are spectrally separated by the FSR of the cavity

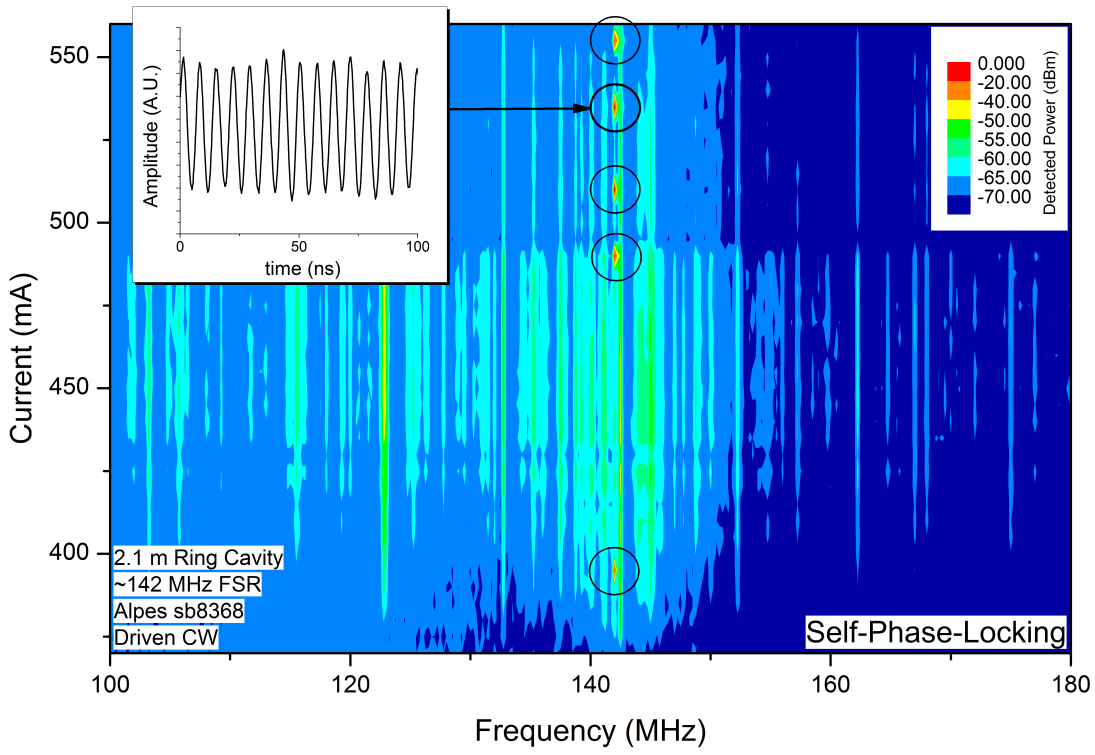

Figure 3.13: Plot showing the detected RF spectrum of a CW driven 2.1 m ERC-QCL system in the vicinity of its FSR (142 MHz) at various driving currents. Circled are the points at which the phase locking was observed. Inset shows an example of the temporal response of the system under this condition.

We have observed this effect in ERC-QCLs based on buried structures with both multi-spatial mode and single spatial mode profiles. Similar behaviour has been documented in multi-spatial mode buried structure systems where the phase locking of different transverse modes can cause oscillations[10]. This would seem a more likely occurrence due to the coincidental thresholds of transverse modes in buried structures as well as the reduced modal competition between transverse modes.

This behaviour in single spatial mode buried structures seems less intuitive. Classically, the expectation would be that modal competition would lead to a single CW mode. This is clearly not the case when these supermodes show such longevity. In the absence of cavity drift it's likely they would continue to oscillate indefinately. Larger, less stable, cavities are needed to bring the FSR within the bandwidth of our detector.

It's understood that the QCL gain medium with its fast gain recovery behaves like a fast reverse saturable absorber. This makes the laser tend to favour constant power (CW) emission. On the otherhand, the broad gain coupled with both spatial and spectral hole burning as well as SA effects favour a multimode regime. The intersubband transitions in QCLs have large non-linearities associated with third order suseptability (χ_3) due to the large optical matrix elements. This creates a strong four-wave-mixing (FWM) regine which can lock together the cavity mode phases and frequencies, mitigating to some extent the GVD of the medium. The combination of these effects is to give rise to the generation of frequency modulated (FM) frequency combs. This has been shown to occur naturally in QCLs and is of vast importance in MIR spectroscopy[11].

While there is likely some causal connection between these combs and our observations, there is one significant difference. In FM comb regimes the phases of the comb cavity modes are arranged in such a way that there is little to no amplitude modulation (AM). The phases essentially cancel each other out, as opposed to AM mode-locked combs where phases are equal and result in intense periodic pulses. FM combs may have constant amplitude, which is favoured by the the reverse saturable absorber characteristic, but the emission is still periodic at the cavity round trip frequency. This periodicity is the single requirement for frequency comb generation.

If a perfectly FM-comb emitting QCL had its output spectrally filtered, removing some of the cavity modes which make up the comb, the remenance of the FM comb will show some AM. This is the basis of intermode beat spectroscopy (IBS) which is one way of measuring the coherency of FM modulated combs which uses a similar arrangment to FTIR spectroscopy but produces an interferogram by plotting frequency components near the round trip frequency against mirror delay. Some unintentional spectral filtering would account for our AM signal if the system is emittig in an FM comb regime. Even if these observations aren't the result of FM frequency combs, the AM emssion would lead to the proliferation of comb modes through the FWM process.

3.9 Conclusion

Shown here for the first time is the possibility of room temperature, unidirectional, wavelength tunable emission from ERC-QCLs based on buried structures. Measurements performed on an untuned system would seem to confirm the theory that SHB causes instabilities in Linear EC-QCL where the effect is suppressed in ERC-QCLs. These results support the established theory as well as demonstrating the suitability of the ERC-QCL as a potential platform for high resolution gas spectroscopy.

The system detailed here suffers from a number of shortcomings that would need further development before being a suitable replacement for the well established Littrow type EC-QCL systems. The first problem is regarding the switching nature of the directionality which would need to behave predictably for the system to be useful in real world applications. There are known passive techniques that exist that may be suitable for this task. Secondly, and much more significantly, the system would need to be adapted to wavelength tune continuously. Littrow type systems simultaneously adjust the grating angle and cavity length allowing a single mode order to be tracked. This means a single mode can be continuously tuned over the full tuning range. Our system lacks the ability to adjust the cavity length and as a result the emission wavelength *hops* along cavity modes as it's tuned. This type of tuning is called multi-mode envelope tuning and lacks the necessary selectivity for high resolution gas spectroscopy.

The observation of the self-phase locking provides an exciting avenue into FM frequency combs generation which is likely to be the basis of future multi-heterodyne spectroscopy platforms.

Bibliography

[1] Papa Lat Tabara Sow, Sinda Mejri, Sean K Tokunaga, Olivier Lopez, Andrey Goncharov, Bérengère Argence, Christian Chardonnet, Anne Amy-Klein, Christophe Daussy, and Benoît Darquié. A widely tunable 10-μ m quantum cascade laser phase-locked to a state-of-the-art mid-infrared reference for precision molecular spectroscopy. *Applied Physics Letters*, 104(26):264101, 2014.

[2] Ariel Gordon, Christine Y Wang, Laurent Diehl, Franz X Kärtner, Alexey Belyanin, D Bour, S Corzine, G Höfler, HC Liu, Harald Schneider, et al. Multimode regimes in quantum cascade lasers: From coherent instabilities to spatial hole burning. *Physical Review A*, 77(5):053804, 2008.

[3] Nikola Vukovic, Jelena Radovanovic, Vitomir Milanovic, and Dmitri L Boiko. Analytical expression for risken-nummedal-graham-haken instability threshold in quantum cascade lasers. *Optics express*, 24(23):26911–26929, 2016.

[4] M Chashnikova, G Monastyrskyi, A Aleksandrova, M Klinkmüller, MP Semtsiv, and WT Masselink. Buried-heterostructure quantum-cascade laser overgrown by gas-source molecular-beam epitaxy. *Applied Physics Letters*, 100(21):213504, 2012.

[5] Hyunyong Choi, Laurent Diehl, Zong-Kwei Wu, Marcella Giovannini, Jérôme Faist, Federico Capasso, and Theodore B Norris. Gain recovery dynamics and photon-driven transport in quantum cascade lasers. *Physical review letters*, 100(16):167401, 2008.

[6] Benedikt Schwarz, Peter Reininger, Hermann Detz, Tobias Zederbauer, Aaron Maxwell Andrews, Stefan Kalchmair, Werner Schrenk, Oskar Baumgartner, Hans Kosina, and Gottfried Strasser. A bi-functional quantum cascade device for same-frequency lasing and detection. *Applied Physics Letters*, 101(19):191109, 2012.

[7] Pietro Malara, Romain Blanchard, Tobias S Mansuripur, Aleksander K Wojcik, Alexey Belyanin, Kazuue Fujita, Tadataka Edamura, Shinichi Furuta, Masamichi Yamanishi, Paolo de Natale, et al. External ring-cavity quantum cascade lasers. *Applied Physics Letters*, 102(14):141105, 2013.

[8] DG Revin, M Hemingway, D Vaitiekus, JW Cockburn, N Hempler, GT Maker, and GPA Malcolm. Continuous wave room temperature external ring cavity quantum cascade laser. *Applied Physics Letters*, 106(26):261102, 2015.

[9] Michael Hemingway, Deivis Vaitiekus, John Cockburn, Nils Hempler, Gareth Maker, Graeme Malcolm, and Dmitry G Revin. Continuous wave room temperature external ring cavity quantum cascade laser. In *CLEO: Science and Innovations*, pages STu4G–6. Optical Society of America, 2015.

[10] Aleksander K Wójcik, Nanfang Yu, Laurent Diehl, Federico Capasso, and Alexey Belyanin. Self-synchronization of laser modes and multistability in quantum cascade lasers. *Physical review letters*, 106(13):133902, 2011.

[11] Andreas Hugi, Gustavo Villares, Stéphane Blaser, HC Liu, and Jérôme Faist. Mid-infrared frequency comb based on a quantum cascade laser. *Nature*, 492(7428):229–233, 2012.

Chapter 4

Mode-Locked External Cavity QCLs

4.1 Introduction

While continuous–wave sources of mid-infrared radiation are best suited for high resolution gas spectroscopy, systems capable of emitting ultra-short pulses can generally be applied to a broader set of experimental tasks. In the visible wavelength range commercial titanium sapphire lasers are capable of emitting pulses as short as a few femtoseconds. This makes them useful for experimentally probing matter to study fast processes which occur over a timescale greater than the pulse's duration. Ultra-short mid-infrared pulses, as well as having much potential as a source for future spectroscopic tasks, can be used to study atomic and molecular dynamics as well as electron transport in solids where pulses from shorter wavelength ranges would be damaging to the material. In biological systems the lower energy photons in the MIR can be used in multi-photon processes in a non-invasive fashion. Two- and three-photon microscopy is currently a cutting edge technique used to image a wide range of molecular chromophores in biological systems where the increased wavelength reduces scattering in the sample. In these techniques, which require multiple photons to coincide at a point in the sample, higher photon numbers reduce the out of focus excitation which produces higher contrast images and increases the achievable penetration depth. To avoid sample photodamage increasingly long infrared wavelengths are needed. Longer wavelengths do experience greater attenuation in biological tissues meaning higher peak powers are required to achieve significant penetration. Currently the sources for these techniques are complex systems made up of titanium sapphire lasers, amplified by second harmonic generating (SHG) optical parametric amplifiers (OPA), a bulky and costly method of producing the required emission. Clearly an alternative system capable of producing these short pulses would become an attractive tool for a number of scientific tasks.

ERC-QCLs have long been understood to provide a promising platform for the generation of short mode-locked mid-infrared pulses. ERC-QCLs should be capable of producing short MIR pulses using a single active device, at high power, room temperature and without relying on complex non-linear optical elements. This is when compared to the more mature platform of optical parametric oscillators (OPOs), or similar systems, which are currently the only reliable means of generating short

MIR pulses. These tend to suffer from low output power but can produce few, or even sub-, cycle MIR pulses.

Here we attempt to study the effects of electrical modulation on EC- & ERC-QCLs at or around the round-trip frequency. This active mode-locking (AML) approach should generate isolated pulses comprised of a number of phase locked cavity modes. This would represent an important first step towards the realisation of short pulse mode-locked ERC-QCLs suitable for spectroscopy and other scientific applications.

This chapter begins with a discussion of the basic principles of mode-locked lasers and the electronics involved in active-modulation. Then details are provided of our initial electronics setup based on a custom made electrical modulator. This includes some initial time domain and spectral measurements of an ERC-QCL under resonant modulation. The remainder of the chapter details the development of an improved electrical scheme based on a custom made power amplifier and a custom made laser mount incorporating a bias-tee and an impedance matching network. This latter system will go on to be used in chapters 5 & 6 where it forms the basis of a harmonic-mode-locking (HML) scheme for the ERC-QCL & EC-QCL respectively.

4.2 Mode-locking Schemes

Mode-Locking schemes, in general, are numerous and varied but are largely based on the system's gain medium characteristics. Unlike a number of other laser systems which can achieve femtosecond pulses using passive mode-locking schemes, the fast gain recovery of QCLs ($\sim$1 ps) prevents the formation of stable pulses using the usual passive optical elements such as Kerr Lenses and saturable absorbers[1]. The effect of this fast gain recovery is to *blur out* the pulses by amplifying the trailing edge. The QCL is said to operate as a fast reverse saturable absorber which will clip high intensity pulses and tends to amplify the tails of a pulse propagating through it. This is more so the case in the large signal limit where pulse intensities reach gain saturation. Under these conditions the QCL operates as a power limiter. While it may be possible to exploit these characteristics to generate short pulses using some form of additive pulse scheme, its likely this would require a more complex

system, comparable in attractiveness to other more complex schemes for generating mid-infrared pulses such as OPOs.

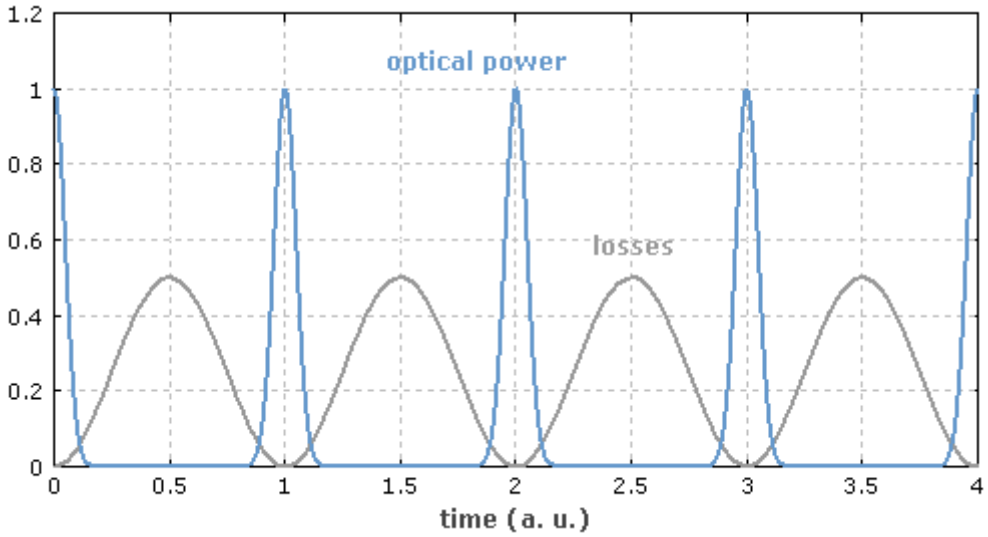

Figure 4.1: Normalised loss modulation and optical intensity of an actively modulated laser cavity. RP Photonics, (2017), active-mode-locking [ONLINE]. Available at: `https://www.rp-photonics.com/active_mode_locking.html` [Accessed 8 November 2017].

Active mode-locking, in general, allows stable pulse trains to form by adding a temporal dependence to the gain function of the laser. Usually a single harmonic tone of some power is coupled into the laser's driving current producing a gain function which varies in time. Fig.4.1 demonstrates how an optical field develops in a laser cavity when the driving current is modulated at the cavity round-trip frequency. When the laser's driving current reaches a maximum the losses are at a minimum. The goal here is to choose the DC and RF components such that the maximum gain briefly exceeds the system's transparency current. This can be visualised as a small window opening briefly and periodically, allowing light to pass through for a time where some net gain exists. If an external cavity of some geometry is formed around the laser then active modulation at the round trip frequency should allow a light pulse to develop and propagate or circulate around the cavity. This round-trip frequency is known as the Free Spectral Range (FSR) of the cavity and, considered in the frequency domain, represents the spacing between adjacent longitudinal cavity modes. In the time domain this represents the frequency at which a light pulse travels one whole length of the cavity, the inverse of this figure being the round trip

time. Fig.4.2 illustrates how mode-locked pulses (in red) are comprised of a number of adjacent phase-locked cavity modes (in blue), each separated from its neighbour by the cavity's FSR.

When the system is electronically modulated at this round trip frequency a single pulse propagates, though there may be two propagation directions in the case of the ring cavity. It's also possible to pump the cavity at multiples of the round trip frequency which leads to a situation where multiple evenly spaced pulses can propagate simultaneously. For this reason the cavity length and the pumping harmonic define the pulse repetition rate. Again, in the frequency domain a short pulse is the superposition of some number of cavity modes, with shorter pulses being composed of increasing numbers of cavity modes. This phenomenon is a manifestation of the Time-Bandwidth product which imposes a lower limit on the product of a pulse's duration and its spectral width.

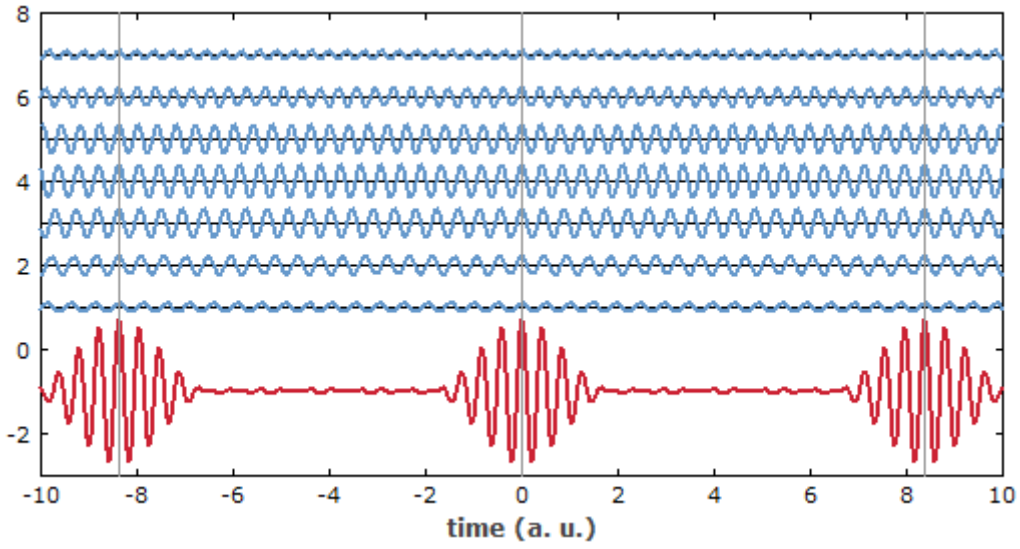

Figure 4.2: Demonstration of the formation of pulses by the superposition of a number of adjacent cavity modes. RP Photonics, (2017), pulse-train-synthesis2 [ONLINE]. Available at: `https://www.rp-photonics.com/mode_locking.htm` [Accessed 8 November 2017].

The aim in mode-locking is to excite a broad range of cavity modes which share a fixed phase relation i.e. share a common phase velocity and have their phases arranged such that one of the antinodes of each mode coincide. At this point the field intensity will be high and outside this region the differing wavelengths will destructively interfere. There are two effects which limit the number of modes which

can be phase-locked together in typical semiconductor lasers. Firstly, only the modes which fall within the laser's gain bandwidth can contribute to the pulse. This puts a limit on the broadness of the emission spectrum and in turn a minimum pulse length achievable by a given gain medium. In a typical QCL (gain bandwidth 100 cm^{-1}) this would impose a lower limit on the pulse duration of about 100 fs. Secondly, group velocity dispersion (GVD) can cause modes to propagate at different speeds through the gain medium. Without specially designed structures and materials this can make it difficult to lock the majority of the gain medium's bandwidth. Instead only regions of relatively flat GVD can be phase locked. GVD is comprised of contributions from the material systems, waveguide design and the gain medium itself. In the case of QCLs this is less problematic than other systems, with relatively low values of GVD for popular material systems such as InP[2]. Nevertheless, some schemes may require GVD to be compensated for which can be done using optical elements such as double-chirped mirrors (DCMs) which can be specially engineered to cancel out any GVD present in the laser device[3].

4.3 Frequency Combs

The set of evenly spaced cavity modes forms a characteristic pattern called a frequency comb. Frequency combs of various types are a subject of much study with a broad set of applications from spectroscopy to ultra-precise clocks[4]. Although a stable repetitive pulse train will always result in a comb in the frequency domain, combs aren't necessarily associated with short pulses. Frequency modulated (FM) combs and Fourier Domain mode-locking are both capable of producing combs. The only real requirement for combs in the frequency domain is a repetitive signal. FM combs are of interest in QCLs, as mentioned at the end of Chapter 3. The QCL may be naturally better suited to emitting combs in this regime than a short pulse one. For the reasons previously mentioned the QCL would seem to be well suited to emitting combs in a constant power FM regime. Indeed, QCLs that have been designed with this task in mind[5] have produced high powered combs spanning 60 cm^{-1}. This was achieved by engineering a near zero GVD device with high levels of second and third order non-linear susceptibilities (χ_2 & χ_3). This is sufficient to lead to

the proliferation of frequency combs through the four-wave-mixing process. Fig.4.3 illustrates how the four-wave-mixing (FWM) process gives rise to FM combs. Starting from a CW regime, lasing on a single cavity mode (ω_1 in fig.4.3), side-modes (ω_2 & ω_3) are generated through multimode instabilities such as spatial hole burning[6]. Once these three adjacent modes are excited, both degenerate and non-degenerate FWM processes excite additional side-modes. This process continues to produce new side-modes at each side of the frequency comb as well as components which reinforce existing comb lines. This gives the FWM process the ability to create broad FM frequency combs. Dispersion causes the cavity mode frequencies to differ slightly from the evenly spaced modes created through the FWM process. Low levels of GVD must be achieved to allow these evenly spaced modes to be sufficiently locked to nearby dispersed cavity modes.

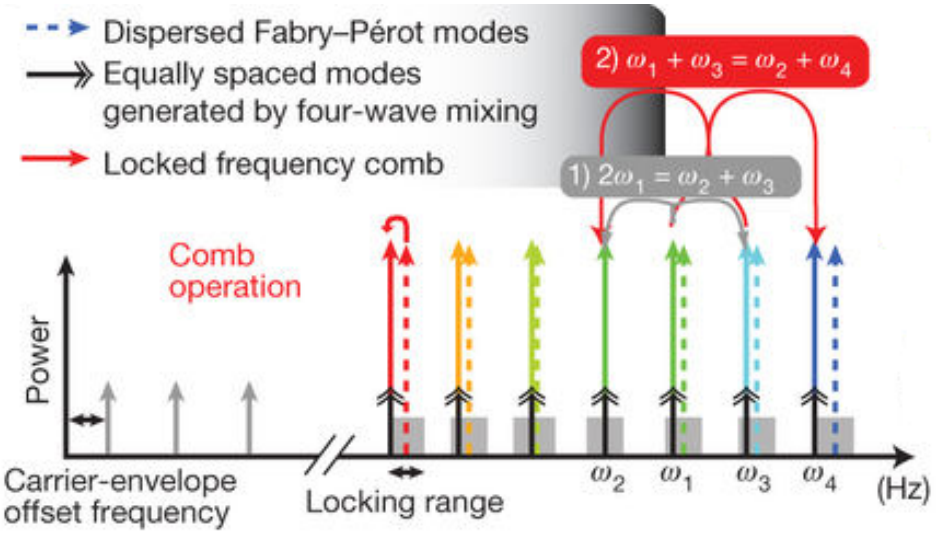

Figure 4.3: Demonstration of how Frequency modulated QCL frequency combs are generated through the Four wave mixing process.[6]

This success, and others, would seem to confirm that FM combs are a far more fruitful method of employing QCLs for spectroscopic tasks. Dual-Comb spectroscopy is a particularly ingenious scheme allowing the multi-heterodyne beating of two slightly differently spaced combs to be measured in the RF range. It's likely that external cavity implementations of dual-comb systems would perform very well with a reduced cavity mode separation leading to greater resolution. Despite this great promise for spectroscopic tasks there still exists good reason to pursue combs based

on short optical pulses. Time resolved measurements and experiments that currently employ visible wavelength mode-locked lasers, such as titanium sapphire, require a short temporal event and can't function under the type of constant power regime seen with FM combs. This alone should be regarded as sufficient motivation to explore short QCL pulses. Furthermore, active modulation at low levels has been shown to enhance the formation of FM combs[6].

4.4 Active Mode-Locking Electronics

While many of the principles of mode-locked laser emission are shared between active and passive schemes, from an engineering point of view, they are entirely different pursuits. The gain characteristics of the QCL are well understood and extensive modelling confirms that passive schemes alone won't spontaneously produce mode-locked pulses. The QCL does, however, lend itself well to electrical modulation with intrinsic modulation limits as high as 100 GHz. This, like most other device characteristics, is subject to engineering tradeoffs. High performance QCL material should have a modulation limit in excess of 30 GHz[7]. Although these figures might seem encouraging they relate to the QCL chip itself, in reality efficient modulation beyond a few hundred megahertz requires increasingly well designed laser mounting. In all cases the practical modulation limit will be defined by the mounting parasitics. Achieving microwave modulation frequencies would likely requires a transmission line approach which sees the QCL mounted directly onto a specialist substrate. If other necessary conditions, such as thermal heatsinking, can be maintained, this approach should allow modulation up to the intrinsic modulation limit of most practical devices.

Because the modulation frequency is matched to the cavity round trip time, the cavity length also defines the pulse repetition rate. Frequencies around 10 GHz and above would only be applied to Fabry Perot (FP) type ridge devices. When an external cavity is employed the modulation frequencies can be reduced to the radio frequency range. This simplifies the drive electronics and is one of the reasons that external cavities are an attractive platform for mode-locking QCLs.

While the fundamental frequency of the current pumping should clearly be equal

to the round trip frequency, or a multiple thereof, additional degrees of freedom exist that define the form of the driving current. This can be largely categorized by two different forms of active modulation. One is harmonic mode-locking(HML) and the other is normal active mode-locking(AML). HML is simply driving the gain medium with a harmonic tone of some RF power while normal active mode-locking, in its purest sense, is driving the device with top-hat like pulses with a repetition rate equal to the round trip frequency.

Due to the increasingly high harmonics required to produce high slew rate switching, it's difficult to produce square pulse shapes beyond even modest radio frequencies. High repetition rate short pulse generators are likely to produce less ideal pulse shapes. Gaussian pulse shapes are often used in theoretical studies[7].

HML follows an approach similar to other RF/Microwave electronics, using some form of bias-tee which combines DC and AC components. Usually the DC is set in the close vicinity of the laser's threshold and the RF power is capacitively coupled into the laser. Semiconductor lasers are in general extremely non-Ohmic with a strong negative second order differential resistance (becoming more conductive at higher voltages) and can also have a considerable light dependent component to their conductance. This is especially true in QCLs. These factors together make exact impedance matching challenging. For a pure harmonic tone a reasonable reactive matching network should be possible when designed to operate around the lasers threshold. Here the I-V curve becomes roughly linear and a normal impedance matching approach becomes effective. Despite excitation with a harmonic signal, non-linearities are introduced through both this non-ohmicity and through the nature of the laser's gain response. Because of this it's highly unlikely that a harmonically mode locked laser will emit light with a harmonic amplitude modulation. While in the small-signal limit there may be good linearity, modulation of any real depth will likely lead to an anharmonic output. This is desirable where short separate pulses are sought.

The opposite end to this is the more classical view of active mode locking where the gain medium is pumped with a top hat like or more likely a Gaussian pulse. This switching type modulation benefits from a more abrupt increase in current and as a result the gain. This produces a more temporally selective window. The difficulty

here is in producing this switching at high repetition rates. If the fundamental frequency is already in the RF/microwave region then the higher harmonics needed to create the high slew rate during switching are at prohibitively high frequencies. This means that significantly anharmonic electrical pulses can only be produced in the RF range using exotic electrical schemes such as reverse breakdown schemes or non-linear transmission lines (NLTLs).

4.5 Active Mode-Locked QCLs

The first unambiguous demonstration of mode-locking in QCLs was achieved using a specially designed multi-section ridge type QCLs[8]. Here the cavity was purely the semiconductor ridge waveguide which at one end had a 120 μm contacting section which could be independently electrically biased. This allowed RF power to be delivered to a small section of the gain medium. The total chip length was 2.5 mm which corresponded to a round trip frequency of around 18 GHz. In addition to the small bias section the QCL also had a specially designed active region design based on a diagonal transition through a thick barrier. Classical mode-locking theory suggests this should produce better conditions for stable pulse formation by increasing the upper state lifetime. The result of this was the generation of pulses with a FWHM duration as short as 3 ps with a pulse energy of 0.5 pJ.

Pulses were stable within a certain operating range beyond which the output departed from that of a single isolated pulse. The authors acknowledge that evidence of spatial hole burning (SHB) was present in the form of the emitted pulses. This is to be expected in a laser ridge which forms a linear cavity.

An actively mode-locked QCL system based on an external ring cavity (ERC) has a number of advantages over a mode-locked ridge QCL. As previously mentioned the increased cavity length reduces the pulse repetition rate down to the RF for even modestly sized cavities. Mechanically altering the cavity length, as well as pumping at higher harmonics, would make it possible to alter the repetition rate of the pulses. As compared to sectioned ridge type QCLs, an ERC system can achieve a much greater ratio between the non-gain and gain section length. Essentially, a relatively smaller gain window can be created. More importantly the use of an ERC would

allow the mode-locked pulses to propagate in a unidirectional fashion. As is the case for CW emission, this would have the benefit of producing more stable emission by suppressing the SHB instability. One theoretical study[7] performed simulations based on Maxwell Bloch equations for an actively mode-locked ERC-QCL. Their simulations modelled both sinusoidal modulation (HML) as well as modulation by a train of Gaussian pulses. The results support the idea that even typical QCL devices are capable of producing picosecond pulses when driven by sufficiently short electrical pulses. A number of other interesting points emerge from their findings. The length of the gain medium determines the minimum duration of a pulse that can be generated before power starts being traded off. The critical duration here being the light transit time through the gain medium. Electrical pulses shorter than this period lead to a position where pulses don't experience gain for the duration of their transit through the gain medium. This principle seems to impose a limit between pulse length and pulse power that can be created in this fashion, that is with a single active device providing the gain.

Also, even with a relatively short modelled QCL (1 mm), HML at a modulation limited 30 GHz is only likely to produce pulses of around 4 ps. Pulses of around the low picoseconds would seem to be the limit of what actively mode-locked QCLs are likely to produce. Achieving this would require rather exotic electronics. Pulses from other ultrafast laser systems routinely emit pulses of the low femtosecond time period. It's clear before experimentation that if the hope is systems based on QCLs are to produce pulses of this timescale, active modulation is a starting point rather than a solution.

A number of potential routes exist to go beyond this limit. First, increasingly short sections of QCL gain medium could be used and driven with pulses that only just extend over threshold. This scheme would produce decreasing power as mentioned before but these pulses could, to a certain extent, be amplified outside the cavity using a number of means. A more attractive option might be to introduce a non-linear element into the ERC. Experimentation of this type is particularly easy to do when using an external cavity. A slow saturable absorber could be used to introduce an intensity dependent loss into the cavity. Some other non-linear element may also become effective when short high intensity pulses can be created. These

part electrical part optical schemes are called hybrid mode-locking. For ERC-QCLs to produce the type of ultra-short pulses needed to replace current complex systems based on OPO/OPAs, the hybrid mode-locking approach is likely to be the most fruitful.

4.6 Initial Electronics Development

To study the active mode-locking of the ERC- and EC-QCL a method of modulating the lasers drive current at frequencies around the round trip frequency was required. The development and manufacture of a resonant pumping system was undertaken. This was achieved using a series of custom made electrical modulators and power amplifiers (PAs) based on LDMOS transistors. Prior to this, experimentation with a number of very basic through hole circuits based on bipolar junction transistors (BJTs) had been explored. Like later systems, these were made to amplify, or be switched by, a signal delivered by a standard RF signal generator. These had very limited success, mostly due to the failure of paralleled transistors, but led to the work on more suitable surface mounted (SMT) solutions.

The first significant design employed an LDMOS as an electrical switch, operating in a quasi class AB fashion. Additionally, to allow measurements using pulsed lasers, the board had to be able to produce pulse trains lasting between 500 ns and 1 ms. This was achieved using a PIC programmable microcontroller which could be programmed to modulate the envelope of the pulse trains so as not to overheat the QCLs.

Fig.4.4 shows the schematic of this board which was designed using CAD software. Fig.4.5a & 4.5b show the layout photomask and a photograph of the finished board respectively. The three BNC connectors that can be seen in fig. 4.5b are the signal in, on the left; trigger out, at the bottom and the laser output, on the right.

This design suffered from a number of shortcomings with some features not functioning as intended, though we later found that these features didn't prohibit the device's function. The microcontroller allowed us to create pulse trains of various lengths which was the main design requirement. The mosfet, in this case, acted as a switch which was in line with the QCL itself. Using the mosfet to modulate a

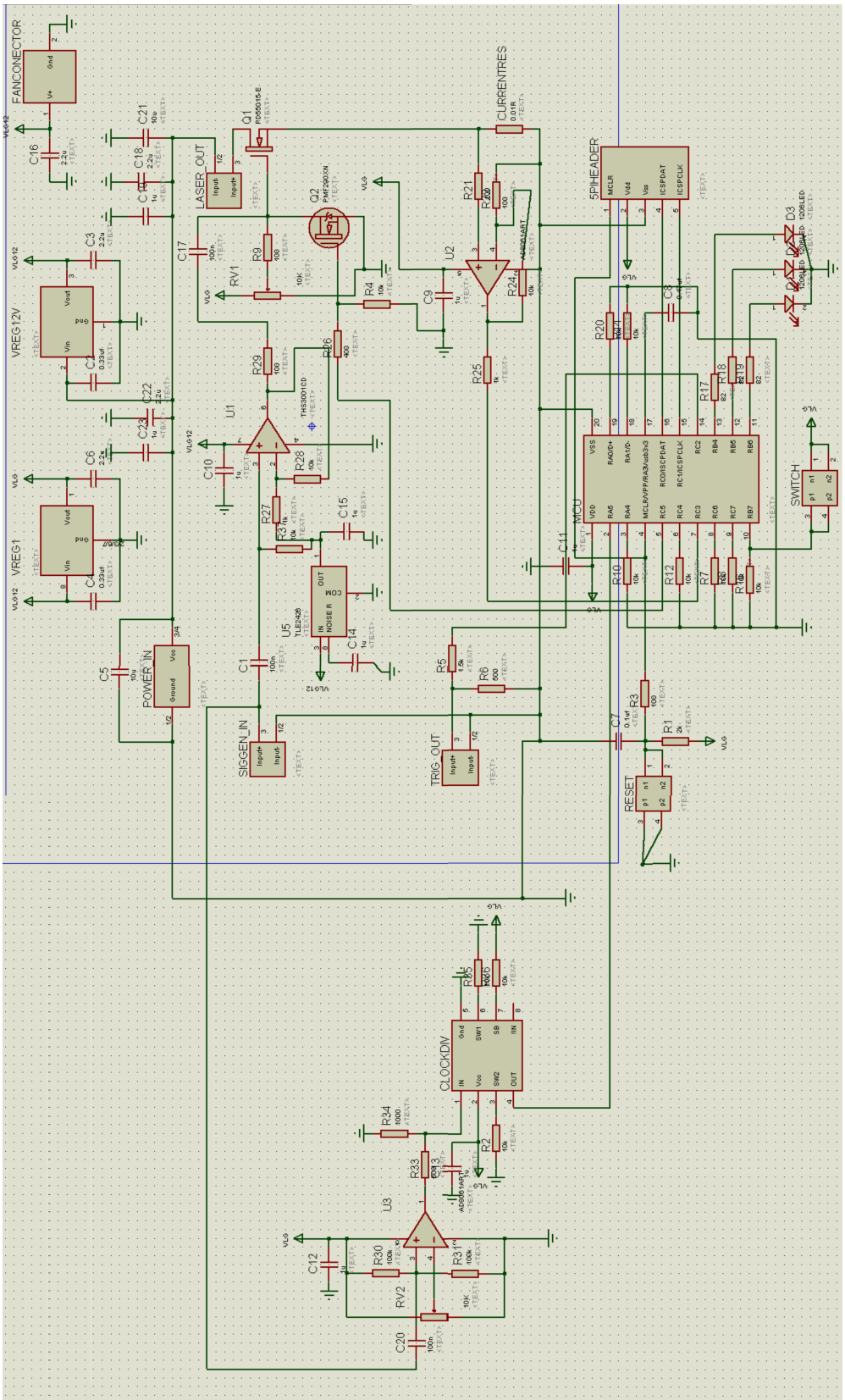

Figure 4.4: Schematic of early mode-locker modulator board.

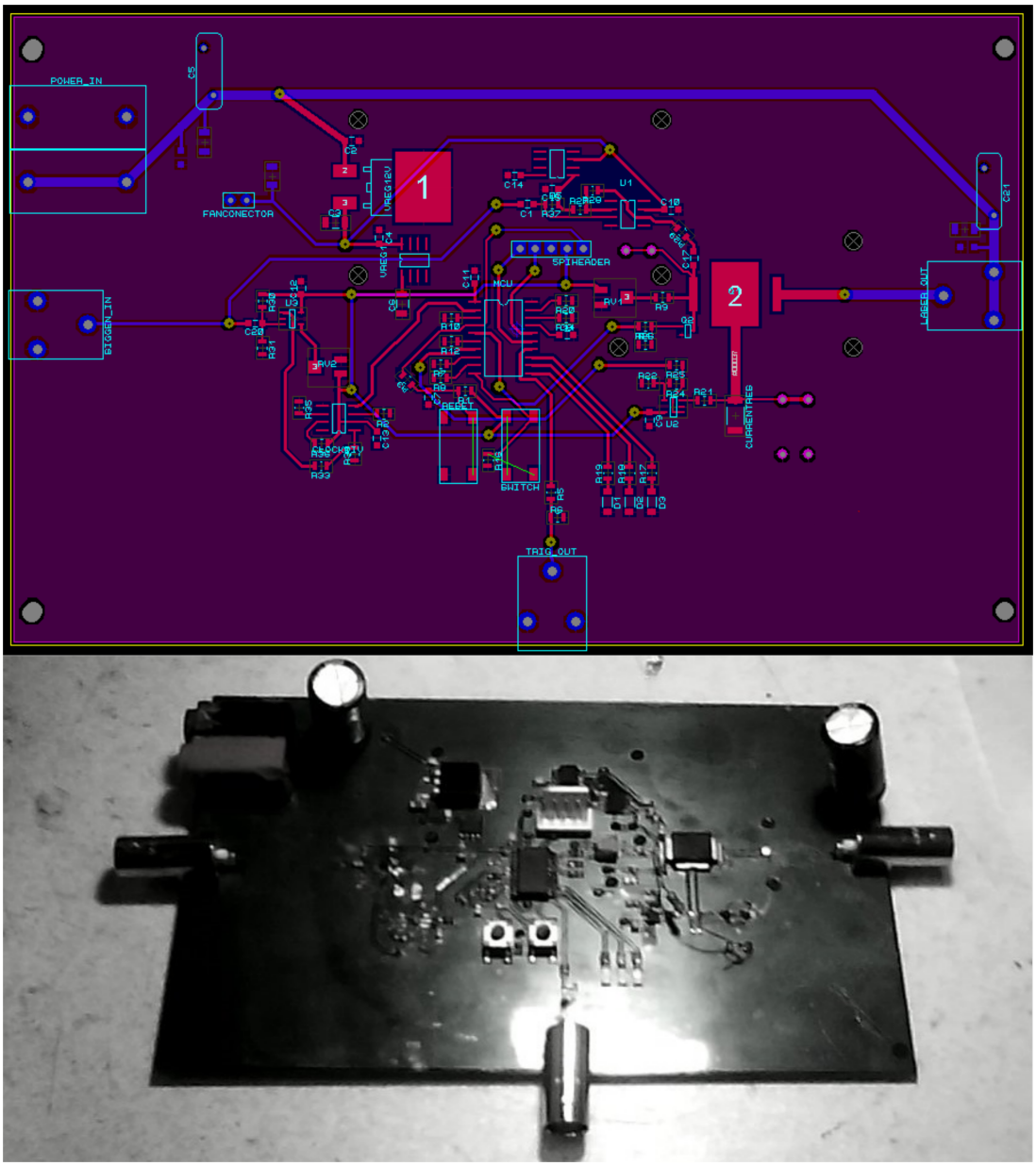

Figure 4.5: **a:** Photomask of Board Layout. **b:** Photograph of manufactured board.

laser in this way, or any other device, has a lot of difficulties, particularly at radio frequencies where transmission line effects usually require good impedance matching for effective power transmission. Difficulties, from a metrological standpoint, meant that the board could only be reliably used for phenomenological study. Any attempt to extract measurements of the driving conditions such as modulation depth lead to implausible results. A current probe could be placed between the board and the laser mount but this was found to interfere with the current pulses. Additionally, because of the polarities involved and the n-type mosfet used, both terminals of the QCL

were held at some positive ground referenced voltage. The grounded optical bench meant special care had to be taken to isolate the laser mount as well as the coaxial cable that connected the board to the laser mount. While most of the problems associated with this scheme could be mitigated to some extent, the real issue is one of measurement which was caused by an inability to separate and extract the DC and AC components. Instead, mosfet biasing was adjusted on a trial and error basis to finds operating conditions that appeared stable over some desired frequency range.

Despite these drawbacks the board produced sufficient modulation depth to observe a resonant response from the ERC-QCLs. This was performed initially using standard ridge QCLs centred at 5.3 μm which were produced at Sheffield. These devices lacked the thermal performance levels needed for continuous-wave or even to be continuously resonantly pumped. The resonant pumping delivered in this way should be thought of as similar to CW pumping. The heating of the device is related largely to the delivered DC component which in the harmonic limit would be around half of the CW DC level. This is still much greater than pulsed operation at low duty cycles.

In these early tests a resonance was observed with a width of around 1 MHz at modest driving currents. Clearly from Fig. 4.6, over the timescales that were deemed to avoid the risk of device failure through overheating, a steady state output had not been achieved despite indications that the current pulses were largely uniform after about 1 μs of modulation. While the optical pulse envelope evolves over the microsecond timescale, the optical spectrum contains a single peak from the very beginning of the emission. Fig.4.7 shows a typical time-resolved spectral measurement from the first 100 ns of emission for a pulse train similar to that of fig.4.6. This is in contrast to the case of long pulses, like those in chapter 2, which consistently cause ERC-QCLs to emit over a wide spectral range for some microseconds before a single emission peak remains.

In the absence of a sufficiently high resolution FTIR to resolve the individual cavity modes for large ERC-QCLs, it may still be reasonable to assume that CW or long pulse emission leads to lasing on a single longitudinal mode, the same can't be said for resonant pumping which in the harmonic limit requires a minimum of

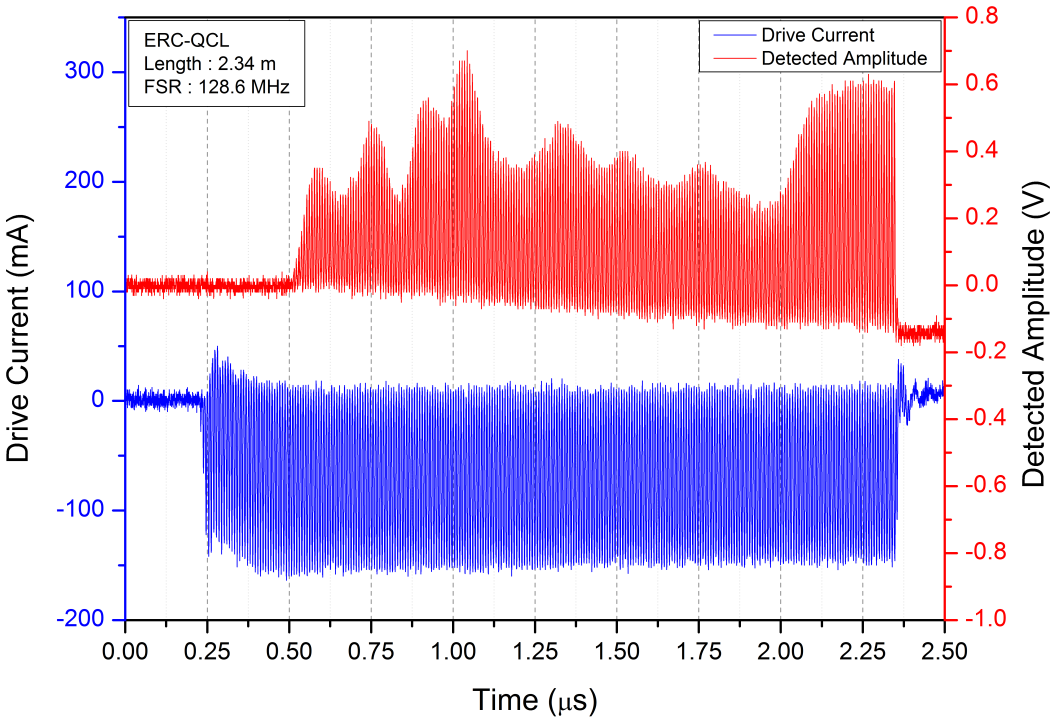

Figure 4.6: Detected emission and current probe measurements of a resonantly pumped ERC QCL. These 2 μs current pulse train contains around 250 pulses with an amplitude of 150mA and were driven at a repetition rate of 1 KHz.

two adjacent modes to produce the fundamental beating frequency. These sets of modes are commonly called *supermodes*. This fast mode selection is likely related to the additional temporal window constraint which may *pick out* a certain part of the developing pulse.

4.7 Further Electronics Development

To build a more robust picture of these processes a modulation scheme based on improved electronics was pursued. Previous drive electronics simultaneously passed the AC and DC through the Mosfet, which effectively acted as a switch. A more conventional approach would be to use a Power Amplifier (PA) to generate an RF AC signal that is combined with DC through a bias-tee. This would allow us to use standard class A amplifier design procedures and would result in a system where

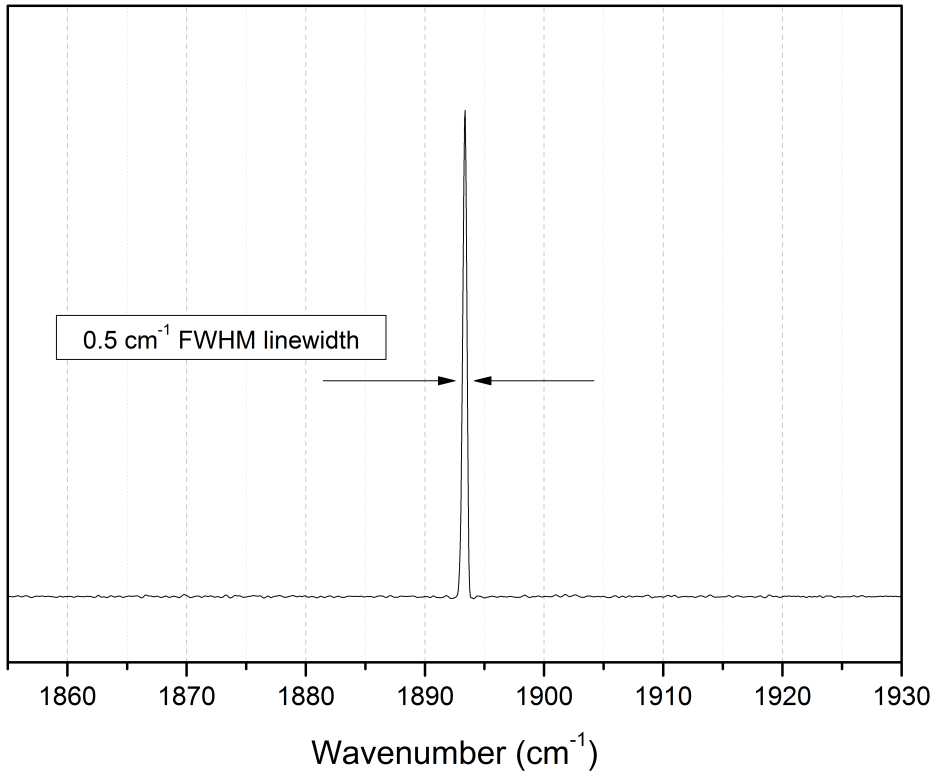

Figure 4.7: Optical spectrum measured from the first microsecond of emission during resonant pumping.

AC and DC components can be controlled in a truly independent fashion. Proper design called for greater consideration of the laser's mounting and heatsinking. To achieve the high level of electrical coupling from the PA to the laser a good level of impedance matching must be employed from end to end. An impedance of 50 Ω is selected to match that of our coaxial cables (RG-58U) and other equipment. The PAs inputs and outputs would be matched at this impedance and the bias-tee's input would also be designed to match this value. The impedance of typical mounted QCL biased around threshold is dominated by its differential resistance. This is known to be in the 5 – 10 Ω range for practically sized ridges. Achieving high levels of non-dissipative coupling requires a reactive impedance matching network to be formed between the bias-tee and the laser device. The growing number of requirements could be solved by producing a new mounting arrangement that combined a DC input, a 50 Ω RF input while being able to be mounted on a TEC cooler that could provide the temperature stabilization to the device. While at modest frequencies,

a number of materials could be used to create matched bias-tees, this final thermal constraint necessitated the use of a more exotic substrate. Direct bonded double copper clad Aluminium Nitride (AlN) provided by Stellar Ceramics had the high levels of thermal conductivity that substrates such as FR4 lack.

4.7.1 Power Amplifier Design

The design of a class A PA suitable for resonant pumping is a task undertaken routinely in many areas of the electronics industry, particularly in communications. As a result, a good deal of documentation and software features are available to support this development. Once the design requirements are known the process is fairly simple. Compared to other PA designs, which may be used in common transmission architectures, this one would only be driven by a single harmonic tone. This reduces the design burden where otherwise certain intermodulation distortion requirements may need to be met. In this case, unlike previous designs that had been used to observe multiple harmonics, the PA would be optimized for a narrow band, around the fundamental cavity frequency, over which good gain flatness would be sought.

The STMicroelectronics PD57006-E LdmoST Lateral Mosfet was chosen on the basis of its low cost and suitable specifications. The PD57006-E specified a minimum gain of 15 dB and a maximum power of 6 W (approx. 38 dBm). Our signal Generator, an Agilent 8648C, could output up to 22 dBm of RF power although power levels above 15 dBm came at the expense of increasing harmonic distortion. This combination would allow powers of at least 30 dBm to be generated before significant distortions would occur. Into an 8 Ω load this would be equivalent to an 8 Vp-p modulation depth, close to the full operating voltage range of a typical QCL.

A centre frequency of 100 MHz was chosen which corresponded to the round trip frequency of a 3 m cavity. Computer optimizations of the PA design would reduce the return loss (S_{11}) to a minimum and flatten the gain (S_{21}) across a band of 40 MHz between 80 and 120 MHz. This range was deemed to be broad enough to capture the response of the cavity under significant detuning as well as providing some safety margin for errors in alignment length.

Once these design decisions had been made and suitable electrical models of the key components have been acquired the engineering of the PA proceeds in the usual fashion. Load-pull and stability analysis are performed using commercial software. These give the ideal operating point for a given frequency. From this point the impedance matching networks can be calculated semi-automatically. One advantage of modern electronic design software is multi goal optimization which can be used as a final step. Here a goal list and optimization parameters can be written and the software, Keysight's Advanced Design System (ADS), will automatically seek the most favourable design solutions. This can include transmission line element dimensions as well as discreet components selection from lists of vendor models such as inductors and capacitors. The mosfet is at the top centre and the other transmission line elements and discrete components make up the impedance matching networks. Fig. 4.8a & b shows the layout photomask and a photograph of the assembled board. The blue features in fig. 4.8a are vias, which connect the top power planes to the bottom side ground plane. These are usually realised using copper through-hole plating but, for simplicity's sake, small copper rivets were used in our design.

The optimization goals used were to produce a gain flatness of 0.5 dB across the band while maintaining a return loss of less than -20 dB. Measuring the return loss (S_{11}) wasn't possible using the available equipment but it was possible to take a rudimentary gain measurement (S_{21}) using a signal generator and an oscilloscope.

The response of the PA is dependent on the mosfet gate bias which was varied experimentally. The measured data of Fig.4.9 shows the operating point that produced optimal gain flatness. At this point the simulated gain is roughly in line with the simulation. The discrepancy is likely the result of a number of factors including component variation, model inaccuracies, unmodeled parasitics, etc. It was also discovered that other electrical elements contributed to this discrepancy and the loss of flatness. The signal generator lacked high levels of power stability across the band though this may have been related to the coaxial cable and its connectors. In this case an oscilloscope was used to measure the power by averaging the pk-pk voltage while on a 50 Ω termination. Greater accuracy might have been achieved using a spectrum analyser.

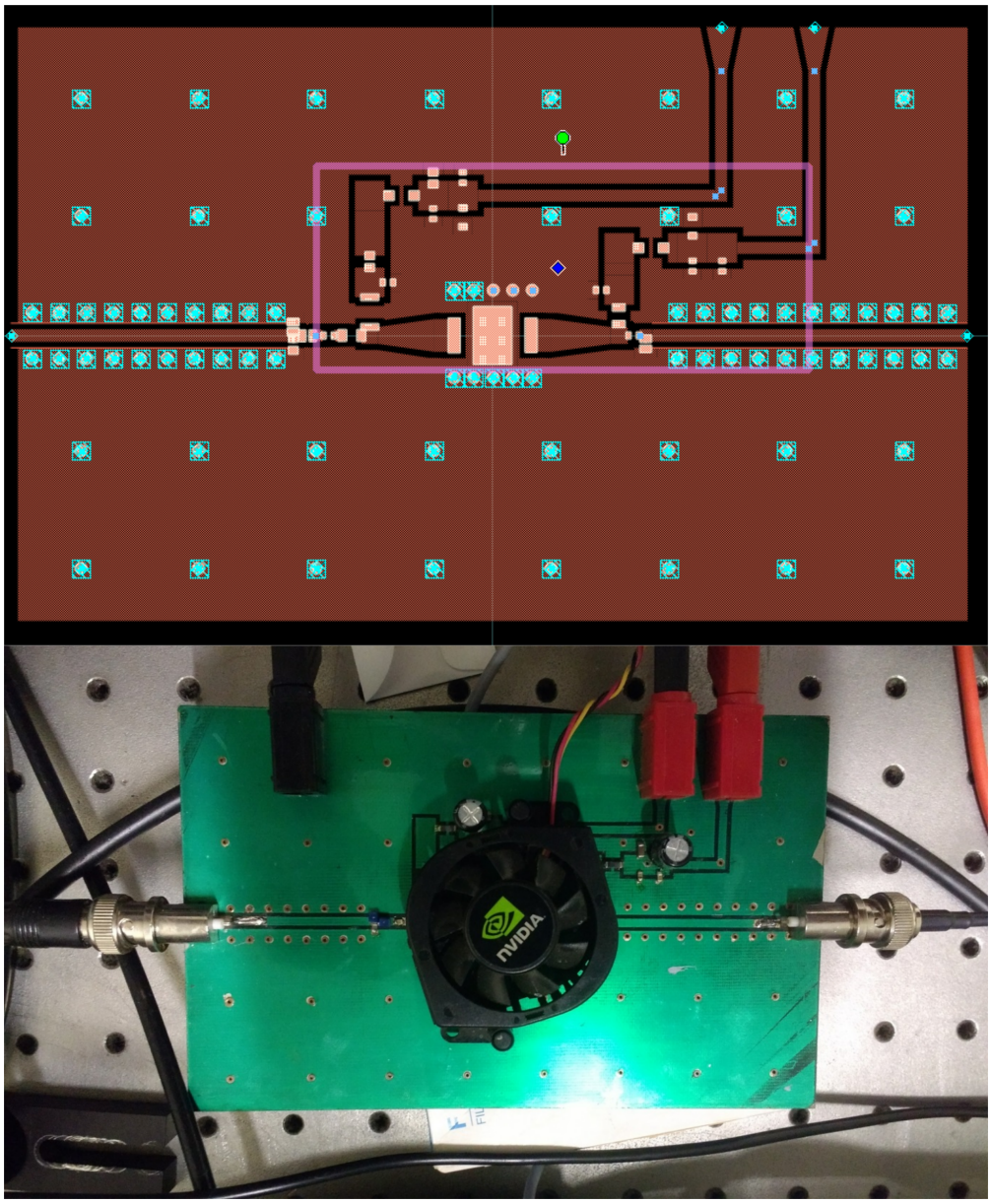

Figure 4.8: **a:** Layout photomask used to fabricate board. **b:** Photograph of finished board fully connected. The periodic vias are used to connect the top and bottom layer ground planes. This is done to suppress EMC issues in the top copper ground plane. The three connectors on the top edge of the board are the ground, gate bias & drain bias which are driven by a dual output bench supply.

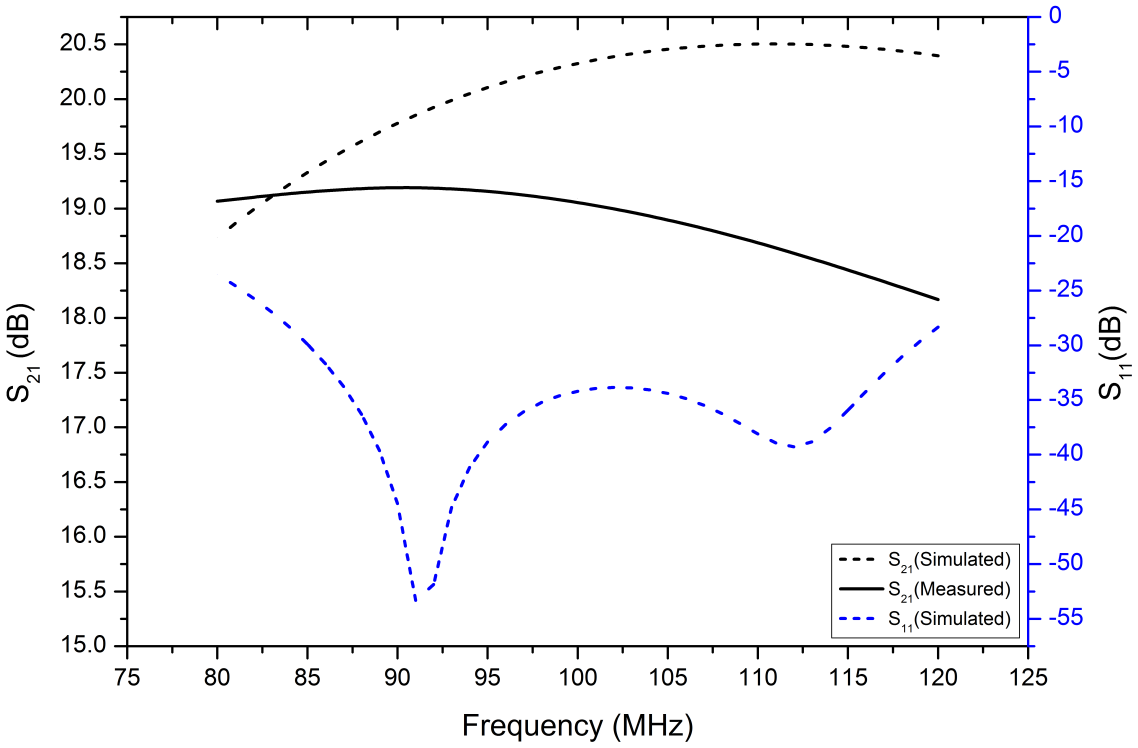

Figure 4.9: Simulated and measured S parameters of Power amplifier with V_{DS} = 15.5 V, I_{DS} = 527 mA. This produced the best real world gain flatness where simulations suggested a slightly different operating point.

It's unlikely that a first revision of a new PA design would have excellent agreement with simulated data when modelled in this way. It's possible that greater accuracy could have been achieved if an EM simulation would have been done once the layout was designed. A further round of optimizations may have improved the situation at the expense of more processing time.

In this case it's very difficult to separate design error from measurement error. A full characterization of the PA would require the use of a calibrated network analyser which could be used to validate the design by extracting the entire scattering matrix. Nevertheless, where only a small band is likely to be needed for a given set of measurements, the PA would seem to operate within tolerances comparable to other elements of the electrical setup.

One further difference between this PA and the previous modulator boards is the true class A operation as opposed to a class AB like operation. Class A operation

ensures lower harmonic distortion by driving the mosfet entirely in its linear region, producing an output which more closely follows the input tone. While the harmonic performance of this board is better the constant bias current means the Mosfet dissipates significantly more heat. The operating point was around 15V V_{DS} and 500 mA I_{DS} with a power added efficiency (PAE) of around 25% which meant almost 6W of heat would need dissipating. To ensure cool operation a small heatsink and fan was cannibalized from an old computer motherboard. Fig. 4.8 shows the board with all the necessary connections made. It requires two separate voltages which provide the drain-source voltage (V_{DS}) and the gate source voltage(V_{GS}). This was conveniently provided by a dual channel bench supply.

4.7.2 Bias-Tee Design

The function of the bias-tee is to combine direct current (DC) from a bench supply with an RF tone from the PA. In our case there is also a need to transform the RF path from the 50 Ω impedance of our PA and coaxial cables to the 5 – 10 Ω of the mounted QCL. Components which form both parts of the bias-tee are subsumed into a single network. This component would be integrated into a laser mount which can accommodate QCL devices on their normal copper submounts. This places an additional thermal constraint on the mount which must provide sufficient cooling for the system to operate continuously. A 40 mm thermoelectric module (TEC) provides this cooling and sits between the bias-tee mount and a 40 mm waterblock. This allows the entire bias-tee mount to be temperature regulated. To realise the electrical network some suitable substrate must be used. Standard FR4 circuit board material satisfies the electrical requirements but has poor thermal conductivity through the substrate. In this scheme the thermal path will go through the electrical substrate, meaning good conductivity is required to sink the watt level heat dissipated by the QCL. Aluminium nitride (AlN) is available in a double copper clad format, similar to standard double sided FR4 boards. AlN has a thermal conductivity of 319 W $m^{-1}K^{-1}$ compared to around 0.3 W $m^{-1}K^{-1}$ for standard FR4. On this basis AlN was chosen as a substrate for the development of a number of thermally regulated bias-tee laser mounts.

Proper design of the bias-tee requires some knowledge of the electrical charac-

teristics of the QCL itself. An electrical model must be created that represents the load seen when looking into the mounted QCL assembly including the QCL chip, the bonding wires and the bonding pad. Fig. 4.10 shows a basic equivalent electrical circuit of the mounted QCL, which is appropriate when the QCL is being driven in the small signal limit while biased in the roughly linear Ohmic region above threshold.

In reality the resistive component of the QCLs impedance is extremely non-Ohmic and requires a far more complex equivalent model[9] to fully capture the behaviour of the device over its full operating range. Under large signal modulation the impedance of the QCL will vary meaning a perfect impedance match is impossible. Attributing values to these equivalent components is done firstly by plotting the I-V curve for the device in the DC limit. A gradient taken at the laser's threshold current will give the differential resistance of the device about that point. This value provides the equivalent value of the resistor. This is true because in the DC limit, which is a steady state condition, the parallel capacitors can be considered open circuit and the series inductor can be considered shorted. The capacitance of QCL ridges is due to the top metal contact and is extremely low, of the order of 0.1 pF. At these values its contribution to the overall impedance is low so this rough estimate will suffice. The bonding pad capacitance can be measured using an LCR meter or calculated, it being an almost ideal parallel plate capacitor with a PTFE dielectric. This gives a value of around 1 pF. Finally, the bonding wire's inductance is estimated from a rule of thumb approximation. These wires generally have an inductance of 1 nH per mm. Depending on the mounting the wires can be between 2 and 5 mm long and number for 4 to 12. Many bonding wires in parallel reduces the inductance according to

$$\frac{1}{L_{tot}} = \sum_{n} \frac{1}{L_n}$$

although a mutual inductance term enters the equation. A figure of around 1 nH is used where a good number of wires are present. All of these figures vary from device to device and the bias-tee needs a reasonable level of performance when used with a number of devices.

These figures can be taken as an average for which the bias–tee will be optimized. Again, this model would have ideally been created using a network analyser which could have performed a one port measurement while the system was biased which

would have produced an S parameter file which could have been used to optimize the bias-tee. This approach becomes more attractive when the circuit is designed for a single device where a good match is required.

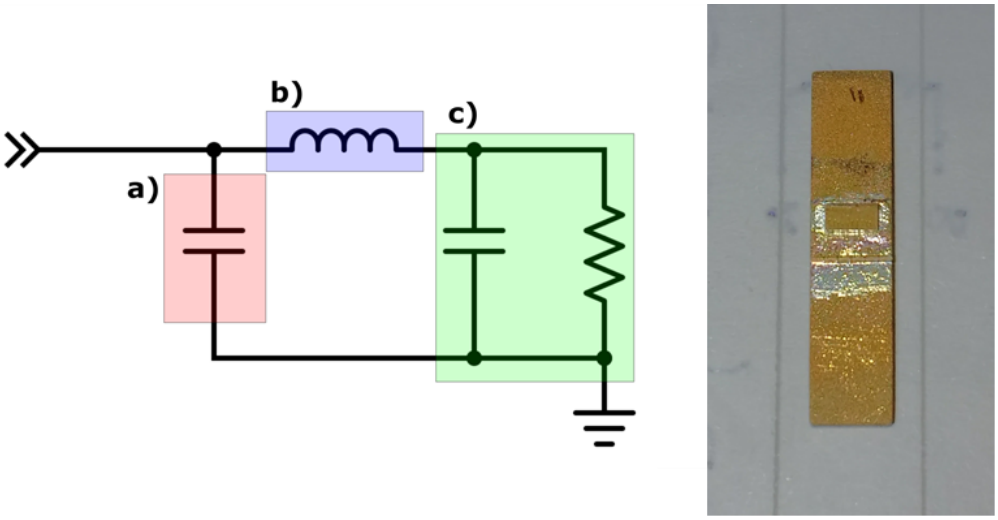

Figure 4.10: Left: Equivalent circuit model comprising a) bonding pad capacitance b) bonding wire inductance and c) Parallel CR of the QCL chip. Right: Photograph of a typical mounted QCL.

A number of problems have to be addressed in order to manufacture these components. The large copper base can be machined in the normal fashion but processing the AlN substrate is more challenging. The copper clad AlN was bought as a single piece of 160 mm by 120 mm. Initially the material underwent an etching using a negative dry film photoresist which removed copper on both sides such that the material could be scribed and snapped into smaller pieces. Due to the thickness of the copper layer (approx. 200 μm) each piece needed to be thinned prior to normal processing. Standard 1 oz copper clad FR4 PCB material has copper 35 μm thick, this thickness is well suited for photolithography and this was set as a target copper thickness for the AlN. Chemical milling using a bubble etch unit with a ferric chloride etchant was tested for this purpose but was found to etch the copper in a non-uniform fashion over such a long range. The best results came from using a surfacing plate with various grades of wet and dry sand paper. This was a painstaking process which required constant measurements to be taken of the thickness using high precision callipers. At some thickness the grade would begin to be increased until finally a polishing with a high speed rotary tool and 0.5 μm diamond

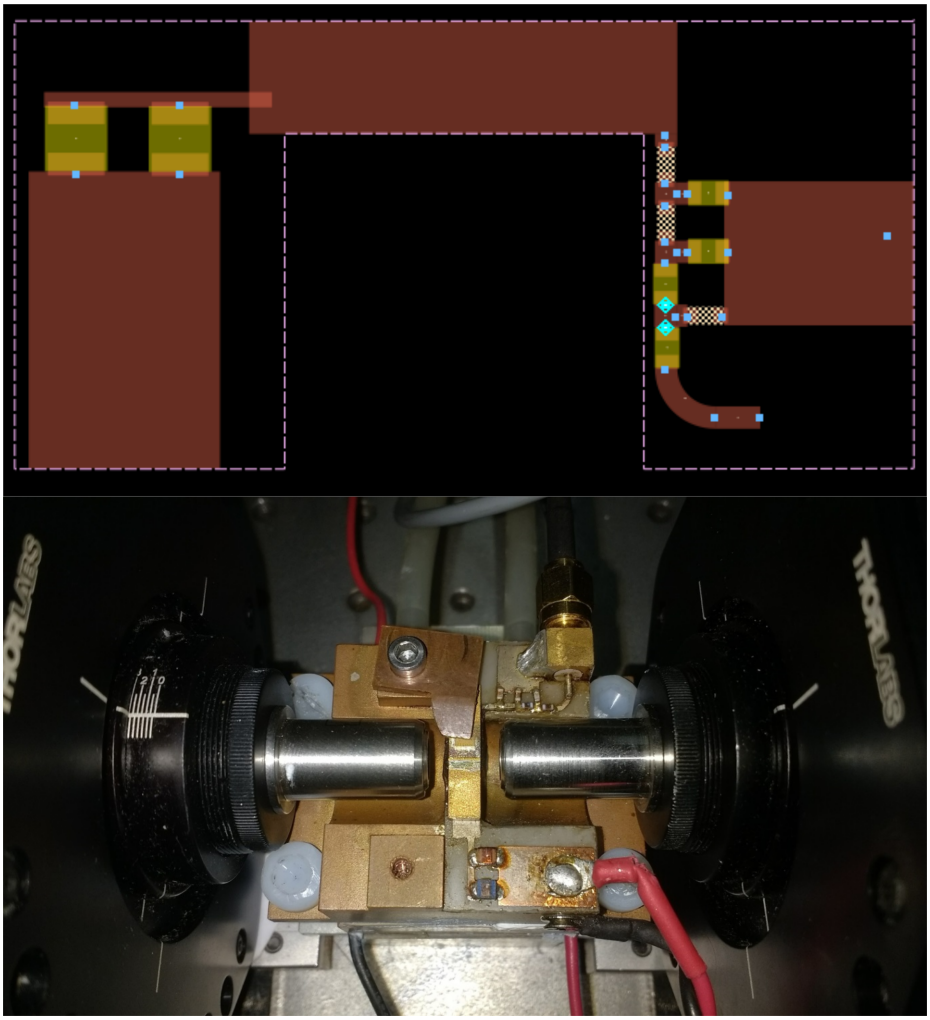

Figure 4.11: **a:** Layout pattern used for the Aluminium Nitride substrate showing the placement of discrete components. The large pad at the top accommodates the QCL submount, the curved track to the right is the RF input which uses a SMA connector and the large pad to the left is the DC input. **b:** Photograph of the assembled Mount in situ. Also visible are the TEC cooler electrodes and the waterblock feeds to the top.

lapping paste left a good quality surface. The opposite side of the AlN received little treatment. This side was to be brazed to the copper base and it was found to be sufficient to remove the oxide layer with a few strokes across the surface plate using a coarse grade of wet and dry emery paper. The quality and cleanliness of the top copper surface was essential for sound application of the photoresist, PRP200, which was sprayed and required about 12 hours drying at room temperature before exposure was possible. The key here is to have an extremely clean, dry and level surface. A photolithography/etching process was the same as used for other PCBs, the chemistry is perfectly compatible with AlN. Also, initial efforts were silver immersion plated in the hope of stopping oxidation of the copper layer and increase the solderability where a silver containing solder would be employed.

The difficulty comes in soldering the assembly together. Brazing the AlN substrate to the copper base is relatively straight forward but populating the AlN circuit with the surface mount components is challenging. A hot plate was used to raise the temperature of the entire assembly to around 160 °C. This made it possible to use a reflow hot air station to flow the solder paste which had a melting point around 200 °C. The real problem here is oxidation. The long periods of high heat was found to rapidly oxidise the surface making it difficult for the solder paste to wet the surface in the normal fashion. The relatively thin silver plate didn't survive very long at high temperature. Even with various fluxes it was still necessary to use a fibreglass pen to abrade the surface prior to each component. Under normal circumstances it would have been possible to apply solder paste to the landing pads and flow it all in one go followed by a brief reflow as each component is added. This approach was possible on pads with some thermal relief but others landed on large ground pads which made it difficult. The use of a solder resist mask was also impossible due to the high temperatures needed. It was also suggested that solder resist mask has poor performance levels at microwave frequencies where dielectric losses became high. Additionally because of the unusual shape needed to accommodate the lens tubes, it was necessary to cut a section out of the AlN between the brazing and soldering phase. This was done with some care using a high speed rotary tool and a number of diamond burr tools. This could be done relatively easily once the AlN was brazed to the copper base. This dictated the order of soldering meaning the

AlN couldn't be populated until already attached to the base.

Fig. 4.11a & b shows the layout photomask and a photograph of the finished bias-tee laser mount. The two larger components in fig. 4.11a are surface mount inductors that provide the DC path, a pair being needed to avoid saturation. The other smaller components are inductor and capacitors which form the impedance matching network for the RF path. The copper base is grounded and contacts the bonding pad through a small copper arm visible in fig. 4.11b.

4.8 Overview

With the power amplifier and bias-tee designed and manufactured the setup is assembled as shown in Fig. 4.12. Testing shows that the thermal performance of the bias-tee is comparable to mounting on raw copper. Clearly the addition of a roughly 1 mm thick Aluminium nitride substrate doesn't add a significant amount of thermal resistance to the assembly. To aid in heat extraction a copper based thermal and electrically conductive compound is used between the top copper of the AlN substrate and the copper QCL submount. This compound has increased thermal conductivity compared to typical ceramic pastes as well as being electrically conductive which ensures there is a large, low inductance, electrical contacting area.

Electrically the system is less noisy than was the case with the earlier designs. One indication of this is the very low levels ($\sim$-60dBm) of pickup noise seen on the spectrum analyser from the detector with the cavity blocked. This is around three orders of magnitude better than before and is likely related to the grounding of the copper mount as well as the correct polarisation being used with the coaxial cables which produces the intended shielding effect.

In this case the RF path has a number of capacitively coupled sections which protect the QCL from failure. This wasn't the case in previous designs which needed to provide a DC path through to the device. Previous designs had, on at least one occasion, destroyed a QCL after the failure of the main mosfet. The single supply provided a convenient method of controlling, limiting and measuring the DC while, with necessary adjustment, the signal generator allows the RF power to be set. The only real uncertainty that remained is the return loss from the bias-tee which

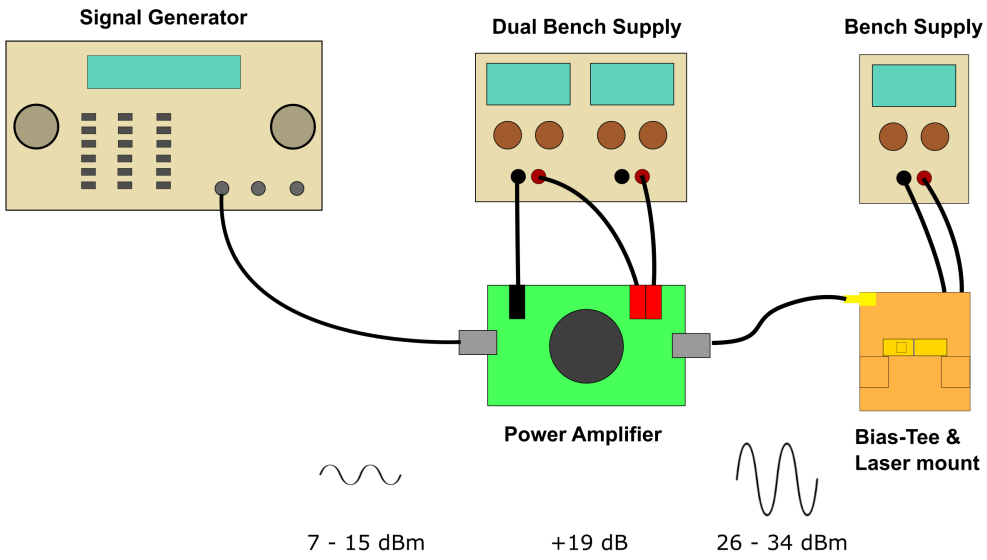

Figure 4.12: Electrical Chain for resonantly pumping the QCLs. A one tone signal is produced by our Agilent 8648C signal generator, undergoes amplification by the power amplifier and is coupled into the QCL through the bias-tee mount. A single bench supply provides the DC bias for the device.

simulations suggest are less than -20 dB and is assumed to be flat across some small modulation band.

The real limitation of this new setup is one of bandwidth, with the system only designed to operate at a single fundamental harmonic of around 100 MHz. Previous drivers had managed to produce resonant excitation up to around 400 MHz or the 4th or 5th harmonic. This means with a slightly longer cavity up to 5 pulses would circulate simultaneously. The electrical coupling was very poor in this case and accurate measurements were impossible. These harmonics were only observed using pulsed lasers and resulted in no differences in the measured optical spectrums. The ability to produce higher frequency/harmonic excitation in a well behaved manner would have been useful. Significant difficulties are encountered when trying to engineer PAs and bias-tees with usable bandwidths that span many octaves. It was decided that the best approach would be to design and manufacture components for certain bands when required. To this end a number of copper mounts were machined at the same time with the intention of producing bias-tees for other frequency ranges.

Bibliography

[1] Yongrui Wang and Alexey Belyanin. Active mode-locking of mid-infrared quantum cascade lasers with short gain recovery time. *Optics express*, 23(4):4173–4185, 2015.

[2] Gorachand Ghosh. *Handbook of optical constants of solids: Handbook of thermo-optic coefficients of optical materials with applications*. Academic Press, 1998.

[3] Raymond J Lanzafame. Ultrashort laser pulse phenomena: Fundamentals, techniques, and applications on a femtosecond time scale, by jean-claude diels and wolfgang rudolph. *Photomedicine and Laser Therapy*, 25(1):58–58, 2007.

[4] Th Udem, Ronald Holzwarth, and Theodor W Hänsch. Optical frequency metrology. *Nature*, 416(6877):233–237, 2002.

[5] QY Lu, M Razeghi, S Slivken, N Bandyopadhyay, Y Bai, WJ Zhou, M Chen, D Heydari, A Haddadi, R McClintock, et al. High power frequency comb based on mid-infrared quantum cascade laser at λ 9 μ m. *Applied Physics Letters*, 106(5):051105, 2015.

[6] Andreas Hugi, Gustavo Villares, Stéphane Blaser, HC Liu, and Jérôme Faist. Mid-infrared frequency comb based on a quantum cascade laser. *Nature*, 492(7428):229–233, 2012.

[7] Aleksander K Wójcik, Pietro Malara, Romain Blanchard, Tobias S Mansuripur, Federico Capasso, and Alexey Belyanin. Generation of picosecond pulses and frequency combs in actively mode locked external ring cavity quantum cascade lasers. *Applied Physics Letters*, 103(23):231102, 2013.

[8] Christine Y Wang, Lyuba Kuznetsova, VM Gkortsas, Laurent Diehl, Franz X Kaertner, Mikhail A Belkin, Alexey Belyanin, Xiaofeng Li, Donhee Ham, Harald Schneider, et al. Mode-locked pulses from mid-infrared quantum cascade lasers. *Optics Express*, 17(15):12929–12943, 2009.

[9] Gui Chu Chen, Guang Han Fan, and Shu Ti Li. Spice simulation of a large-signal model for quantum cascade laser. *Optical and quantum electronics*, 40(9):645–653, 2008.

Chapter 5

Mode-Locked External Ring Cavity QCLs

5.1 Introduction

In addition to the reduced pulse repetition rates generated by free air coupled external cavities, the ring geometry has been suggested as a platform for robust short mode-locked pulse generation in QCLs on the basis of its ability to avoid the spatial hole burning (SHB) instability. SHB has already been shown to distort, or even prohibit, pulses in mode-locked ridge QCLs[1]. In principle ERCs should be able to emit mode-locked pulses which are generated as a result of uni-directional emission, suppressing all SHB effects. Despite the mode-locking of ridge QCLs having already been demonstrated and the promise of mode-locked ERC-QCLs having been highlighted in theoretical studies[2], up to this point there has been no demonstration of mode-locked QCLs in either ERC or even Linear ECs. This provided us with an interesting opportunity, one that allowed us to exploit the knowledge we had gained while working on pulsed and CW ERC-QCLs.

In this chapter we discuss how the setup developed in chapter 4 is used to study the ERC-QCL under resonant modulation. Data is presented showing the temporal response as well as spectral information. This is presented firstly for the case of a single spatial mode (Sb9710) then for a multi-spatial mode device (Sb9709).

5.2 Setup

To study the effects of resonant pumping of the ERC-QCL the setup detailed in chapter 4 was employed. The expectation would be that with sufficient DC and RF power and at modulation frequencies at or around the cavity round trip frequency, some modulated output would be seen at the detector. Because the main benefit of using ring geometries lies in the decoupling of propagation directions, and subsequent suppression of SHB, an ability to measure asymmetries between the two directions is essential. For this purpose a second Vigo systems fast MCT detector is employed, allowing both directions to be measured simultaneously. These detectors differed slightly in detectivity and bandwidth. The slower detector lacked the bandwidth to temporally resolve pulses at the 100 MHz target frequency, meaning an optical chopper was needed to produce a measurable signal. Some scaling of the data was necessary to correct the difference in detectivity between these two detectors.

Having two different outputs does make it difficult to build an accurate picture of the spectral response of the system. Spectral measurements require one output from the beam splitter to be coupled into the FTIR. Given that asymmetries are anticipated, ideally both propagating directions would be spectrally measured. One method of achieving this would be to rotate the beam splitter to change the propagating direction sent to the FTIR. This would most certainly perturb the system, meaning the two sets of data wouldn't correspond to each other. In reality the only measurements that firm conclusions can be drawn from are those measured simultaneously which for spectral measurements would require the use of a second FTIR. For this reason one propagating direction is chosen for spectral measurements while the opposite direction has a detector aligned to provide a RF signal to the spectrum analyser as well as the oscilloscope. As in previous experiments the cavity is aligned at a length of around 3 m which results in a pumping frequency of around 100 MHz, matching the design frequency of our electronics.

Two different Alpes Buried Structures were used for the mode-locking ERC-QCL experiments; both emitted at 5.3 μm and were 4.5 mm long. Buried structures are discussed in chapter 3. Both devices are capable of continuous-wave (CW) emission. The difference between the two devices was the width of their ridges with one at 5.6 μm, designated Sb9710 and one at 11.6 μm, designated Sb9709. This meant that the narrower of the two would only support a single fundamental spatial mode while the wider of the two would likely support a number of additional higher order spatial modes. The hope was that this would provide some insight into the role played by higher order spatial modes in resonantly pumped systems. Both devices had both facets anti-reflection (AR) coated to supress their Fabry-Perot modes.

A 3 m bow-tie ring cavity is aligned in the usual fashion, detailed in section 3.3. This is possible because although the specially made AlN laser mount, detailed in chapter 4, accepts a DC input and a RF input, it was found to be the case that pulses of the order of a microsecond could be coupled through the DC path despite its inductive coupling being designed to block RF power from being coupled into the bench supply. In general, pumping a partly capacitive load through a inductor can lead to a ringing with the potential for an overshoot. In this case the relatively long pulses as well as the nature of the resistive component of the load meant this

wasn't an issue. The only noticeable difference being a slightly less abrupt shape to the current pulse caused by the effective blocking of the high frequency components of the current pulse. This meant the system could be aligned using pulses then the electronics could be switched to the resonant pumping setup without otherwise disturbing the alignment of the cavity.

5.3 Single-Mode Mode-Locked ERC-QCL

With the cavity in good alignment and with DC level set below the laser's CW threshold (331 mA in this case), relatively low levels of RF power are added. With the signal generator set to around 0 dBm, approximately 20 dBm of power is delivered to the mount. Starting from this low base the frequency can be swept across the target range using the signal generator. While the mirror positions needed to create a ring cavity of a given length can be measured out on the optical bench there is usually some error that is difficult to judge. This equates to some small uncertainty in the round-trip frequency. Sweeping the frequency across some generous band ensures that resonance is passed through. If no emission is detected the RF power and DC can be increased incrementally. When the limits of the laser are well known this approach isn't necessary. In that case the laser can have its DC and RF power set to a maximum so as to find the emission quickly. A reasonable expectation here would be that for a given DC and RF power pulse amplitudes would be at a maximum at exact resonance, where the optical pulse from a previous cycle perfectly coincides with current pulse from next.

Indeed, pulse amplitudes are seen to increase up to some modulation frequency before diminishing as the frequency is further increased. Fig.5.1a shows an example of the pulses detected from one propagating direction near the presumed cavity resonance. Over a timescale of 50 – 100 ns the pulses look fairly consistent in amplitude. Taking a look at these pulses over a longer period, as in the right side of fig.5.1a, it's clear that very little amplitude noise exists in the pulse envelope when driven at the cavity resonance. With greater detuning from resonance, as in fig.5.1b, the amplitude noise increases.

Allowing the oscilloscope to trigger from the waveform means that pulses will

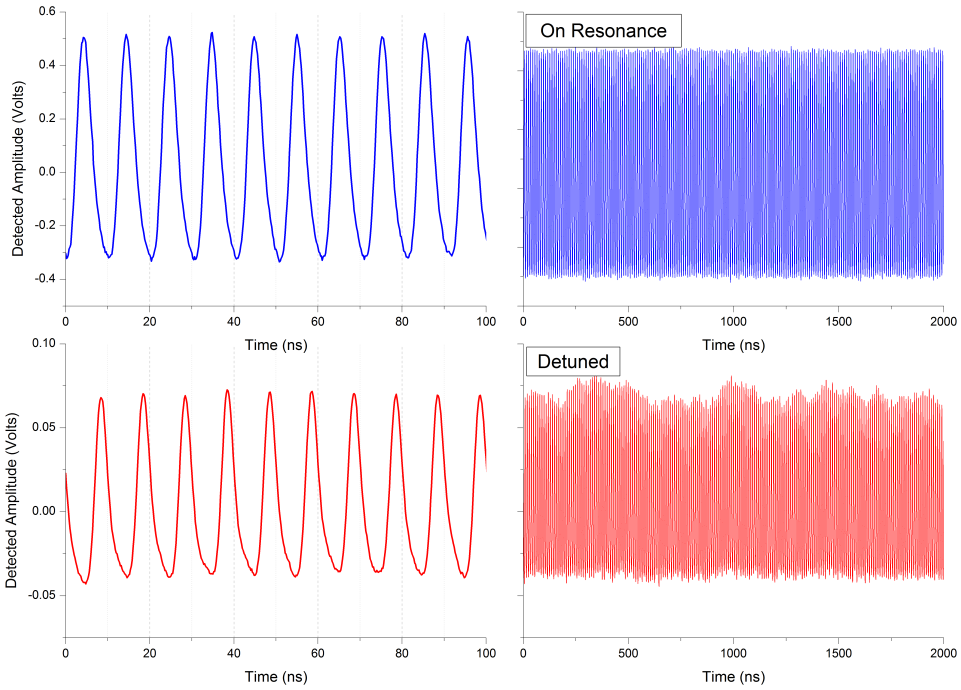

Figure 5.1: Detected transient response of an approximately 3 m harmonically pumped ERC-QCL. A DC level of 200 mA and an RF power of around 34 dBm drives the buried structure QCL. In this case resonance is around 98.5 MHz and the detuned example is set at 99.5 MHz.

appear stationary during successive waveform updates. This allows averaging to be used and peak to peak pulse amplitudes to be extracted. Taking these average pulse amplitude measurements provides a means of studying the response of the cavity to resonant pumping. While this method gives some idea of the response of the system to a certain operating point (DC, RF power, modulation frequency), it suffers from certain limitations. Triggering in this way tends to preferentially select high amplitude pulses, leaving collapsed parts of the wave form from the average. This would likely distort the figures much more at large detuning where the pulse train collapses more frequently. Plotting these average pulse amplitude against the operating point clearly shows the response of the cavity to active modulation.

Because pulses should, in principle, be shortest when the ratio of RF power to DC is highest, i.e. when the modulation is the deepest, RF power tended to be fixed towards the top end of what was available (26 -34 dBm). Average pulse measurements were taken at fixed RF power, at various DC levels and plotted against modulation frequency. The ring geometry meant that there were two average pulse

amplitude readings for each operating point, one for each propagating direction. Fig.5.2 shows the results of this measurement for a number of DC levels.

Pulse amplitude measurements at frequencies around resonance reveal unambiguously the tendency of mode-locked ERC-QCL systems to emit in a unidirectional, or at least asymmetric, fashion. In this system there is a clear pattern in the emission, with the CW direction being favoured on the low frequency side and a switching occurring to favour the CCW direction as the frequency increases. This pattern seems to hold across the entire DC range with the switching occuring at roughly the same frequency, around 98.3 MHz. This would seem to coincide with the resonance of the cavity. It would also suggest that there is some physical asymmetry in the system which makes it favour this regime, the most likely candidate being some small difference in the residual reflectance of the AR coatings. This could be tested by rotating the laser device with respect to the cavity, the difficulty being that this would require the cavity to be realigned. It's likely a large number of realignments would be needed to prove this hypothesis. An exact mechanism which explains how this switching at resonance occurs may be complex and requires significant analysis but a general tendency of mode-locked ERC-QCL systems to favour unidirectional regimes can be understood to occur for reasons similar to those of the continuous-wave ERC-QCL.

Starting from a symmetric position where two equal pulses pass each other in the gain medium, a small perturbation to the amplitude of one would mean that during the time the pulses occupy the same region of the gain medium one would maintain a travelling wave component that would be able to access the gain at the nodes of the gain grating created by the interfering pulses. This would mean the greater pulse would *starve* the lesser while being able to consume the gain in the non-competing regions of the gain medium. This spatial hole burning related effect creates, in ring cavities, a *pulse avoidance* mechanism which gives rise to unidirectional pulse propagation[3]. This could be viewed as an example of the general principle that laser systems tend to find regimes that maximize the amount of gain consumed. While strictly speaking this modulation frequency dependence on emission asymmetry isn't necessary for unidirectional pulse propagation, which theory suggests should be observed on resonance, it does strongly support the suggestion that actively modulated

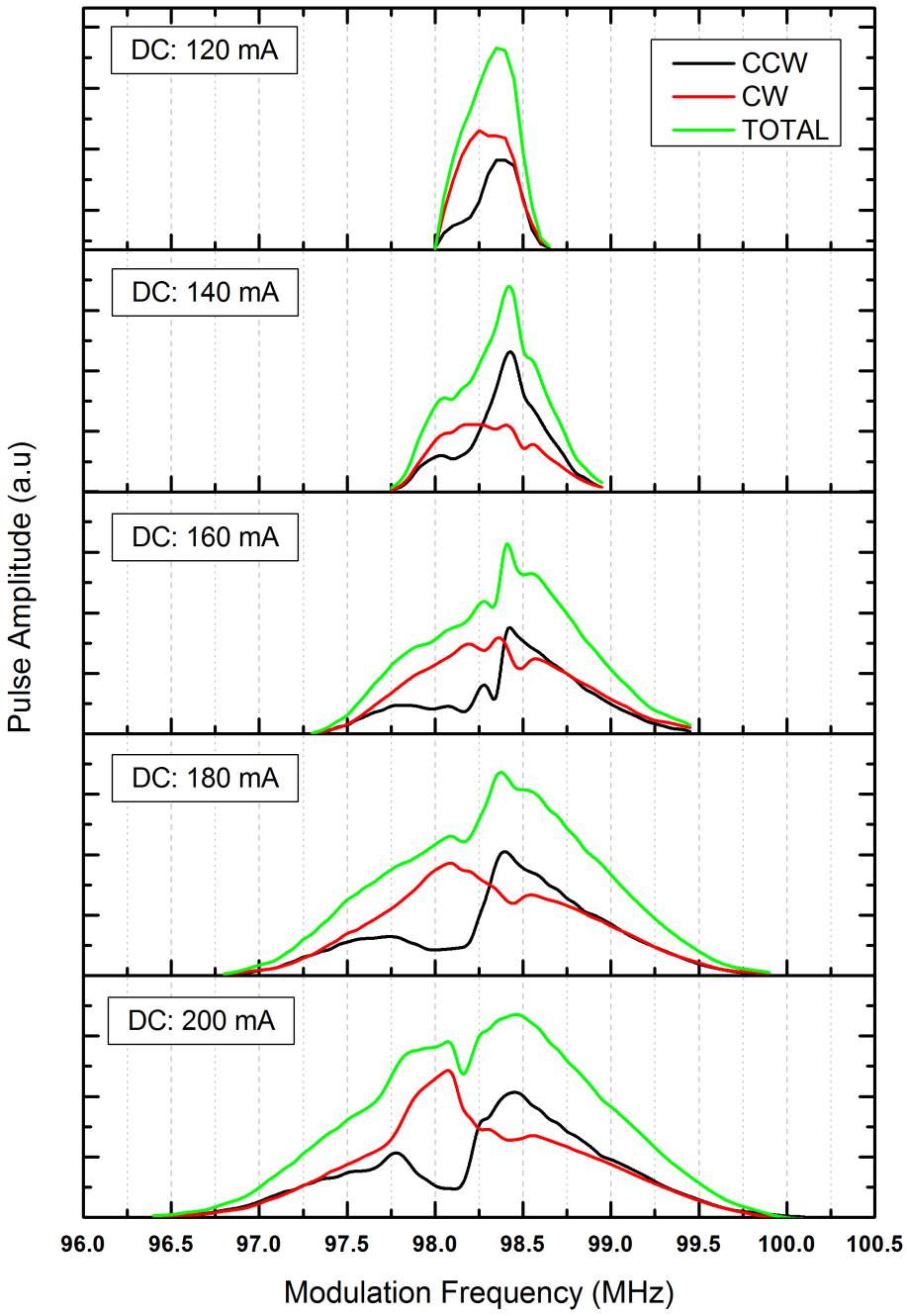

Figure 5.2: Maximum peak to peak pulse amplitude of counter-propagating pulses of a single-spatial-mode ERC-QCL at various DC levels with an modulation RF power of 34 dBm. At every DC level a clear asymmetry exists between the two propagating directions.

ERC-QCLs have the ability to emit pulses in a unidirectional fashion.

While these measurement clearly demonstrate the resonant response of the ERC-QCL, more insightful results can be found in the frequency domain. To this end the detector signal is measured using a spectrum analyser which allows frequency components in the vicinity of the round-trip frequency to be measured. This is done using a HP E4411B spectrum analyser and helps us understand the characteristics of the field envelope. In a stable mode-locked system the expectation is that a single narrow line will exist in the RF spectrum. Any sideband noise or any significant width to the peak would in this case signify a collapsing or otherwise unstable pulse train. These measurements are combined with spectral measurements at optical frequencies from our Bruker IFS 66v/S FTIR. Again a single peak in the optical spectra would signify a stable mode-locking condition.

With the RF power and DC fixed, both optical and RF spectra are taken at various modulation frequencies in the vicinity of the round trip frequency. The results shown here are characteristic of all devices that we measured and remain qualitatively similar over most of the usable range of operating conditions. The system, depending on the operating point, lases in one of three distinct ways, characterised by its optical spectrum; single-peaked, multi-peaked or broad. Examples spectra of these three regimes are shown in fig. 5.3.

Fig. 5.4 shows both the optical and RF spectra of the system when modulated at frequencies around the round trip frequency. A strong resonant response is seen with the highest intensity emission occurring roughly in the middle of the band at around 98.3 MHz. Here the emission is largely single peaked. At some level of detuning emission becomes broad and of low intensity. These regions coincide with the RF spectra where single peaked optical emission has a low associated RF sideband noise. Conversely, where the optical regime collapses to low intensity broad emission the RF spectra picks up a significant amount of sideband noise.

The easiest to understand is the broad regime which exists under relatively large detuning. This chaotic regime has a low intensity broad optical spectrum which appears on both sides of resonance. The broad features in the RF spectrum coincide with the onset of broad emission and show an unstable pulse train which collapses randomly. These features quickly broaden as detuning is increased signifying a pulse

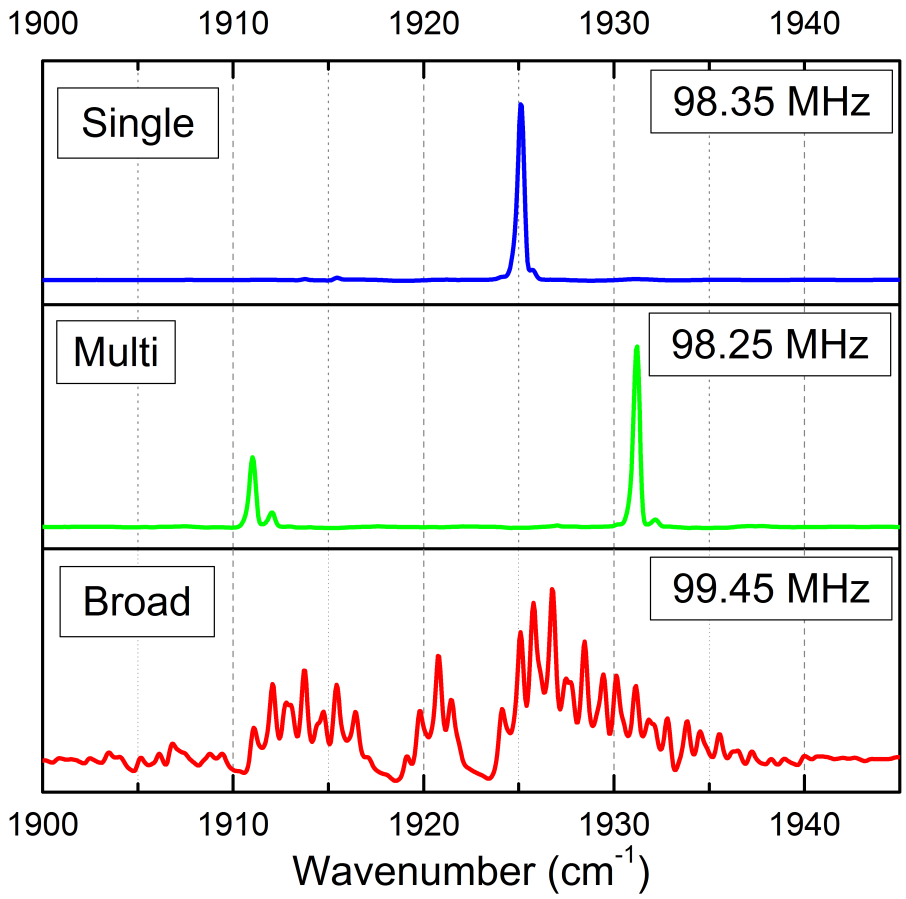

Figure 5.3: Characteristic optical spectra of the three regimes; single peaked, multi-peaked & broad, seen under resonant modulation of an ERC-QCL.

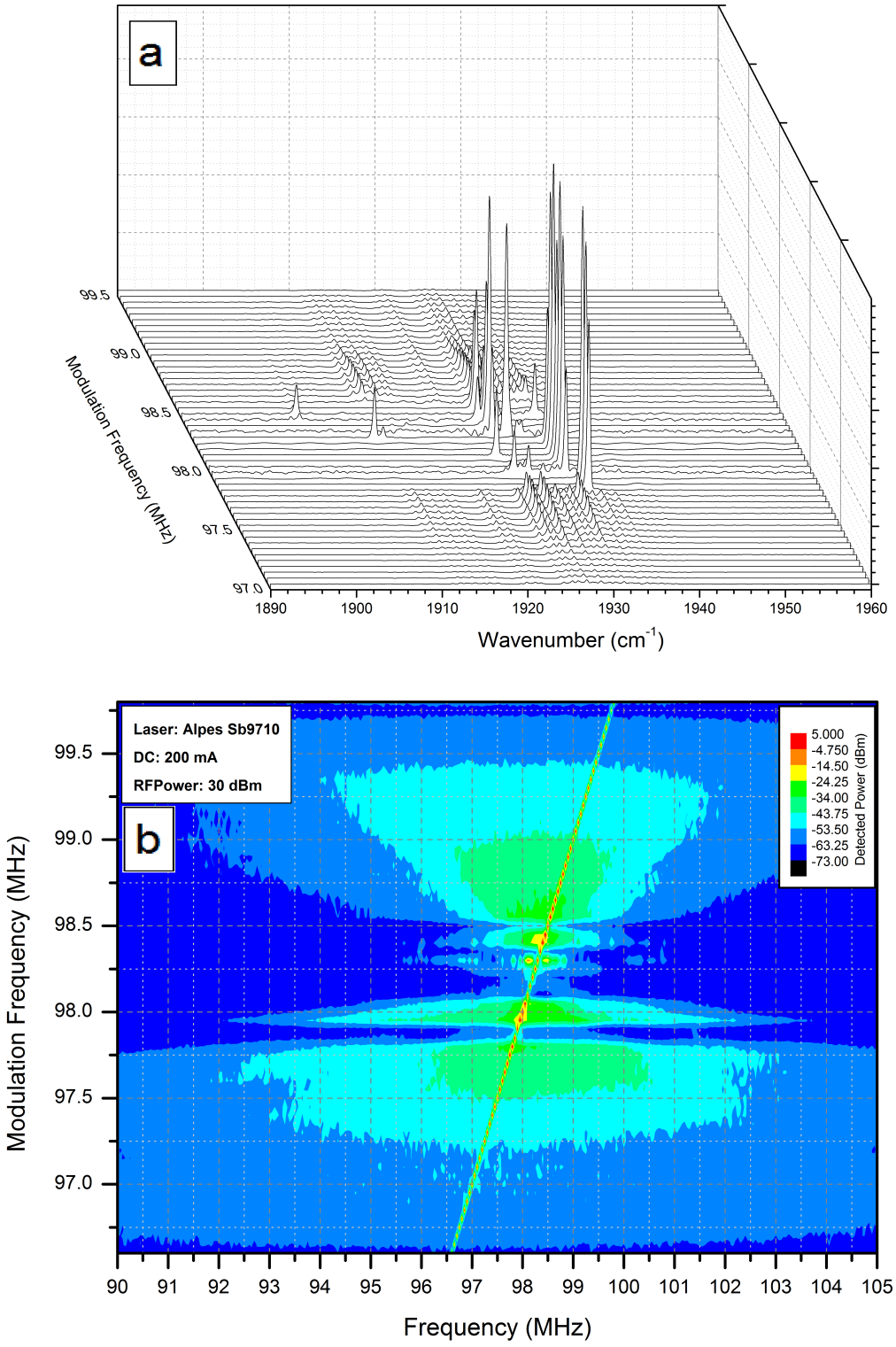

Figure 5.4: a: Optical spectra, b: RF spectra; of a 3 m ERC-QCL under near resonant modulation at a DC level of 200 mA.

train that collapses with increasing frequency until the detuning reaches a point at which no significant emission is sustained.

Under large detuning, the laser's gain would reach a maximum with some delay relative to the optical pulse envelope, amplifying one of the pulse tails to a greater extent. These pulse tails would be composed of broad electroluminescent (EL) photons which would be amplified on the following cycle. This could be regarded as super electroluminescent (SEL) light, with the majority of the intensity likely coming from EL photons which were amplified for a single or low number of cycles.

Between these broad features is a region of single and multiple peaks. Here the intensity of the emission indicates normal laser action, the result of many cycles of amplification. Despite these two spectral sets coming from opposite directions there still seems to be a strong correlation between them, with low sideband noise in the RF spectrum coinciding with a single peak in the optical spectrum. These stable single peaked regions are present at a number of modulation frequencies. Conversely, higher levels of sideband noise in the RF spectrum always coincide with multi-peak emission in the optical domain. This is likely to be the result of a switching behaviour rather than a stable multi-wavelength output. This would certainly account for the noise in the RF spectrum. At this operating point, the region between the broad emission regimes has significant bandwidth, approx. 750 KHz in this case. This would seem to suggest that the pulses have a minimum duration of around 1 ns.

The picture is slightly complicated by the fact that asymmetry is present in the two propagation directions. In this case the optical spectra are from the CW direction which is consistently dominant on the low frequency side of resonance, presumed to be around 98.35 MHz. In the region from 97.8 to 98.25 MHz the two domains from the two different directions coincides very well. Optical spectra beyond 98.3 MHz become erratic and multi-peaked which would seem to coincide with the switching of the dominant direction from CW to CCW.

All the measurements at a modulation frequency of 98.35 MHz suggest that stable mode-locking is achieved. Fig. 5.5 shows spectra at this modulation frequency. A narrow, resolution limited optical spectrum along with a very narrow RF beat-note both occur at the peak of intensity, as found from peak amplitude measurements, strongly suggesting the presence of a stable mode-locked pulse train.

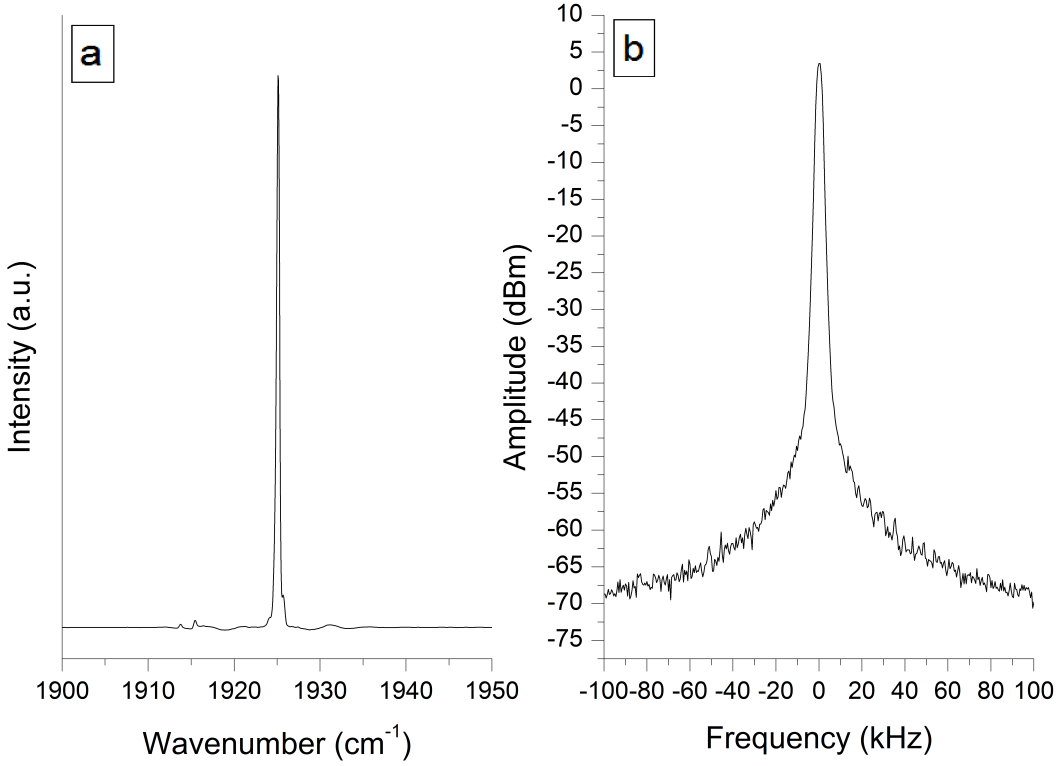

Figure 5.5: Mode-locking condition of an External Ring Cavity QCL at 98.35 MHz. Both optical and RF spectra are resolution limited at 0.5 cm^{-1} and 1 kHz repectively.

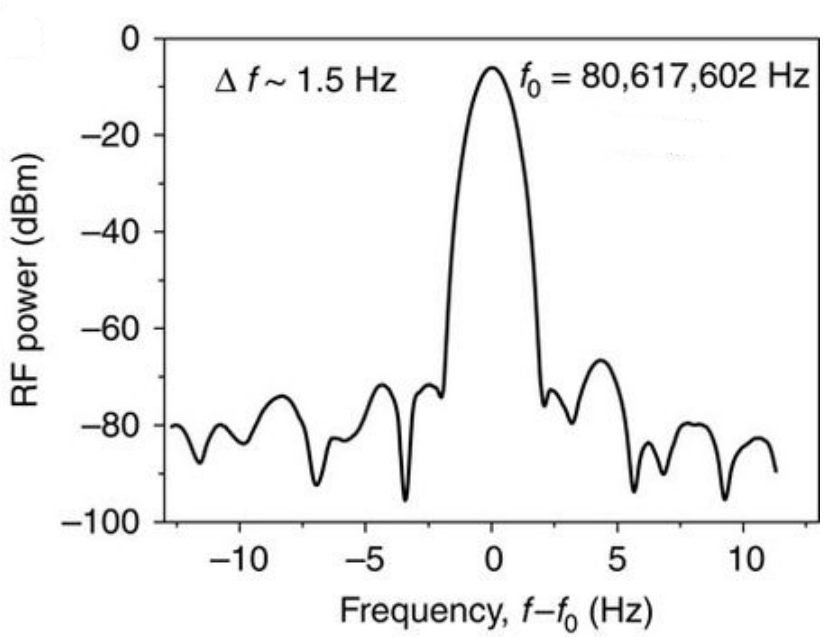

Figure 5.6: High resolution RF spectra of a 3.7 m ERC-QCL resonantly pumped at 80.6 MHz [3].

Fig. 5.6 is a RF spectrum which was measured for a longer (3.7 m) ERC-QCL system using a higher resolution spectrum analyser. This shows, under the right conditions, the system can emit pulse trains with a RF linewidth of less than 1.5 Hz, suggesting that pulse trains remain stable for around 10^8 pulses.

5.4 Conclusion - Single Mode

We have shown unambiguously the mode-locking of the ERC-QCL by active gain modulation of the QCL device. We have shown that in the case of the ERC-QCL it is possible to produce asymmetric or unidirectional pulses that could avoid the effect of spatial hole burning to which mode-locked ridges are prone. This first step towards well behaved, short mid-infrared pulses from ERC-QCLs demonstrates the sensitivity of such systems to resonant pumping.

A single narrow peak was observed in both the optical and RF domain. The RF intensity spectrum has a very narrow, resolution limited, peak with a FWHM of 10 kHz which suggests stable pulse trains of at least 10^4 pulses. The single peaks in the optical domain are also limited by the resolution of our FTIR but can be presumed to contain a number of cavity modes. Full characterisation would require an second order interferometric autocorrelation setup or a similar pulse characterisation setup such as electro-optic sampling but the modulation band would suggest the pulses have a minimum duration of around 1 ns for cavities pumped at a fundamental frequency of 100 MHz.

5.5 Multi-Mode Mode-Locked ERC-QCL

Unlike the previous section where we used a narrow ridge QCL (5.6 μm wide), supporting only a single fundamental spatial mode, now a wider (11.6 μm) ridged QCL is deployed. Both devices, from Alpes Lasers, were processed from the same wafer and so have closely matched characteristics. This higher powered device supports a number of higher order spatial modes. While beam prolife measurements would be needed to accurately quantify these spatial modes, a strong sense can be gained by breaking the beam under continuous-wave pumping. When this is done a number of emission regimes are observed.

When a gain medium capable of supporting higher order spatial modes is used the picture becomes increasingly complex. Unlike the case of single mode gain mediums, now the system develops a number of different lasing solutions for each operating point i.e for each modulation frequency, RF power and DC. Breaking the beam in different directions allows for a number, usually 3 to 5, of different emission regimes to be observed. This selection by beam breaking is clearly having the effect of introducing spatial mode dependent losses during laser start-up. It's known that buried heterostructure QCLs tend to have spatial modes with similar threshold currents[4]. This would suggest that the laser has a number of different lasing regimes accessible to it for a given pumping operating point. Breaking the beam vertically, for example, would briefly create a condition where one vertical lobe of a higher order vertical mode is blocked, giving favour to spatial modes less concentrated at one of the vertical extents. In some frequency ranges near resonance this can be done in a predictable way, with stable results, at other times the response is less predictable and can be short lived, quickly switching to some preferred regime. While this same behaviour can be seen from multi-spatial mode EC-QCLs, in an ERC configuration there is an additional element of asymmetry which can exist between the two propagating directions. Fig. 5.7 shows a number of regimes that can be tracked as the modulation frequency is increased towards resonance. Similar colours indicate measurements taken simultaneously using two detectors. Breaking the beam allows a number of different regimes to be accessed. A significant number existed beyond the three illustrated here but these were the most stable examples which show a CCW (blue lines in fig. 5.7) and CW (red lines in fig. 5.7) dominant regime as well as one which is largely coupled (green lines in fig. 5.7).

In the case of the multimode device there are great difficulties in measuring pulse amplitude as has been done in previous experiments. Here certain regions exist where a large number of regimes, of varying stability, exist for a given operating point. In some regions these can be tracked like in Fig. 5.7 where nearer the presumed resonance the regimes become more sporadic. In this case the region around the resonance, which was found to be around 97.2 MHz using the previously described method, had two different regimes which were stable and could be tracked over some small band. Fig. 5.8 compares the spectra of these regimes.

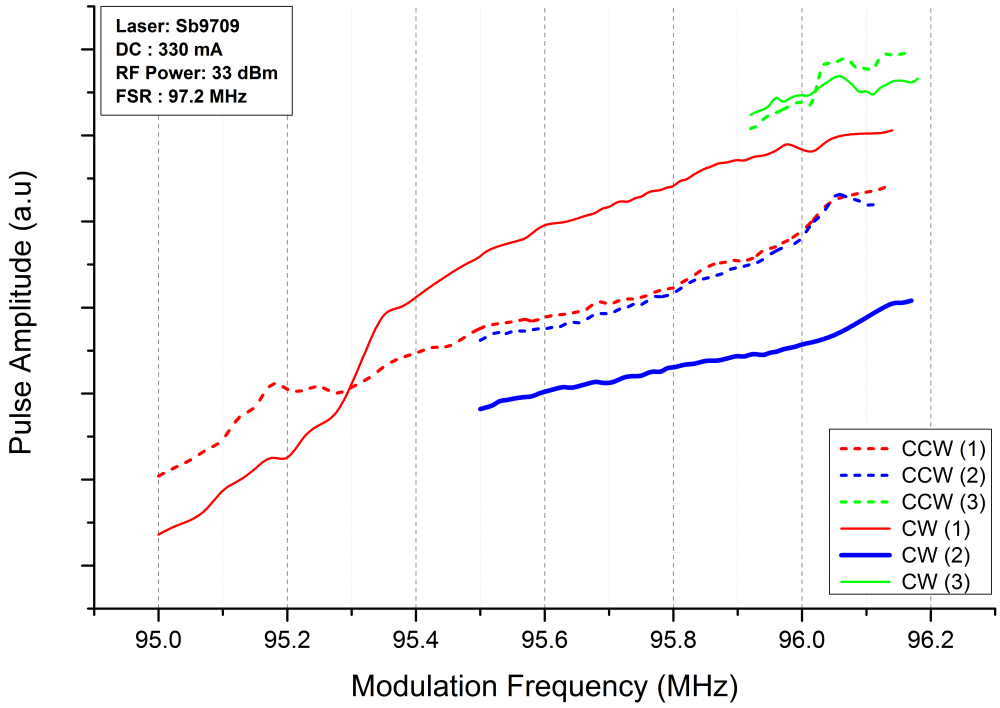

Figure 5.7: Maximum peak to peak pulse amplitude of a multi-spatial–mode ERC-QCL under near resonant modulation. Here lines and dashes of a similar colour represent the emission of oppositely propagating pulses that were emitted simultaneously.

The difference here being that one regime is largely single peaked while the other has two clear emission wavelengths. Associated with each is a strange comb structure in the RF domain. This clearly indicates some coherent process. It could be the case that at such small detuning from resonance the pulse train collapses at regular intervals producing this sideband pattern. One thing that is clear in this and previous experiments is the dominant effect that the beam splitter is having on the emission wavelength of the output. The parasitic etalon effect of the CaF_2 is creating a low finesse filter with a FSR of just below 8 cm^{-1}. Careful examination of optical spectra from the single mode ERC-QCL also show some significant etalon effect, just as in the continuous-wave experiments. In this sense the difference between these two near resonance regimes is that one is lasing on a single etalon order while the other lases on an adjacent pair.

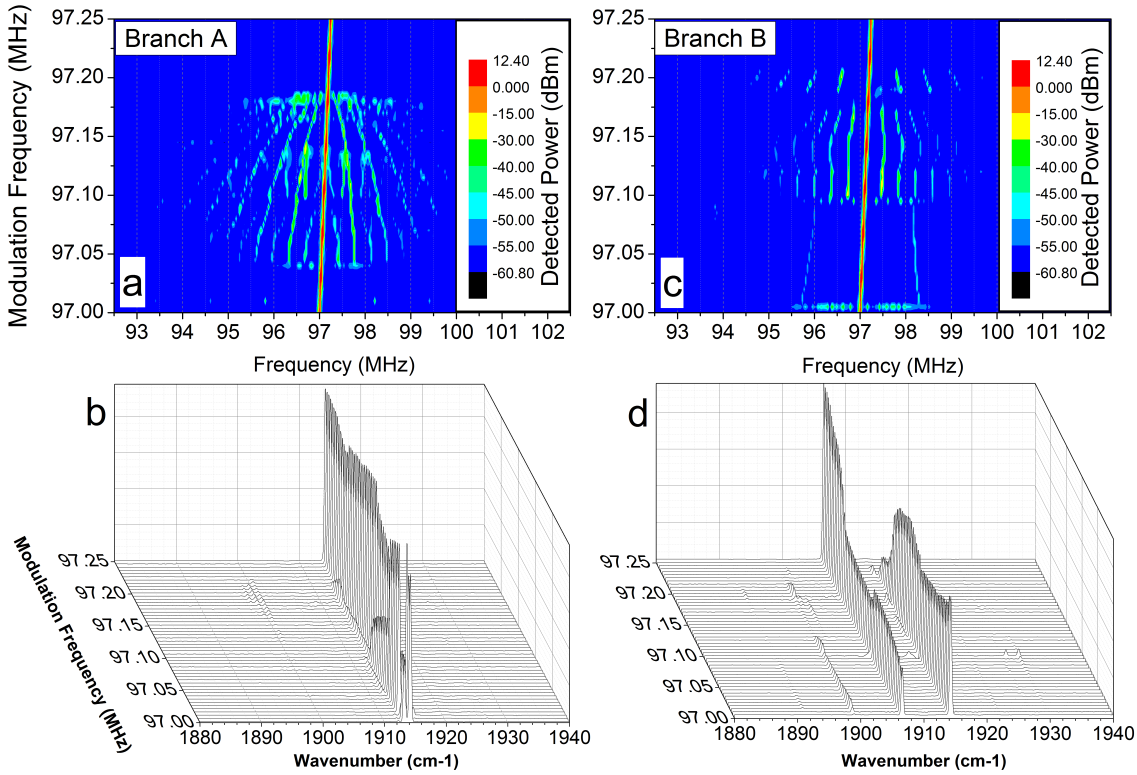

Figure 5.8: **a:** RF spectrum, **b:** Optical spectrum; of an emission regime characterised by a multi-wavelength optical spectrum. **c:** RF spectrum, **d:** Optical spectrum; of an emission regime characterised by a largely single-peaked wavelength. Both sets measured from the same multi-spatial-mode ERC-QCL with a modulation RF power of 34 dBm and a DC of 350 mA.

5.6 Conclusion - Multimode

In the case of the broader ridge, no data was presented for the mode-locking condition as it was discovered that the AR coating on one facet was damaged and this may have had some effect near resonance. The multi-mode effects observed here are qualitatively similar to those observed for other resonantly pumped multi-mode QCLs. Exact resonance, in this case, is likely to be less well defined with each spatial mode having a slightly different resonant frequency due to differing effective modal indices.

Bibliography

[1] Christine Y Wang, Lyuba Kuznetsova, VM Gkortsas, Laurent Diehl, Franz X Kaertner, Mikhail A Belkin, Alexey Belyanin, Xiaofeng Li, Donhee Ham, Harald Schneider, et al. Mode-locked pulses from mid-infrared quantum cascade lasers. *Optics Express*, 17(15):12929–12943, 2009.

[2] Aleksander K Wójcik, Pietro Malara, Romain Blanchard, Tobias S Mansuripur, Federico Capasso, and Alexey Belyanin. Generation of picosecond pulses and frequency combs in actively mode locked external ring cavity quantum cascade lasers. *Applied Physics Letters*, 103(23):231102, 2013.

[3] DG Revin, M Hemingway, Y Wang, JW Cockburn, and A Belyanin. Active mode locking of quantum cascade lasers in an external ring cavity. *Nature communications*, 7, 2016.

[4] Aleksander K Wójcik, Nanfang Yu, Laurent Diehl, Federico Capasso, and Alexey Belyanin. Self-synchronization of laser modes and multistability in quantum cascade lasers. *Physical review letters*, 106(13):133902, 2011.

Chapter 6

Mode-Locked Linear External Cavity QCLs

6.1 Introduction

In chapter 5, mode-locking of the ERC-QCL was demonstrated with the sustained emission of stable pulse trains. Both theoretical studies[1] and ridge mode-locking experiments[2] have shown that spatial hole burning (SHB) can destabilize or distort the pulses of mode-locked systems when in a linear cavity configuration. Currently, there have been no reports of the active mode-locking of EC-QCLs. Here we use our existing electronics system to investigate the ability of the EC-QCL to be mode-locked using active modulation.

Using a harmonic pumping scheme in a linear cavity would be analogous, in some ways, to the already demonstrated ridge QCL mode-locking experiment. For this purpose a number of non-buried ridge QCLs with 5.3 μm wavelength, produced in Sheffield, were prepared and anti-reflection coated on one facet while being high-reflectivity coated on the other. This means that the gain medium can sit at one end of an external linear cavity with a high finesse cavity being formed between the single external mirror and the high reflectivity facet. In this way the gain medium is equivalent to the small modulated section in the ridge mode-locking device.

The difference being, other than the much reduced round trip frequency, that in the sectioned ridge mode-locking device the pulse's round trip is entirely inside the semiconductor material of the QCL. Even though only a small section at the end of the ridge was electrically modulated to produce the pulses, there may have been some significant gain experienced by the pulse while transiting through the longer non-modulated section of the device. This is likely to have had a dramatic impact on the formation of pulses which were observed.

The experimental setup used to study the external cavities under resonant pumping was similar to that used for the mode-locked ERC work. In addition to the DC pumping provided by a standard bench supply there was also the RF pumping which was generated using the system detailed in chapter 4. Of the QCLS which were prepared for this work only a few were deemed to perform well enough to be used for this work. The best of these was designated 8A and was 3 mm in length with emission centred at around 5.3 μm. To suit the electronics a cavity with a physical length of 1.5 m was aligned. This corresponded to a round-trip frequency of approx. 100 MHz. Optical spectra as well as RF spectra were measured for modulation

frequencies around the round trip frequency.

This chapter begin with a discussion of the setup, similar to that used in chapter 5, detailed in chapter 4. Measurements, similar to chapter 5, including temporal and spectral data is presented. Firstly for the case of a linear EC-QCL is modulated at the cavity's fundamental frequency and then, using a custom made high frequency bias-tee, for the case of high harmonic pumping, up to a frequency of around 3 GHz.

6.2 Fundamental Pumping

As in the ERC case, it was found to be considerably easier to align the cavities using pulses of a few microseconds from our Avtech pulse generator than using CW or resonant pumping. The low duty cycle pulses create relatively high levels of gain which makes it easier to find correct alignment during the final stages of the alignment procedure. These pulses could be coupled through the DC path of the bias-tee without any problems.

The setup here is similar to that of the ERC under resonant pumping. With DC and RF power being delivered to the QCL and the oscilloscope triggering from the detector channel, pulses are observed at modulation frequencies in a band of a few MHz around the round trip frequency. Fig.6.1 shows the pulses seen by the detector. As was the case in the ERC, while pumped close to the round trip frequency, a stable pulse train is generated. This can be seen in the upper right part of fig.6.1. Detuning from resonance leads to instability in the pulse train, as can be seen from the bottom right part of fig.6.1.

To investigate the response of the system we follow a similar approach to chapter 5. Using the oscilloscope's averaging, pulse amplitudes are extracted for a given operating point (DC, RF power, Modulation Frequency). This allows the response of the cavity to varying modulation frequencies to be plotted for different DC and RF levels. Like before, we fix the RF power and take measurements at various DC levels. Although in principle shorter pulses are likely to form at higher RF powers, with the QCLs reliability in question, both DC and RF components were limited to relatively modest levels.

Fig.6.2 shows that in contrast to the ERC, the single effective propagating di-

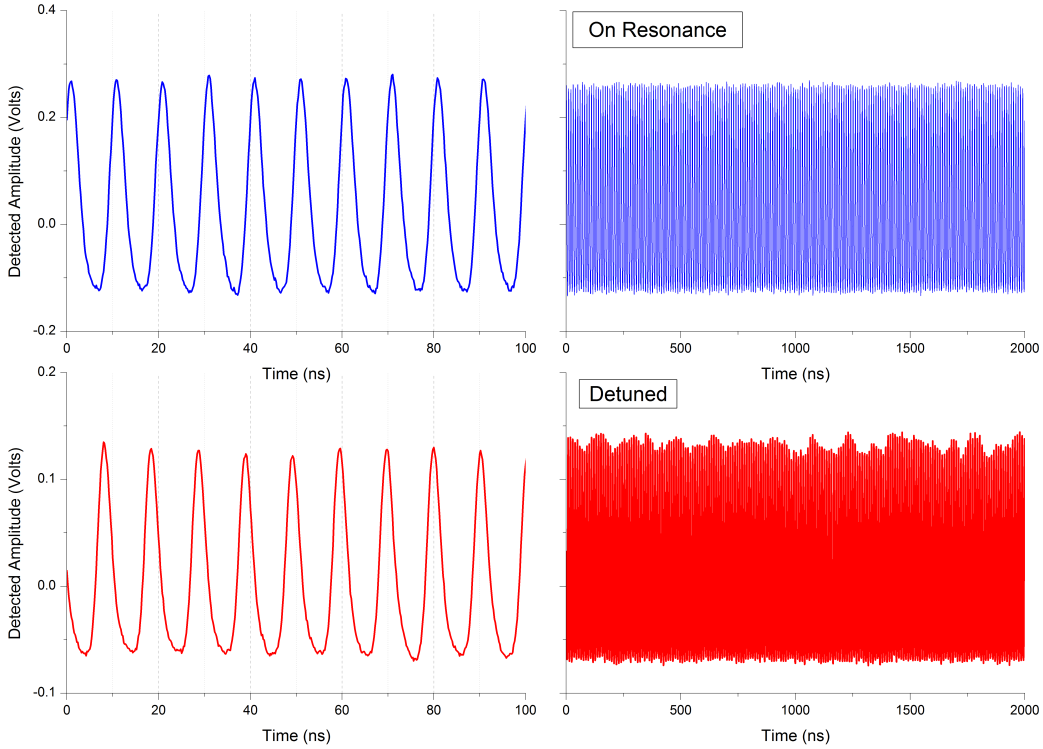

Figure 6.1: Detected transient response of an approximately 1.5 m harmonically pumped EC-QCL. A DC level of 100 mA and an RF power of around 34 dBm drives the ridge QCL. In this case resonance is around 100.0 MHz and the detuned example is set at 97.5 MHz.

rection leads to the response becoming symmetric, sharing an apparently simple relationship with the detuning frequency. The asymmetric switching behaviour in the ERC clearly introduces some significant perturbation into this more ideal looking form. Either side of resonance the amplitudes diminish in an almost linear fashion, though the detectors non-linear response and the averaging used here may convolute this to some extent. What can be said is that the maximum pulse amplitudes are observed at some resonant modulation frequency, in this case around 99.5 MHz and, for a given RF power, increase with the DC component. The DC component can be thought of as lifting an increasing amount of sine wave above threshold allowing pulses of greater detuning to be sustained for some time.

This idea of increasing window size under in detuned system is detailed in a theoretical study[3]. With emission being produced with a detuning of as much as 5% of the modulation frequency it's doubtful that this signifies the formation of ultra-short pulses. This would after all represent a pulses peak from a previous

cycle being 15 cm short of the gain medium when the next electrical pulse is at its maximum, at least on the high frequency side of resonance. This would seem to suggest that pulses in this relatively high DC case have lengths in the order of at least a nanosecond. If this is the case then detuning would be resulting in the tails of the pulse being amplified, shifting the pulse envelope with each successive round trip. This is likely to be a noisy and chaotic process, similar to that observed in other detuned mode-locked systems.

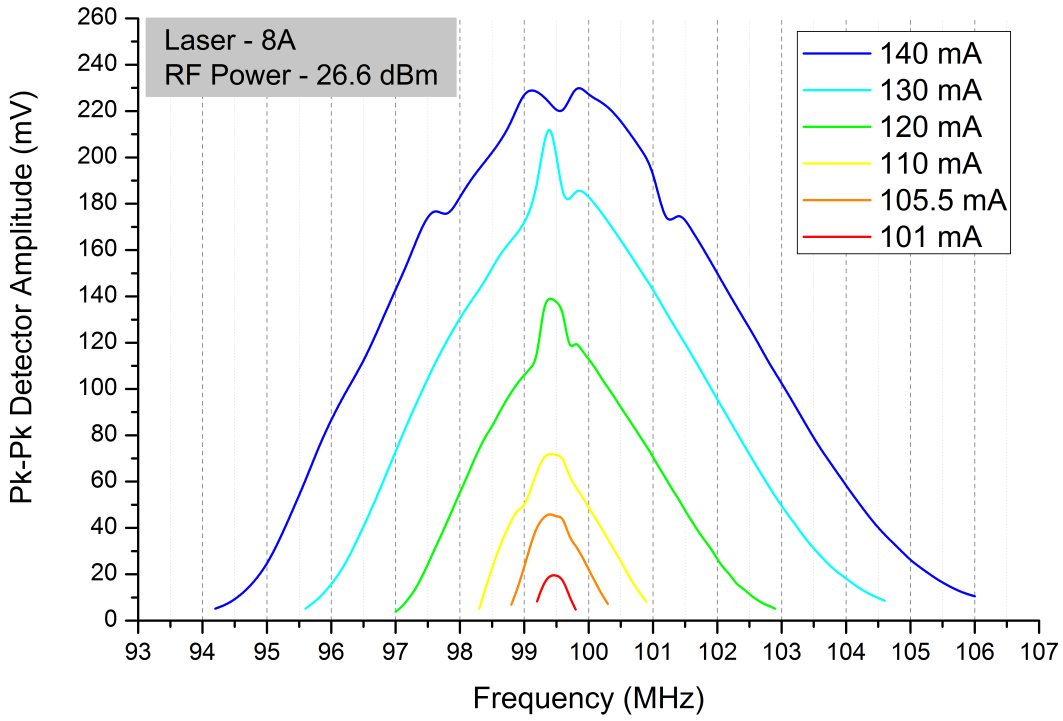

Figure 6.2: Maximum detected pulse amplitude vs modulation frequency at various DC levels for fixed RF power of a 1.5 m EC-QCL.

These pulse amplitude measurements show nicely the resonant response of the cavity but again we turn to the frequency domain to build a more comprehensive picture of the system's behaviour. A number of other QCL devices from the same batch had failed during testing at higher current. With this in mind as well as the time required to measure optical spectra, it was decided that measurements should be performed at modest DC levels.

When the spectral data is compared to the ERC-QCL a very similar picture

emerges. The combined optical and RF spectra reveal a number of behaviours which seem to be characteristic of both resonantly pumped EC & ERC QCLs. The optical spectra show that over the tuning range, the emission can be largely divided into three categories; single-peak, multi-peak or broad.

In the low DC limit (fig. 6.3), a broad emission regime is observed only on the high frequency end of the detuning. This coincides with the feature present in the RF spectrum starting at around 99.8 MHz. This broad emission regime with its associated RF sideband noise is the most unstable and highly chaotic emission seen under modulation. The explanation for this regime is based on super EL emission, exactly the same as was detailed in the previous chapter for the case of the ERC. As the DC is increased, as in fig. 6.4, this broad regime is observed on both ends of the detuning and the large features in the RF spectrum seem to support a view that at this level of detuning the pulse train is collapsing and restarting rapidly and in different spectral positions.

While it's not clear why this regime initially appears only on the high frequency end, one explanation may be that the leading edge of an early electrical pulse contributes electro luminescent (EL) photons to the leading edge of the optical pulse that will then coincide with the peak of the current pulse on the subsequent cycle. This isn't the case in low frequency limit where the EL is added to the trailing edge of the pulse envelope. The EL that will coincide with the peak of the electrical pulse on the following cycle, in this case, comes from the trailing edge of the current pulse. Despite the relatively short electrical pulses, thermal effects occur on a picosecond timescale. The trailing edge of the current pulse will have experienced some device heating and will contribute less EL to the leading edge. This is due to normal thermal non-radiative scattering. This would mean that some additional pumping would be required to compensate for the thermal losses before this broad super EL regime achieves threshold in the low frequency limit. The initial appearance of broad emission in the high frequency modulation limit is also observed in ERCs for the same reason. While this explanation is difficult to confirm, the EL photons that occupy the *dark* part of the cavity are known to play a role in detuned actively mode-locked systems[3].

At higher currents (fig. 6.4), broad emission is observed on either end of the

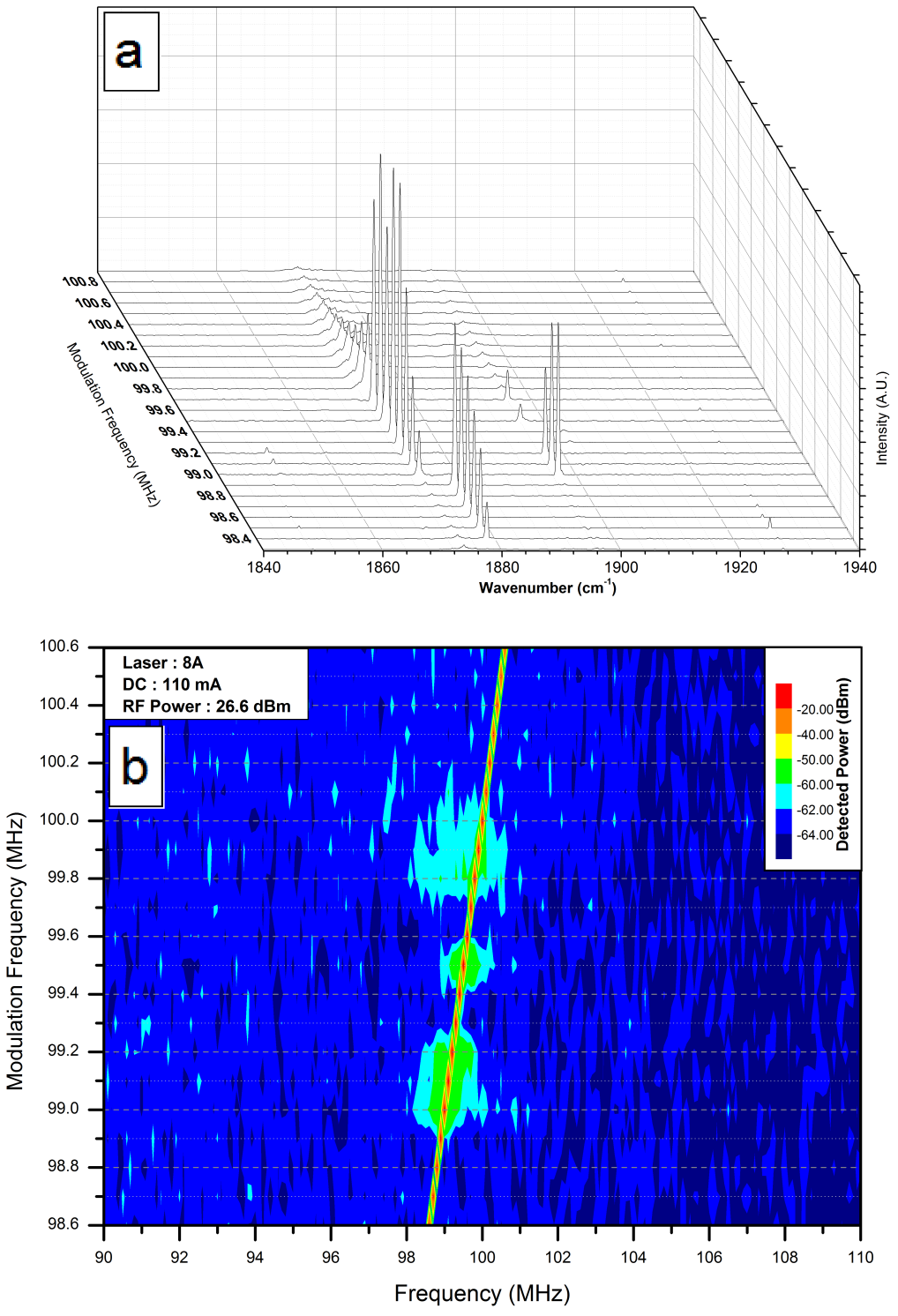

Figure 6.3: **a:** Optical spectra, **b:** RF spectra; of a 1.5 m EC-QCL under near resonant modulation at a DC level of 110 mA.

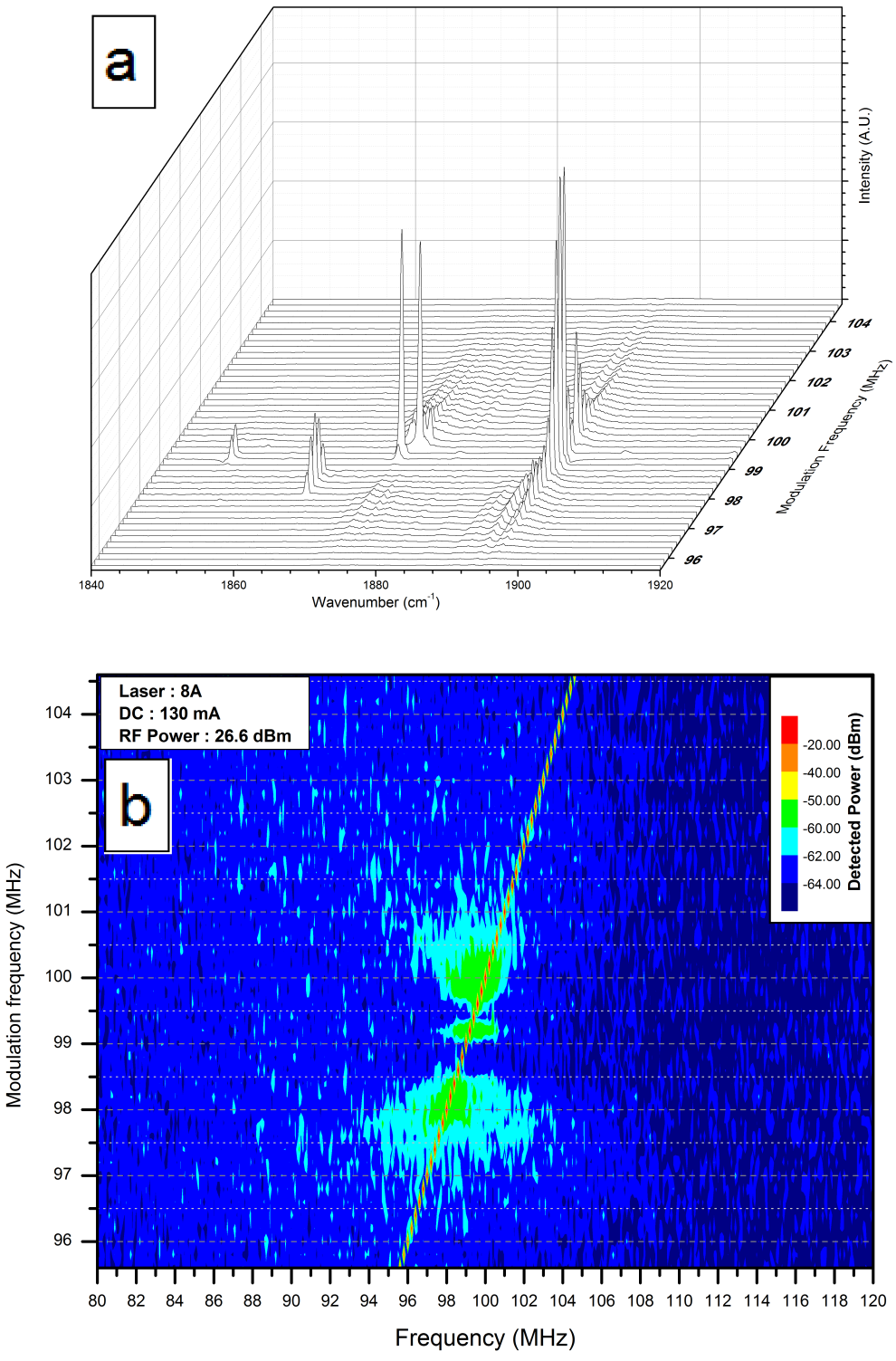

Figure 6.4: **a:** Optical spectra, **b:** RF spectra; of a 1.5 m EC-QCL under near resonant modulation at a DC level of 130 mA.

detuning, with the broad features in the RF spectrum (fig. 6.4b) coinciding with broad\multimode optical spectra (fig. 6.4a). The resonance or mode-locking condition can be expected to lie in the region between them. A stable mode-locked condition is expected to have a single peak in the optical domain and the narrowest of peaks in the RF spectrum. This would indicate a stable pulse train which persists for many cavity round trips. As can be seen at both DC levels, the most intense single peaks in the optical spectra coincide with regions of very low sideband noise in the RF spectrum. There are also multi-peak optical spectra which seem to coincide with RF noise. The RF noise suggests this is likely to be a switching behaviour in the optical domain rather than a stable multi-wavelength pulse train. Accounting for the single and multi-peak emission region is more challenging. A reasonable expectation might be that the maximum intensity would be observed at the exact cavity resonance. At both DC levels there does exists a central band where high intensity single peaks dominate. On the most part the multi-peak spectra are either side of this assumed resonant band. This seems to create a sensible picture where increased detuning from resonance causes the cavity to transition from a stable single peak regime to one of switching then finally to a vanishing chaotic broad regime. Fig. 6.5. shows the combined interferograms characteristic of the three spectral regimes.

There are, however, a few exceptions. At 110 mA DC the optical spectrum corresponding to a modulation frequency of 99.5 MHz has a small but significant second peak at 1896 cm^{-1} even though it would appear to be in the centre of the resonant band. Further, the entire band of single peaks between 98.4 and 98.9 MHz of the 110 mA run are assumed to be on the low side of resonance whereas at 130 mA DC this band now seems to form the central band. This is despite these data runs having been taken consecutively, without adjustment to the cavity. While the effect of increased DC pumping is likely to cause a change in the index of the QCL, a rough calculation shows this should only account for a shift in the FSR of a few KHz at most. It would, however, seem possible that in both DC cases the resonance, and the onset of a multi-peak instability, is very close to the vicinity of the reading taken at 99.4 MHz. In this case the small difference made by the additional current may have shifted this regime boundary by a single reading.

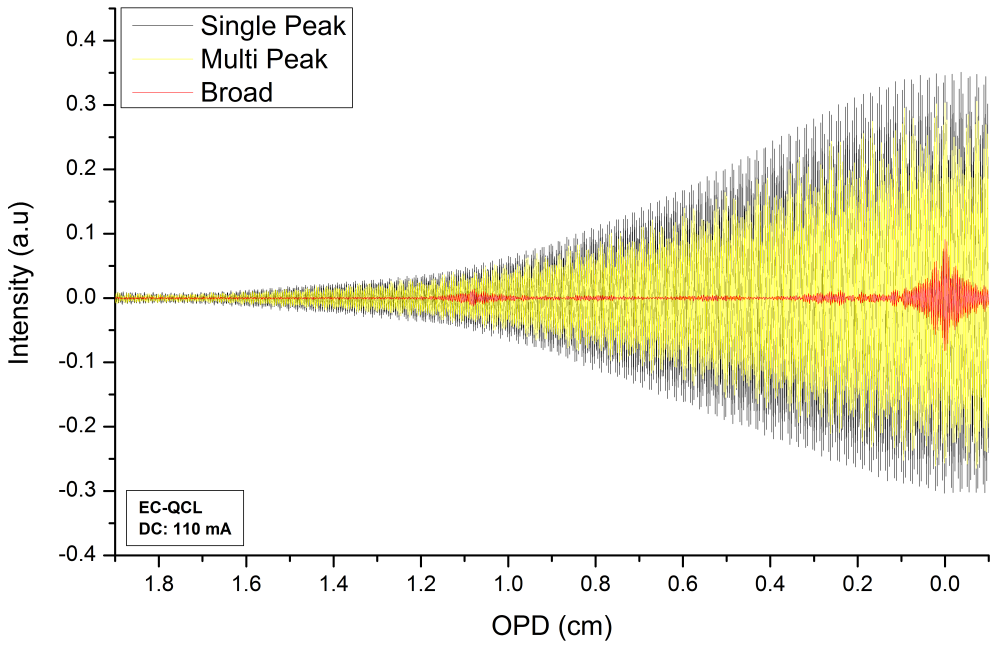

Figure 6.5: Characteristic interferograms of the three emission regimes: broad, in red; multimode, in yellow; single peaked, in black; seen from a resonantly pumped 1.5 m EC-QCL.

Looking at the features present in the two RF spectra of figs. 6.3 & 6.4 it's clear that the two upper features present at 110 mA coalesce into the upper feature present at 130 mA. This area at around 99.4 MHz would then seem to have both expected characteristics of highest intensity emission and a narrow RF linewidth. This figure would also seem to be supported by the pulse amplitude measurements in fig. 6.2. The lowest DC current used here was 101 mA but with care increasingly low DC currents can be used to narrow in on the resonance, the assumption being that for a given RF power, emission will be observed at the lowest possible DC level when modulated at the exact round-trip frequency. This can be done quickly, in an iterative fashion, prior to each data run to give a good indication of the cavity's FSR.

To examine more closely the pulse stability around resonance, RF spectra were taken at a higher resolution with a reduced video bandwidth (VBW). This reduction in VBW helps reduce the noise which can expose features at lower power levels. Fig. 6.6 shows the same device measured with increased VBW. In this instance the cavity

had been adjusted which may have caused a slight shift in the resonant frequency. The resonance was found to be around 98.78 MHz using the aforementioned technique at low DC levels. The same characteristic pattern is present despite being at a higher DC level with a broad feature quickly developing as the detuning increases on the high frequency side of resonance. Here the feature that broadens with increased detuning is symmetric about the cavity resonance and shows nicely the effect of the fixed FSR of the external cavity. These pedestal like features can be understood in the time domain as a consequence of the fundamental frequency been modulated randomly by a lower frequency, in this case the pulse-train collapsing. A broader pedestal would signify more rapid formation and collapse. In mode locked systems with very broad optical combs these pedestals in the RF spectrum can instead be evidence of mode locking where it is created by the difference in mode beat frequencies caused by the significant index variation over the comb band[4]. This can't be the case here with such significant detuning.

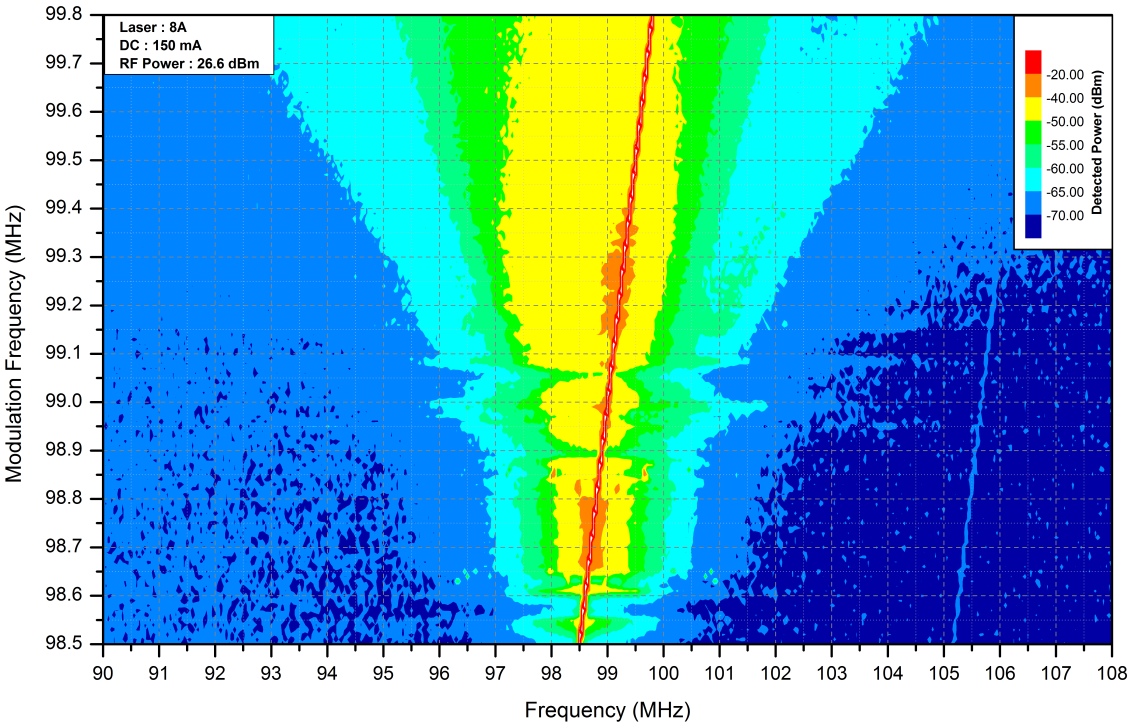

Figure 6.6: RF spectrum of a 1.5 m linear EC-QCL modulated around resonance.

Increasing the resolution even further, as in fig. 6.7, reveals a rather counterintu-

itive picture. Where all previous measurements suggest a resonant frequency close to 98.78 MHz, this measurement would seem to suggest that more stable pulse trains are generated when the cavity is modulated in the 98.82 to 98.84 MHz region. One possible explanation could be the effect of hysteresis which can govern the behaviour of these external cavity systems in a profound way. Whether resonantly pumped or driven CW, where different possible lasing solutions exist, the system will generally remain in a metastable state until some perturbation causes an effective reset. This can be anything from mechanical shock to some electrical transient. In this case adjustments to the modulation frequency have been in very small increments which are less likely to perturb the system than the larger steps taken in previous data runs.

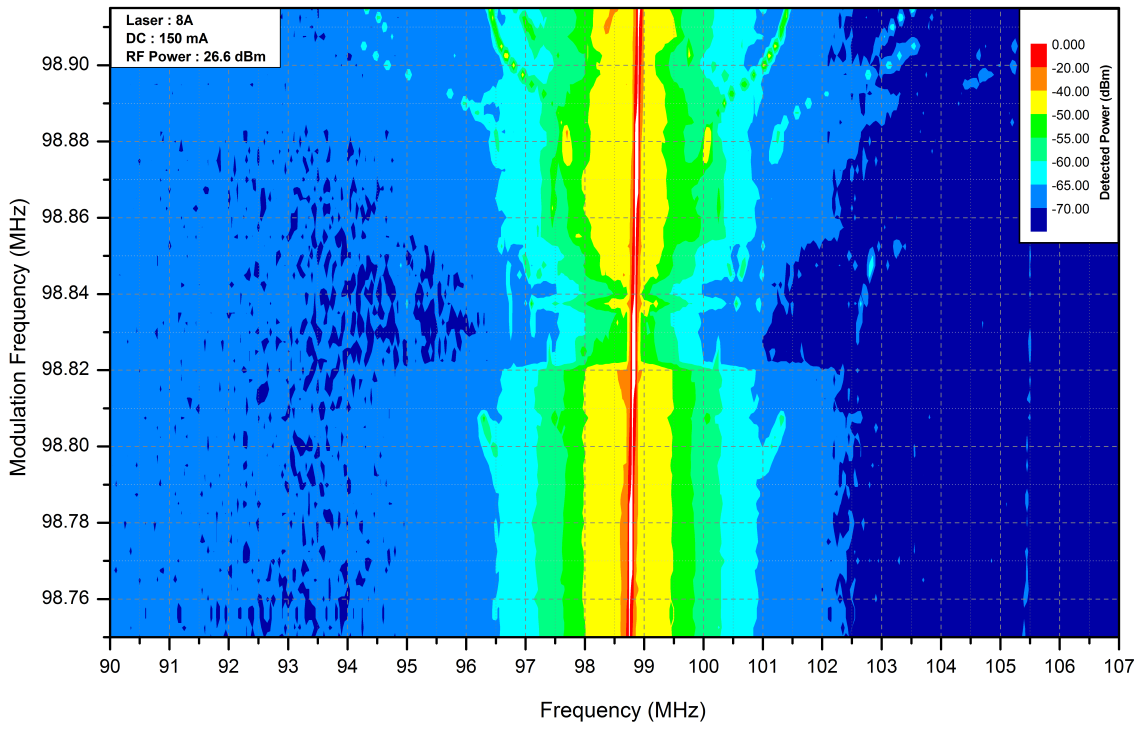

Figure 6.7: Increased resolution RF spectrum of a 1.5 m linear EC-QCL modulated around resonance.

In this vicinity the conditions suggestive of stable mode-locking are both present. Fig. 6.8 shows the two spectra at this point. Similar to the ring cavity case, both spectra are resolution limited.

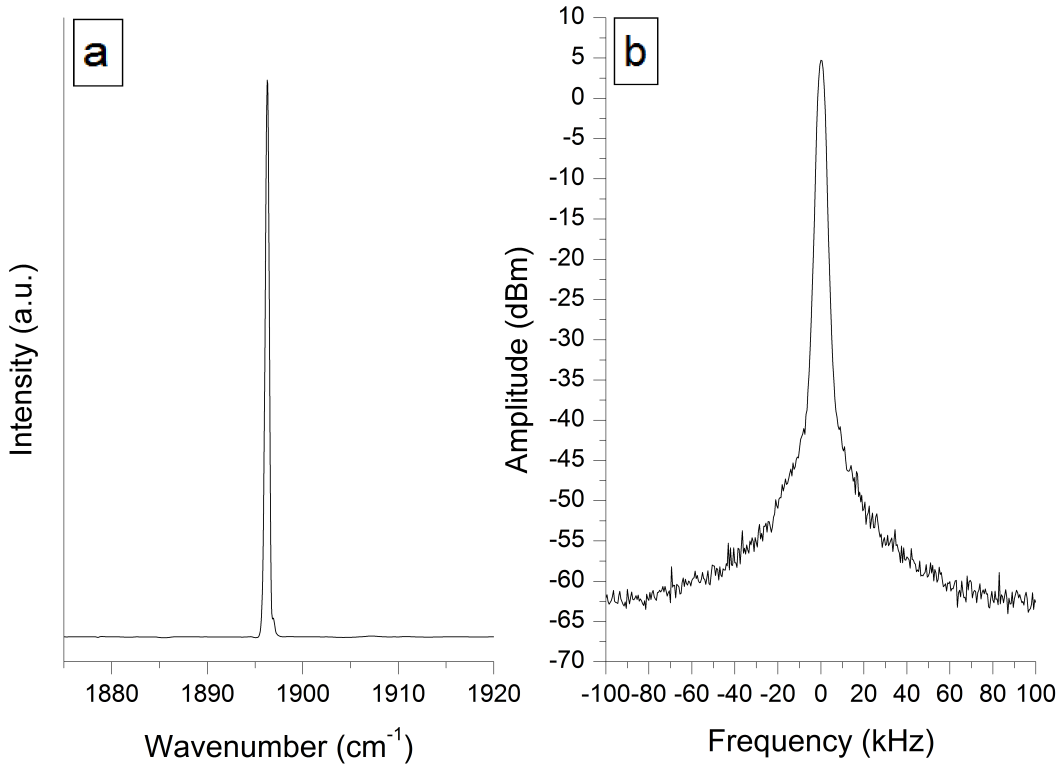

Figure 6.8: Mode-Locking condition for the External Cavity QCL at 98.78 MHz. Both optical and RF spectra are resolution limited at 0.5 cm^{-1} and 10 kHz repectively.

With a modulation frequency fixed at a resonant frequency of 98.78 MHz the effect of the DC level and RF power on the RF spectrum of the laser output were measured. In both cases the picture is a complex one. The DC level is likely to have a significant effect on the devices characteristics due to heating of the ridge. This shouldn't be expected to be the case for varying RF power although this may break down to a certain extent when the modulation depth is high enough to reach beyond the Ohmic region of the QCL. One stark difference is the disparity between the two pumping components as they are increased. In both cases the detected power at resonance increases with the pumping but only in the DC case do we see the sideband noise increasing in kind. Also the appearance of combs in the RF spectrum are difficult to account for. Particulaly those observed while varying the

RF power starting at around 22.5 dBm. The form clearly suggests some coherent process adding an aditional modulation component, starting at around 500 KHz, to the output. It's likely that these features, like most, are the result of the complex interplay between optical, electrical and thermal effects.

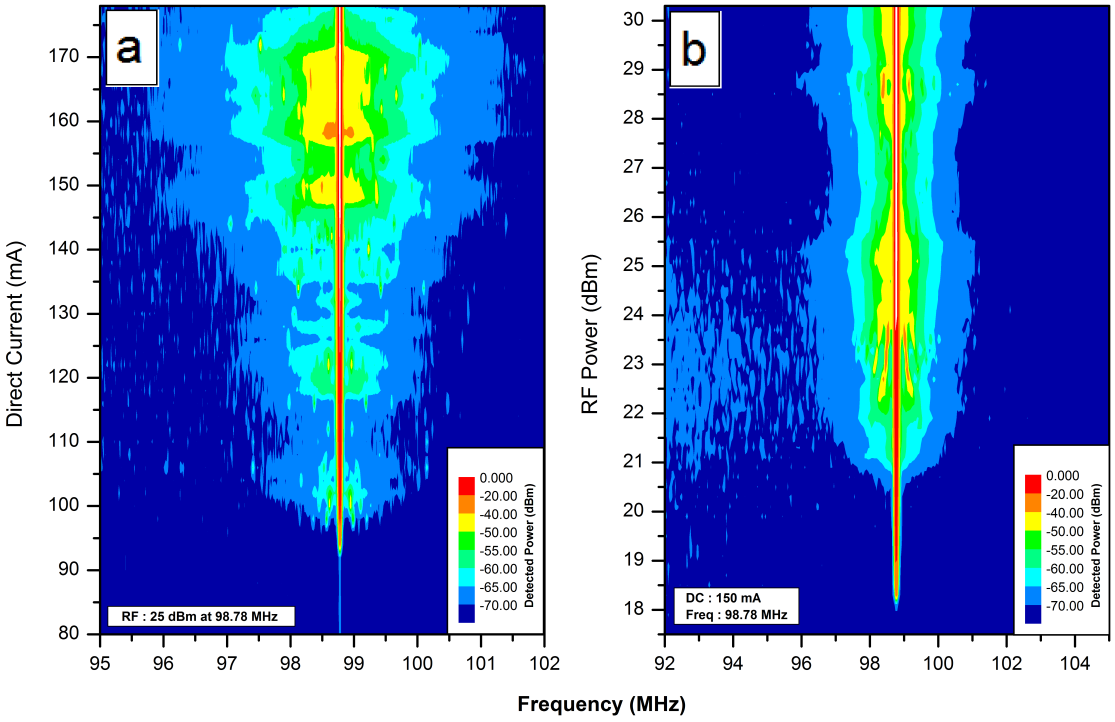

Figure 6.9: **a:** RF Spectrum of EC-QCL at resonance under varying DC bias levels. **b:** RF Spectrum of EC-QCL at resonance with varying RF power levels.

6.3 Fundamental Pumping Discussion

A number of limitations existed in this setup. Firstly, the detector used to measure the RF spectrum of the laser output had a bandwidth of around 300 – 400 MHz. When measuring the RF spectrum of cavities with a FSR (round trip frequency) of around 100 MHz this is more than sufficient. This measurement around the FSR gives an indication of the pulse's stability. A narrow line around the FSR would indicate a stable pulse train whereas a broader line, one with significant sideband noise, would indicate a periodically collapsing pulse train. Calculations based on

the FWHM linewidth of the RF/microwave peak gives a rough indication of the number of round trips over which the pulses remained stable. The difficulty comes when wanting to study the temporal form of pulses emitted by the cavity. The hope is that highly anharmonic pulses can be created at the FSR frequency and having a higher bandwidth detector would have allowed us, to a greater extent, to temporally resolve the pulse envelope which may have provided further insight. In the first real ridge mode-locking experiment[2], where the FSR frequency was around 17.8 Ghz, the group used a quantum well Infrared photodetector (QWIP) which had a bandwidth of around 20 GHz. Clearly their detector could only be used to observe the microwave spectrum around the FSR of the ridge in a similar fashion to ours.

Pulse characterization in the mid-Infrared is almost entirely done using second order interferometric autocorrelation (IAC), as was the case for the ridge mode-locking experiment. Autocorrelation can be divided into three classes: field, intensity and interferometric. The key difference is whether or not phase information can be extracted from the measurements. Where conclusive proof of short isolated pulses is sought, second order IAC can provide both the spectral and phase information needed to completely reconstruct the electric field. These setups can be complex and usually rely on second harmonic generation (SHG) in a non-linear crystal although a good number of different schemes exist[5].

Field autocorrelation measurements were the limit of our setup and were provided by a Brucker IFS 66v/s FTIR spectrometer. While an IAC setup is the gold standard for demonstrating short, isolated pulse-trains a strong case is made here without relying on any unreasonable assumptions.

6.4 High Harmonic Pumping

One route to creating shorter pulses is to modulate the cavity at a higher harmonic, that is a multiple of its FSR. Attempts using prior electronics had shown some emission up to a frequency of around 400 MHz without any serious considerations for the electrical conditions around the QCL submount. While our PA was limited to a band around 100 MHz, 22 dBm of RF power could be generated up to 3.2 GHz

by our signal generator, albeit with some harmonic distortion. A broadband (1 – 3 GHz) impedance matched bias-tee was designed and manufactured using a similar AlN substrate brazed to a copper TEC mount. This time the impedance matching network relied partly on a distributed element approach with only a few discreet components.

Observing pulses in the time domain was impossible beyond 300 MHz due to the limited bandwidth of our detector. This meant an optical chopper had to be used to produce a signal that could be detected when a cavity resonance was found. As previously mentioned, the presence of short isolated pulses is difficult to prove without a full IAC setup but one indication may be the spectral broadening, in the optical domain, of the emission peak. All of our high intensity, single peak spectra taken from resonant pumping, and CW, tended to be resolution limited with a FWHM of around 0.4 cm^{-1}. The time-bandwidth product ensures any pulse of a duration shorter than around 35 ps would have a FWHM bandwidth of more than 0.5 cm^{-1}, the stated resoution of our FTIR. Observing spectral linewidths under increasing modulation frequency may in this way help support a case for the generation of short optical pulses.

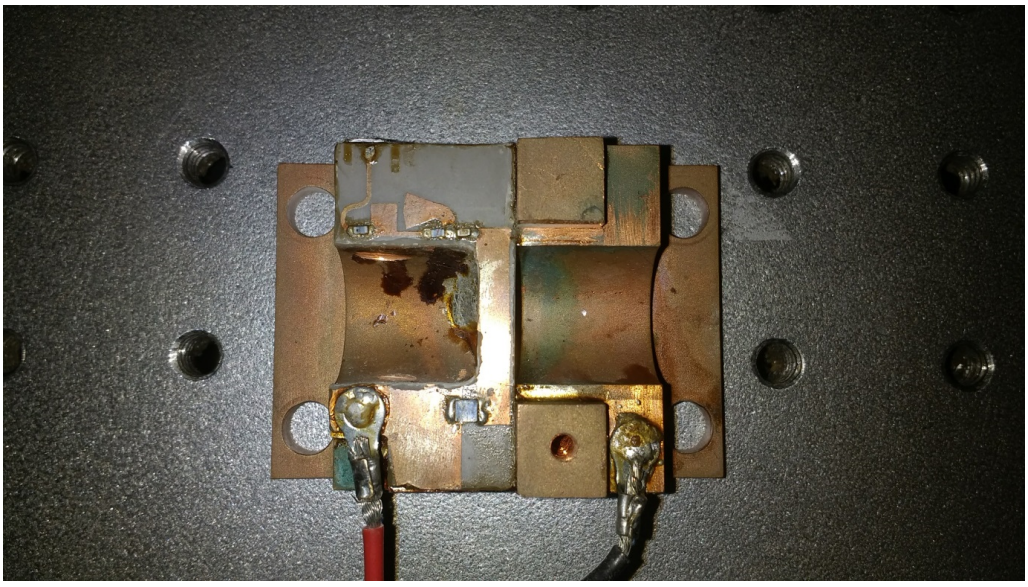

Figure 6.10: Completed high frequency bias-tee used for high harmonic pumping of the EC-QCL. Missing here is the SMA connector which was removed to be reused. This sat at the RF input at the top left of the mount.

This bias-tee was used with the same laser (8A) as in the previous experiments

Nº	Peak frequency (MHz)	$\frac{f}{n}$ (MHz)
1	174.3	174.3
2	347.8	173.90
3	521.8	173.93
4	697.5	174.38
5	869.7	173.94
6	1044.8	174.13
7	1218.5	174.07
8	1392.7	174.09
9	1566.6	174.07
10	1740.5	174.05
11	1915.1	174.10
12	2089.3	174.11
13	2263.39	174.11
14	2437.48	174.11
15	2611.57	174.10
16	2785.66	174.10
17	2959.75	174.10
18	3133.84	174.10

Table 6.1: List of detected resonances in the 0 to 3.2 GHz band with a maximum RF power of 22 dBm at a DC close to threshold of a 85 cm EC-QCL.

aligned into a linear cavity of approx. 85 cm in length. Under modulation from the signal generator resonances were observed at every harmonic from the first at 174.3 MHz up to the 18^{th} at 3.13 GHz. As expected, it was only possible to observe individual pulses for the first two harmonics. Beyond this the oscillations quickly diminished and the signal resembled a CW response, where a chopper is also employed. The signal detected becomes an average illumination analogous to a DC level in electronics.

The high frequency bias-tee worked well outside the lower edge of its 1 GHz design band and generally reduced in coupling efficiency as the frequency increased.

With the RF power set to a maximum of 22 dBm the first harmonic required very little DC compared to the laser's CW threshold. Maintaining the RF power at the maximum, the trend was that the DC required to see emission increased with frequency. By the 18th harmonics the coupling of the RF power was so poor that a reduction of only 1 mA from the CW threshold was possible. While it was clear at the design stage that the high frequency and bandwidth requirements would come at the expense of electrical coupling efficiency, simulations had suggested that a manageable return loss of around -3 dB would be maintained over the band. These return loss (S_{11}) simulations didn't accurately represent what was observed in this instance.

This made it impossible to measure accurate spectra much beyond 2 GHz. At these frequencies the resonant response could only be observed on the oscilloscope and were at such low power levels that extracting clear time domain data was impossible. Fig. 6.11 shows a number of spectra from various harmonics of the system. Despite the modulation frequencies been over many octaves the interferograms all look very similar. The jump in wavelength after the 4th harmonic at 697 MHz was probably due to the increased DC that was required to generate emission. Other harmonics lased at a number of different wavelengths but in all cases the FWHM linewidth was resolution limited at around 0.4 cm^{-1}.

Taking the 12 th harmonic (2089 MHz) as an example, at this frequency a half cycle has a duration of approx. 240 ps which can safely be assumed to be the upper limit on the pulse duration given the DC level was below CW threshold. It's clear from the spectra that harmonic mode locking with such poor coupling cannot generate pulses which are significantly shorter than a half cycle. A theoretical study[1] based on ERC-QCLs has shown that under the right bias conditions, with deep sinusoidal modulation, pulse durations below a quarter of the cycle time should be possible. In their model this required a DC gain of 0.8 times threshold and a modulation amplitude of 0.65 times threshold. A quick calculation, ignoring non-ohmicity, shows this would, for a typical buried structure, require in excess of 23 dBm of microwave power being delivered to the QCL. From the level of DC needed to detect a response at the 18th harmonic (3.134 GHz) it's likely as little as -30 dBm was coupling into the chip.

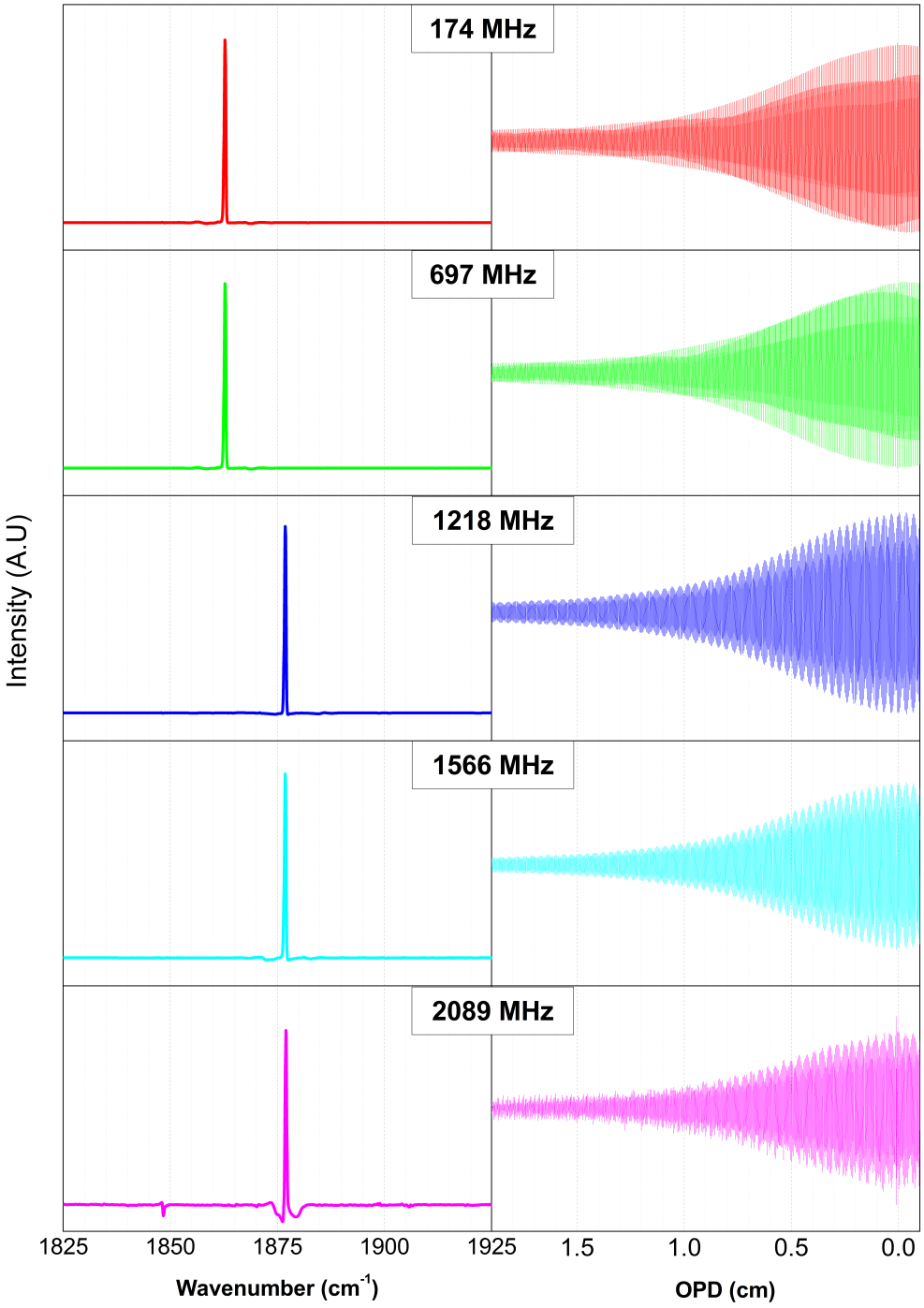

Figure 6.11: Optical spectra and associated interferograms of a 85 cm EC-QCL under high harmonic pumping. 22 dBm of RF power and various DC levels were used.

A number of reasons could explain this poor high frequency performance. Like in the previous bias-tee design there was a hope that the module could be used with multiple lasers, but primarily for high performance Alpes buried structures. This meant targeting a differential resistance of around 8 Ohms. A quick measurement of this figure for 8A gave a figure of over 14 Ohms in the vicinity of threshold. There is clearly a significant mismatch here which would modify the frequency response of the bias-tee. Optimizations at 8 Ohms suggested that deviations tended to deteriorate the high frequency performance to a greater extent. The plan had been to use this high frequency mount for the ERC-QCL but unfortunately time didn't permit any measurements to be taken.

Even with a correctly matched chip it may have been the case that the design procedure was lacking for work at these frequencies. While the software used here models non-idealities for its transmission line and distributed elements beyond normal spice simulations, optimizations weren't performed in an EM environment. It would have been relatively straight forward to produce 2D EM co-simulations which would have taken account of a number of additional effects and may have led to a more accurate optimal design. The problem with this being the amount of processing power required. Multi-variable optimizations in even a 2D EM environment would require a great deal of time on the hardware that was used. In reality the nature of the bias-tee and laser submount means only a full 3D EM simulation would have given an accurate indication of performance. Wherever possible, sound design principles were employed, however certain aspects of the design were limited by the submounting of the QCL. The copper finger which contacts the bonding pad (absent in fig. 6.10) remained entirely unmodelled. While it was designed to be substantial and short to avoid significant inductance, it represents a major departure from a transmission line, introducing a significant asymmetry in the current return patch. Without the use of full 3D EM simulations and a network analyser the only thing that can be said is at some frequency this feature becomes a limiting factor.

6.5 Conclusion

We have shown, for the first time, the mode locking of a linear EC-QCL. A harmonic mode locking scheme was used at the fundamental frequency of the cavity which showed good pulse stability with a narrow linewidth RF spectrum and a single peak in the optical domain. Pulse durations in this regime are estimated to be around 1 – 2 ns, similar to the ERC. The suggestion that SHB effects limit the ability of linear resonators to sustain mode-locked pulse trains isn't evidenced here. Little difference is seen between the case of the EC and ERC-QCL systems in this regard. The reason for this may lie in the relatively long, low intensity pulses that are generated by this fundamental pumping scheme. While in the CW regime, the SHB instability is present from threshold, it can be expected to exert the greatest effect on short high intensity pulses.

High frequency modulation of an 85 cm cavity up to the 18 th harmonic at 3.13 GHz is achieved with a pulse duration that can be safely estimated to not exceeding 150 ps, containing a minimum of around 30 phase-locked cavity modes. Full pulse characterization wasn't possible in the absence of an IAC setup. Shorter pulses could be created by this harmonic mode locking scheme by employing higher frequencies at a higher microwave power. This would require more exotic electronics including microwave bias-tee design well impedance matched to the QCL with an ultra-low parasitic mounting scheme. Simulations in an EM environment may be needed to achieve this. The high frequency bias-tee was designed for use in the ERC-QCL system but time didn't permit these measurements to be taken. If the impedance match resulted in significantly better electrical coupling then at the upper limit of the attainable band (around 3 GHz), it may have been possible to achieve pulses with a duration below 100 ps which would have begun to approach the limit where even bandwidth limited pulse would have produced a broadening resolvable by our FTIR.

Bibliography

[1] Aleksander K Wójcik, Pietro Malara, Romain Blanchard, Tobias S Mansuripur, Federico Capasso, and Alexey Belyanin. Generation of picosecond pulses and

frequency combs in actively mode locked external ring cavity quantum cascade lasers. *Applied Physics Letters*, 103(23):231102, 2013.

[2] Christine Y Wang, Lyuba Kuznetsova, VM Gkortsas, Laurent Diehl, Franz X Kaertner, Mikhail A Belkin, Alexey Belyanin, Xiaofeng Li, Donhee Ham, Harald Schneider, et al. Mode-locked pulses from mid-infrared quantum cascade lasers. *Optics Express*, 17(15):12929–12943, 2009.

[3] D Zumbuhl, N Matuschek, and FX Kartner. Turbulence in detuned mode-locked lasers. In *Lasers and Electro-Optics, 1998. CLEO 98. Technical Digest. Summaries of papers presented at the Conference on*, pages 336–337. IEEE, 1998.

[4] Roberto Paiella, Federico Capasso, Claire Gmachl, Harold Y Hwang, Deborah L Sivco, Albert L Hutchinson, Alfred Y Cho, and HC Liu. Monolithic active mode locking of quantum cascade lasers. *Applied Physics Letters*, 77(2):169–171, 2000.

[5] Raymond J Lanzafame. Ultrashort laser pulse phenomena: Fundamentals, techniques, and applications on a femtosecond time scale, by jean-claude diels and wolfgang rudolph. *Photomedicine and Laser Therapy*, 25(1):58–58, 2007.

Chapter 7

Future Work

7.1 Wavelength Tunable External Ring Cavity QCLs

In chapter 3 we demonstrated, for the first time, a room-temperature continuous-wave wavelength-tunable external ring cavity QCL system, potentially suited to high resolution gas spectroscopy. The findings support the suggestion that ring cavity geometries have an advantage over linear cavities due to the suppression of the spatial hole burning instability. Replacing an external mirror with a diffraction grating allowed the wavelength to be tuned across the entire gain bandwidth of the QCL gain medium. One significant shortcoming of this system is the tuning regime it employs. The path to developing this system into one which could rival its linear counterparts is clear.

Unlike Littrow and Littmann Metcalf linear cavities, which are capable of continuous wavelength tuning, our system is limited to a regime known as multi-mode envelope (MME) tuning. This regime is unfavourable to high resolution spectroscopy which calls for high levels of sensitivity and selectivity. MME tuning allows groups of adjacent external cavity modes to lase simultaneously and with our system lacking the ability to alter the cavity length during a wavelength sweep these modes remain stationary. This means during a wavelength sweep there exists the possibility that a number of closely spaced modes lase simultaneously, compromising the systems selectivity. The fixed wavelength position of the evenly spaced external cavity modes also allows the narrow spectral features of some analytes to be missed entirely. In larger cavities the FSR creates closely spaced modes which could be used to resolve the broad features of some analytes without significantly distortion. If, on the other hand, spectral features are narrow compared to the systems FSR and its wavelength position falls between adjacent cavity modes, the feature could remain entirely undetected.

Both of these issues are resolved in Littrow type systems which are capable of producing a single narrow linewidth emission peak that can be swept continuously across some bandwidth. This ensures that a sample's absorption spectrum can be measured in an almost idea fashion. The key to this mode-hop-free operation is the mechanical synchronization of the grating angle and cavity length. This is usually achieved by attaching the grating to a pivoting arm which can be engineered such that the gratings filter function tracks a single mode order. This quite elegant

solution allows tuning to be achieved using a single mechanical actuator, usually a piezoelectric actuator or a linear stepper motor. While our ring system uses a diffraction grating in the same way as these linear cavities, no method of adjusting the cavity length was employed.

To further the ring cavity as a tool for high resolution gas spectroscopy a geometry must be found that that allows this mode-hop-free condition to be satisfied while maintaining the circular boundary condition that gives ring cavities their advantage. Producing appreciable changes in the cavity length of ring based systems is more challenging than is the case for linear types. From an engineering viewpoint, it's desirable to minimize the number of optical components. It would also be highly undesirable if multiple mechanical actuators had to be electrically synchronized during a wavelength sweep. A novel solution was found that allowed an external ring-like geometry to be continuously tuned using a single actuator, in the same fashion as its linear counterparts. It employs less optical components than the system detailed in chapter 3 and requires no specialist components. An early prototype has shown much promise and this system is currently being considered as the basis of a spin-off company.

7.2 Phase-locking

At the end of chapter 3 we detailed a strange self-phase-locking regime observed while driving certain buried structure QCLs in both linear and ring cavities. This effect is assumed to be related to frequency modulated combs and the four-wave-mixing process. This is a matter of interest in QCL research and is likely to be the future of MIR gas spectroscopy where FM combs can be exploited using dual heterodyne techniques. In our case, little time was available to explore this exciting phenomenon which showed some strange characteristics when compared to the literature. To fully explore this effect some experimental setup would need to be developed, most significantly an intermode beat (IMB) spectroscopy setup. This could be realised using our FTIR spectrometer, a Vigo fast detector, a spectrum analyser and a labview script. An IMB spectrum is similar to the field autocorrelation measurements of a standard FTIR except instead of the mirror path difference

being measured against intensity, it's measured against the frequency component corresponding to the cavity's free spectral range. This is a standard technique used to study QCL FM frequency combs where comparison between intensity and IMB spectra shows the phase coherence of broad emission. Another idea, also borrowed from QCL FM comb studies, is that broad FM combs can be enhanced with the addition of very low levels (around -25 dBm) of RF power at the cavity's FSR frequency. This could be realised quickly using some elements of our resonant pumping setup. The use of our longer path length external cavities under FM comb regimes could lead to the realisation of a dual comb spectroscopy system with an increased resolution compared to those based on Fabry Perot devices.

7.3 Mode-locked External Cavity QCLs

The mode-locking work detailed in chapters 5 & 6 employs an active harmonic mode-locking technique to make comparisons between linear and ring cavity mode-locked pulses. With the exception of the high frequency modulation in section 6.4, the fundamental pumping likely resulted in pulses of a duration on the nanosecond timescale for both linear and ring configurations. The scientific value of mode-locked MIR pulses from QCL based systems in spectroscopy and other applications is dependent on the ability to create ultrashort pulses. Clearly the foundational work presented in this thesis falls short of this classification with ultrashort pulses generally being those with a duration on a pico- or femtosecond timescale. This is certainly true of systems that operate at visible wavelengths, with commercially available systems able to generate mode-locked pulses with a duration of around 10 femtoseconds. It's highly unlikely that actively modulated external cavity systems, similar to those detailed in this thesis, will be able to produce pulses of this duration. With a practical modulation limit of around 30 GHz, it's likely that pulses of around a few picoseconds are the limit of what's attainable using a purely active approach.

Finding these limits was the goal of our ongoing work, with a number of approaches being pursued. Using our harmonic mode-locking scheme in a linear cavity (section 6.4) produced high harmonic pulse formation with 18 circulating pulses, each with a duration of around 150 ps. The poor electrical coupling limited this setup

which was engineered to be used with a high performance Alpes buried structure QCL in a ring cavity configuration. Using this setup with the correctly impedance matched device may have produced pulses of a shorter duration. This approach was practically limited by the bandwidth of our signal generator which had a maximum frequency of 3.2 GHz and could produce 22 dBm of power. Producing a power amplifier which could operate at around 3 Ghz would have allowed us to study high harmonic regimes at powers comparable to those generated by our fundamental pumping setup. While low cost transistors are available at these frequencies, usually HEMT FETs, designing power amplifiers at these frequencies can be more challenging. The development of robust power amplifiers at these frequencies would require the use of a network analyser setup as well as an oscilloscope of sufficient bandwidth.

Aluminium Nitride provides a highly thermally conductive substrate for the development of bias-tees above 3 GHz. While it suffers from a high dielectric constant (around 8.9) which results in short electrical wavelengths, proper design should allow microwave bias-tees to be made up to the bandwidth limit of typical QCLs. A number of improvements could have been made to its processing if proper resources were available. Gold plating would have been more appropriate for very high frequency work. Gold is the preferred plating material for microwave work due to the low losses compared to other plating materials such as tin. Silver plating is close but the immersion process only produces a very thin plate whereas the gold electroplating process can build a more robust layer, though this involves the use of toxic chemicals. Either CNC routing or Laser cutting could have been employed to produce the shape needed prior to brazing and may have made it possible to populate the substrate beforehand. A second, lower temperature, solder could have been used for the brazing which would have removed the risk of reflowing the component solder.

These harmonic schemes are a reliable method of decreasing pulse duration in actively mode-locked EC- & ERC-QCL systems. In the short pulse limit, the time-bandwidth product ensures that pulses are comprised of broad frequency combs. Using high harmonic pumping would produce broad combs but would have comb lines separated by the pumping frequency. For example, when a cavity is pumped

at its 10th harmonic, i.e. ten times the cavity's FSR, only one in every ten of the external cavity modes (ECMs) would be excited. For many applications it would be preferable to have frequency combs which include all ECMs. This can only be achieved when a single pulse circulates. To achieve this the device needs to be pumped with short electrical pulses at a repetition rate matching the cavity's fundamental frequency. Developing an electrical system capable of producing high powered short electrical pulses at RF repetition rates was the main aim of our ongoing work.

Figure 7.1: Photograph of completed NLTL realised on Rogers Duroid 5880 microwave laminate. A 100 MHz input tone is coupled in though the SMA connector on the left hand side. The small cluster of components adjacent to the left connector is the bias network used to bias the varactors to 5 V. RF signals are capacitively coupled in and out, providing a DC block.

At the heart of this system is a tapered non-linear transmission line (NLTL) which is capable of compressing the pulses which make up a 100 MHz harmonic tone. Fig.7.1 shows the completed NLTL which was fabricated using a Duroid microwave laminate substrate. This low index material allows coplanar waveguides

(CPW) with high characteristic impedances to fabricated, with very low losses into the tens of gigahertz. In our design the CPW transmission line is periodically capacitively loaded with varactor diodes. These diodes have a voltage dependent capacitance which is the key to the pulse compressing effect. The NLTL is made up of around 30 stages, each stage being comprised of a series inductance and a shunt capacitance. The inductive sections are a combination of surface mount RF inductors and some length of transmission line. The shunt capacitance sections being one or two varactor diodes. Some small value ceramic capacitors were added to bring each section closer to its optimum value. The key design requirement for these type of NLTLs is to match the impedance across the line while geometrically tapering the bragg frequency. Where pulse compression is sought, this generally results in inductance and total capacitance values which reduce along the length of the transmission line. This is complicated by the fact that the capacitance of the varactor diodes are voltage dependent, meaning parameters have to be calculated for a certain pulse amplitude. In our case a 10 V peak pulse was chosen.

The design process required the modelling of a large set of varactor diodes. From this large set around 15 different diodes were used in the final design. This painstaking process, taking months, led to a set of models which were used in a series of simulations that were used to optimize the design. Fig.7.2 shows a transient representation of a harmonic balance simulation for the NLTL pumped with a 10 V pk-pk 100 MHz tone. This simulation shows that the NLTL should be able to produce high amplitude pulses with a FWHM duration of under 100 ps, close to the 50 ps limit imposed by the transit time of light through a 4.5 mm QCL. While some small improvements may be possible, this would likely be close to the limit of what's possible using electrical modulation.

Electrical pulses of these short durations have frequency components starting from the fundamental pumping frequency up to around 10 GHz. The high frequency components are highly sensitive to parasitics along the electrical path to the QCL and could suffer high attenuation if improperly designed. High efficiency coupling requires low loss transmission lines to be used from the output of the NLTL to the QCL device. This meant using semi-rigid coaxial cables and a completely redesigned QCL mount based on the Aluminium nitride substrate similar to those detailed in

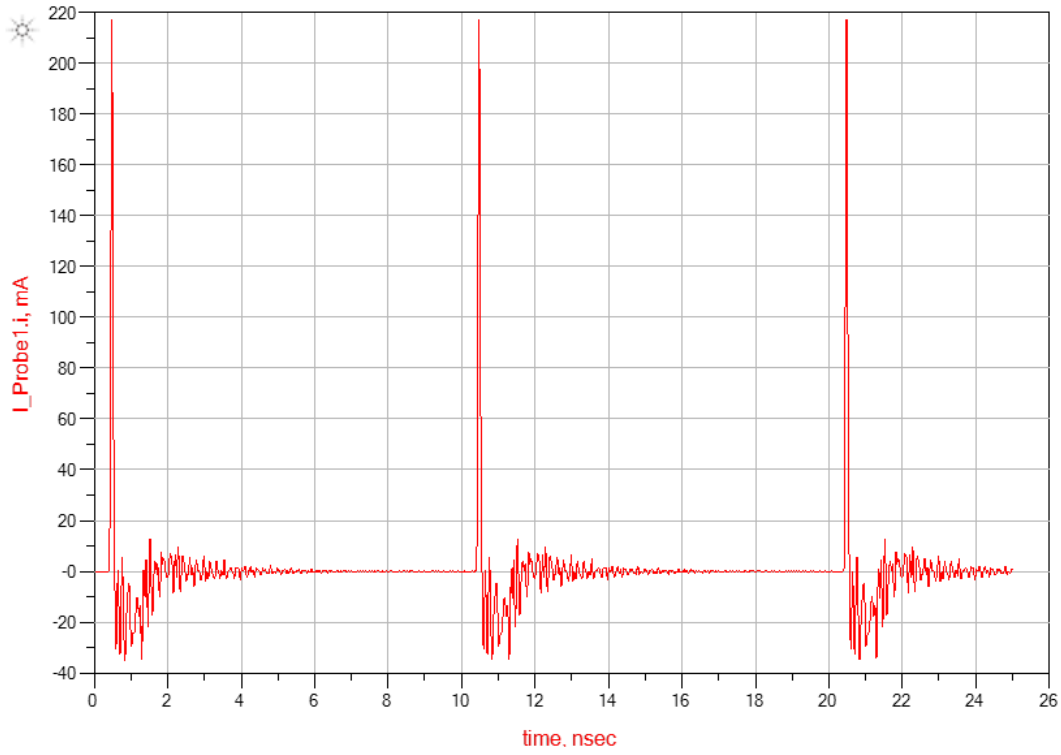

Figure 7.2: Transient representation of a harmonic balance simulation performed in Agilent ADS. This response shows the current flow into the QCL when resistively matched to 50 Ω. Electrical pulses with a FWHM duration of around 75 ps with amplitude in excess of 200 mA are generated.

chapter 4. Fig.7.3 shows the completed QCL mount. To reduce mounting parasitics a QCL device was affixed to the mount, meaning the wire bonds could join directly to the base, avoiding the need for a bonding pad or a contacting arm. These were the most significant limitations in previous mounts and are expected to form a parasitic filter network which rolls off above at a few GHz. Unlike the reactive impedance matching networks of previous systems, these high bandwidth electrical pulses call for a simple resistive match. This was achieved using a single high frequency SMD resistor.

From a fabrication point of view, the NLTL was relatively straight forward with the greatest difficulty being the use of Duroid laminate which required the application of a photoresist layer. This can be difficult over such a large surface which must be well cleaned and must be extremely level. Some care must also be taken when soldering the smaller varactor diodes which are on the limit of what can be manually soldered at 0402 size. This is possible, with some care, using a reflow soldering station. The difficulty came when manufacturing the QCL mount. This

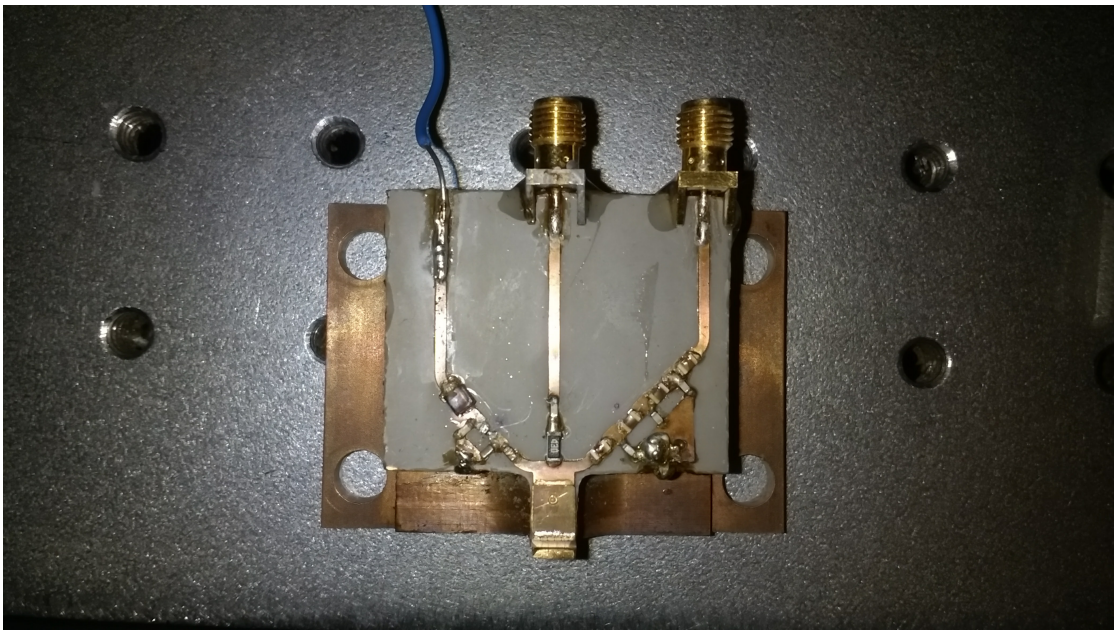

Figure 7.3: Photograph of the damaged QCL low parasitic mount. Three paths are present: a DC through on the left, a resistively matched microwave input for the NLTL in the centre, a 100 MHz RF path on the right. The QCL can be seen at the very bottom.

was manufactured using a similar procedure as that detailed in chapter 4. This was complicated by the fact that the QCL device needed to be affixed directly to the mount. Ideally, the QCL would have been indium soldered directly to the end of the transmission line on the aluminium nitride substrate. This size of the copper mount meant that anti-reflective coatings couldn't be applied once the device was mounted. Furthermore, soldering the QCL after the coatings had been applied would likely damage the coatings. This necessitated the use of a small copper submount ($0.5 \times 4.5 \times 6mm$) which allowed the device to be coated. The AlN substrate was engineered to accommodate this submount which was joined using an electrically conductive gold based epoxy resin. This allowed the connection to be made without exposing the coated device to high temperatures. The final stage of fabrication was the wire bonding which would join the QCL top contact to a raised base copper area adjacent to the QCL. Unfortunately during the wire bonding process the device was irreparability damaged. This was due to a clearance issue resulting from the unusual size of the mount.

This failure made it impossible to continue with this short pulse system, with no unmounted QCL devices remaining. This was the most promising thread of our

research, failing only due to the lack of a suitable replacement QCL. It's expected this system would have generated mode-locked pulses of a duration short enough to create a measurable spectral broadening from our FTIR. Without modifying the QCL device itself, this would have likely represented the limits of electrical modulation and would have been an excellent platform for the development of a hybrid mode-locked ERC-QCL system. In these schemes, non-linear optical elements such as saturable absorbers and kerr lenses could be introduced into the cavity with the aim of further compressing the propagating optical pulses. These elements are unable to produce passive mode-locking regimes in EC- & ERC-QCLs but may be effective when short high intensity pulses are imposed by active modulation.

To pursue ultrashort pulses from EC- & ERC-QCL systems it would be helpful to develop other elements of our experimental setup. The most important addition would be a quantum well infrared photodetector (QWIP) and an oscilloscope of sufficient bandwidth. QWIPs are the main component of a second order interferometric autocorrelation setup. This is the gold standard in short pulse characterization and is capable of reconstructing the complete electric field of a periodic pulse train. This would become increasingly important as it's expected that the difference between actively modulated EC- & ERC-QCLs would be most pronounced when short high intensity pulses can be generated. It would be of particular interest to see the effect of such short electrical pulses on the directionality of ERC-QCLs and compare pulse structures between bidirectional and unidirectional regimes.